ASSOCIATIONS BETWEEN AMOUNT OF VIRUS OR ANTIGEN EXPOSURE WITH DISEASE OUTCOMES AND IMMUNOLOGICAL RESPONSES

by

YANG GE

(Under the Direction of Andreas Handel)

ABSTRACT

This dissertation focus on the impact of virus or antigen exposure levels on infectious diseases outcomes and immune response. We explored three issues in subsequent studies: 1) the association between inoculum dose and norovirus infection outcomes; 2) norovirus antibody kinetics comparisons between infection and vaccination; 3) the impact of seasonal influenza vaccine dose on homologous and heterologous immunity. Our results provide a further understanding of the impact of exposure dose.

INDEX WORDS: Norovirus, Influenza, Vaccine, Antibody

ASSOCIATIONS BETWEEN AMOUNT OF VIRUS OR ANTIGEN EXPOSURE WITH DISEASE OUTCOMES AND IMMUNOLOGICAL RESPONSES

by

YANG GE

BACHELOR OF SCIENCE, CHINA, 2010

MASTER OF MEDICINE, CHINA, 2013

A Dissertation Submitted to the Graduate Faculty of the University of Georgia in Partial Fulfillment of the Requirements for the Degree.

DOCTOR OF PHILOSOPHY

ATHENS, GEORGIA

2022

ASSOCIATIONS BETWEEN AMOUNT OF VIRUS OR ANTIGEN EXPOSURE WITH DISEASE OUTCOMES AND IMMUNOLOGICAL RESPONSES

by

YANG GE

Major Professor:	Andreas Handel
Committee:	Benjamin Lopman
	Justin Bahl
	Ye Shen

Electronic Version Approved:

Ron Walcott
Dean of the Graduate School
The University of Georgia
May 2022

DEDICATION

To Yuwei Wang, Bowen Ge and my parents without whom this wouldn't be possible.

ACKNOWLEDGMENTS

I would like to extend my deepest gratitude to my advisor, Dr. Andreas Handel. Also, I appreciate my committee members Dr. Benjamin Lopman, Dr. Ye Shen, and Dr. Justin Bahl for their instructions. Further, I very much appreciate the collaborations I received from W. Zane Billings, Amanda Skarlupta, Ted Ross, Juan Leon, Katia Koelle, Robert L. Atmar, Antone R. Opekun, Mary K. Estes, David Y. Graham, and Paul Thomas.

CONTENTS

Acknowledgments **v**

List of Figures **viii**

List of Tables **xxviii**

1 Introduction **1**

1.1 Summary of Objectives 2

2 Analyzing the association between inoculum dose and norovirus infection outcomes **5**

2.1 Abstract 6

2.2 Introduction 7

2.3 Methods 8

2.4 Results 13

2.5 Discussion 19

2.6 Acknowledgements 20

3 Norovirus antibody kinetics comparisons between infection and vaccination **21**

3.1 Abstract 22

3.2 Introduction 24

3.3 Methods 26

3.4 Results 29

3.5 Discussion 38

4 Impact of seasonal influenza vaccine dose on homologous and heterologous immunity 40

4.1 Abstract 41

4.2 Introduction 43

4.3 Methods 45

4.4 Results 48

4.5 Discussion 57

5 Conclusion 59

Bibliography 63

Appendices 78

A Appendix: Analyzing the association between inoculum dose and norovirus infection outcomes 78

A.1 Overview 78

A.2 Analysis of virus shedding 79

A.3 Analysis of symptom outcomes 89

A.4 Results from additional analyses 97

B Appendix: Norovirus antibody kinetics comparisons between infection and vaccination 110

B.1 Overview 110

B.2 Accounting for limits of detection 111

B.3 Modeling antibodies kinetics 111

C Appendix: Impact of seasonal influenza vaccine dose on homologous and heterologous immunity 136

C.1 Description of the multi-center cohort study 136

C.2 Main multilevel model 140
C.3 Further analyses 159

LIST OF FIGURES

2.1 Virus shedding in feces or vomit. The straight lines and shaded regions indicate the mean and 89% credible intervals of the fitted Bayesian model. Points with circle shape are raw data. A) Cumulative virus shedding in feces during the first 96 hours. B) Cumulative virus shedding in feces during the full observation period (up to 91 days). C) Cumulative virus shedding in vomit. Only a few of the infected individuals had vomiting episodes, all within the first 96 hours. 14

2.2 Fitted fecal virus concentration curves. The red lines show mean of estimations. The grey areas show 89% equal-tailed credible interval (CI). LOD1 and LOD2 indicate the two limits of detection. Points with triangle shape represented samples that are positive qRT-PCR. Points with circle shape represented samples that are positive IMC and negative qRT-PCR. Points with square shape represented samples that are negative IMC and negative qRT-PCR. . . 15

2.3 Fitted virus concentration (GEC/g) in feces. The lines show mean of estimations. The colored areas show 89% equal-tailed credible interval (CI). A) The fitted curves for 90 days. B) The fitted curves for the first 7 days. 16

2.4 Model predictions for viral kinetics as a function of inoculum dose. The lines show mean of estimations. The colored areas show 89% equal-tailed credible interval (CI). A) Shedding onset (time at which virus load reaches LOD1). B) Time to virus peak shedding. C) Shedding duration (amount of time where virus load was above LOD1). D) Total virus load (area under virus concentration curve). . . 17

2.5 Association between dose and symptom scores. The lines show mean of estimations. The colored areas show 89% equal-tailed credible interval (CI). Points with circle shape are raw data. A) Incubation period, i.e., time between infection and onset of first symptoms. B) Severity using the modified Vesikari score. C) Severity using the comprehensive symptom score. 18

3.1 Fitted longitudinal antibody results in the HC study. The first row of the panel is the exponential decay model. The second row is the power-law decay model. The lines show the means of estimations. The colored areas show 89% equal-tailed credible intervals (CI). 32

3.2 Fitted GI.1 longitudinal antibody results in the HV study. The first row of the panel is the exponential decay model. The second row is the power-law decay model. The lines show the means of estimations. The colored areas show 89% equal-tailed credible intervals (CI). 33

3.3 Fitted GII.4 longitudinal antibody results in the HV study. The first row of the panel is the exponential decay model. The second row is the power-law decay model. The lines show the means of estimations. The colored areas show 89% equal-tailed credible intervals (CI). 34

3.4 Fitted peak level of antibodies and half-list time in the HC study. The lines show means of estimations. The colored areas show 89% equal-tailed credible intervals (CI). 36
3.5 Fitted peak level of antibodies and half-list time in the HV study. The lines show means of estimations. The colored areas show 89% equal-tailed credible intervals (CI). 37

4.1 The impact of HD vaccine compared to SD on strain-specific, homologous HAI responses. The median and 89% equal-tailed credible interval (CI) of the overall effect (HD vs. SD) are shown. The numbers under each line show the sample size (HD/SD) for that specific strain or the overall effect size. 50
4.2 The impact of HD vaccine compared to SD on strain-specific, heterologous HAI responses. The median and 89% equal-tailed credible interval (CI) of the overall effect (HD vs. SD) are shown. The numbers under each line show the sample size (HD/SD) for that specific strain or the overall effect size. Figures for seroconversion and seroprotection outcomes show similar results (see supplementary material). 51
4.3 The impact of HD vaccine compared to SD on strain-specific, heterologous HAI responses. The median and 89% equal-tailed credible interval (CI) of the overall effect (HD vs. SD) are shown. The numbers under each line show the sample size (HD/SD) for that specific strain or the overall effect size. 52

4.4 The impact of HD vaccine compared to SD on strain-specific, heterologous HAI responses. The median and 89% equal-tailed credible interval (CI) of the overall effect (HD vs. SD) are shown. The numbers under each line show the sample size (HD/SD) for that specific strain or the overall effect size. 53
4.5 The impact of HD vaccine compared to SD on vaccine-specific, homologous HAI responses. The median and 89% equal-tailed credible interval (CI) of the overall effect (HD vs. SD) are shown. The numbers under each line show the sample size (HD/SD) for that specific strain or the overall effect size. 54
4.6 The impact of HD vaccine compared to SD on vaccine-specific, heterologous HAI responses. The median and 89% equal-tailed credible interval (CI) of the overall effect (HD vs. SD) are shown. The numbers under each line show the sample size (HD/SD) for that specific strain or the overall effect size. 55

A.1 Daily comprehensive symptom score stratified by inoculum dose group. 93
A.2 Daily comprehensive symptom score stratified by inoculum dose group. 97
A.3 Virus shedding in feces or vomit. The bars show 89% equal-tailed credible intervals (CI). Points with circle shape are raw data. A) Fecal virus shedding in the first 96 hours. B) Fecal virus shedding with all data. C) Vomit virus shedding. The points show mean of estimations. 98

A.4 Fitted fecal virus concentration curves. The red lines show means of estimations. The grey areas show 89% equal-tailed credible intervals (CI). LOD1 and LOD2 indicate the two limits of detection. Points with triangle shape represented samples that with positive qRT-PCR results. Points with circle shape represented samples with positive IMC and negative qRT-PCR results. Points with square shape represented samples with negative IMC and negative qRT-PCR results. 100

A.5 Fitted virus concentration (GEC/g) in feces. The lines show means of estimations. The colored areas show 89% equal-tailed credible intervals (CI). LOD1 and LOD2 represent the two limits of detection. A) The fitted curves for 90 days. B) The fitted curves for the first 7 days. 101

A.6 Model predictions for viral kinetics as a function of inoculum dose. The points show means of estimations. The bars show 89% equal-tailed credible intervals (CI). A) Time to detection (above $15,000$ GEC). B) Time to peak. C) Shedding duration (period that virus concentration above $15,000$ GEC). D) Total virus load (area under concentration curve). 102

A.7 Estimated dose impact on symptoms. The points show means of estimations. The bars show 89% equal-tailed credible intervals (CI). Points with circle shape are raw data. 103

A.8 Virus shedding in feces or vomit. A) Total fecal virus shedding in the first 96 hours. B) Total fecal virus shedding with all data. C) Total vomit virus shedding. The lines show means of estimations. The grey areas show 89% equal-tailed credible intervals (CI). Points with circle shape are raw data. 104

A.9 Fitted fecal virus concentration curves. The red lines show means of estimations. The grey areas show 89% equal-tailed credible intervals (CI). LOD1 and LOD2 indicate the two limits of detection. Points with triangle shape represent samples that are positive for qRT-PCR. Points with circle shape represented samples that are positive for IMC and negative for qRT-PCR. Points with square shape represented samples that are negative for IMC and negative for qRT-PCR. 106

A.10 Fitted virus concentration (GEC/g) in feces. The lines show means of estimations. The colored areas show 89% equal-tailed credible intervals (CI). LOD1 and LOD2 represent the two limits of detection. A) The fitted curves for 90 days. B) The fitted curves for the first 7 days. 107

A.11 Model predictions for viral kinetics as a function of inoculum dose. The lines show means of estimations. The grey areas show 89% equal-tailed credible intervals (CI). A) Time to detection (above $15,000$ GEC). B) Time to peak. C) Shedding duration (period that virus concentration above $15,000$ GEC). D) Total virus load (area under curve). 108

A.12 Estimated dose impact on symptoms. The lines show means of estimations. The grey areas show 89% equal-tailed credible intervals (CI). Points with circle shape are raw data. 109

B.1 Description of serum antibodies in the HC study. 118
B.2 Description of serum antibodies in the HV study. 119
B.3 Fitted individual kinetics of GI.1 HBGA antibody in the HC study (Exponential decay). The lines show means of estimations. The colored areas show 89% equal-tailed credible intervals (CI). 120
B.4 Fitted individual kinetics of GI.1 HBGA antibody in the HC study (Power-law decay). The lines show means of estimations. The colored areas show 89% equal-tailed credible intervals (CI). 121
B.5 Fitted individual kinetics of GI.1 HBGA antibody in the HC study (Power-law decay). The lines show means of estimations. The colored areas show 89% equal-tailed credible intervals (CI). 122
B.6 Fitted individual kinetics of GI.1 IgA antibody in the HC study (Power-law decay). The lines show means of estimations. The colored areas show 89% equal-tailed credible intervals (CI). 123
B.7 Fitted individual kinetics of GI.1 IgG antibody in the HC study (Exponential decay). The lines show means of estimations. The colored areas show 89% equal-tailed credible intervals (CI). 124

B.8 Fitted individual kinetics of GI.1 IgG antibody in the HC study (Power-law decay). The lines show means of estimations. The colored areas show 89% equal-tailed credible intervals (CI). 125
B.9 Fitted individual kinetics of GI.1 HBGA antibody in the HV study (Exponential decay). The lines show means of estimations. The colored areas show 89% equal-tailed credible intervals (CI). 126
B.10 Fitted individual kinetics of GI.1 HBGA antibody in the HV study (Exponential decay). The lines show means of estimations. The colored areas show 89% equal-tailed credible intervals (CI). 127
B.11 Fitted individual kinetics of GI.1 IgA antibody in the HV study (Exponential decay). The lines show means of estimations. The colored areas show 89% equal-tailed credible intervals (CI). 128
B.12 Fitted individual kinetics of GI.1 IgA antibody in the HV study (Power-law decay). The lines show means of estimations. The colored areas show 89% equal-tailed credible intervals (CI). 129
B.13 Fitted individual kinetics of GI.1 IgG antibody in the HV study (Exponential decay). The lines show means of estimations. The colored areas show 89% equal-tailed credible intervals (CI). 130
B.14 Fitted individual kinetics of GI.1 IgG antibody in the HV study (Power-law decay). The lines show means of estimations. The colored areas show 89% equal-tailed credible intervals (CI). 131

B.15 Fitted individual kinetics of GII.4 IgA antibody in the HV study (Exponential decay). The lines show means of estimations. The colored areas show 89% equal-tailed credible intervals (CI). 132
B.16 Fitted individual kinetics of GII.4 IgA antibody in the HV study (Power-law decay). The lines show means of estimations. The colored areas show 89% equal-tailed credible intervals (CI). 133
B.17 Fitted individual kinetics of GII.4 IgG antibody in the HV study (Exponential decay). The lines show means of estimations. The colored areas show 89% equal-tailed credible intervals (CI). 134
B.18 Fitted individual kinetics of GII.4 IgG antibody in the HV study (Power-law decay). The lines show means of estimations. The colored areas show 89% equal-tailed credible intervals (CI). 135

C.1 Flow diagram of the multi-center cohort study. 138
C.2 The hierarchical features of the study. 139
C.3 Homologous pre- and post- vaccination titer. The dashed horizontal line is the seroprotection criterion. criterion. . . 160
C.4 Heterologous pre- and post- vaccination titer (H1N1-California-2009). The dashed horizontal line is the seroprotection criterion. 161
C.5 Heterologous pre- and post- vaccination titer (H1N1-Michigan-2015). The dashed horizontal line is the seroprotection criterion. 162
C.6 Heterologous pre- and post- vaccination titer (H3N2-Texas-2012). The dashed horizontal line is the seroprotection criterion. 163

C.7 Heterologous pre- and post- vaccination titer (H3N2-Switzerland-2013). The dashed horizontal line is the seroprotection criterion. 164
C.8 Heterologous pre- and post- vaccination titer (H3N2-Hong Kong-2014). The dashed horizontal line is the seroprotection criterion. 165
C.9 Heterologous pre- and post- vaccination titer (H3N2-Singapore-2016). The dashed horizontal line is the seroprotection criterion. 166
C.10 Heterologous pre- and post- vaccination titer (B-Brisbane-2008). The dashed horizontal line is the seroprotection criterion. 167
C.11 Heterologous pre- and post- vaccination titer (B-Massachusetts-2012). The dashed horizontal line is the seroprotection criterion. 168
C.12 Heterologous pre- and post- vaccination titer (B-Phuket-2013). The dashed horizontal line is the seroprotection criterion. 169
C.13 Heterologous pre- and post- vaccination titer (B-Colorado-2017). The dashed horizontal line is the seroprotection criterion. 170
C.14 Pre- and post- vaccination titer by each vaccine. The top row is homologous response, the bottom row is the heterologous response 171
C.15 Repeated vaccination description 172

C.16 The impact of HD vaccine compared to SD on strain-specific heterologous seroconversion (H1N1 strains). The median and 89% equal-tailed credible interval (CI) of the overall effect (HD vs SD) are shown. The numbers under each line show the sample size (HD/SD) for that specific strain or the overall effect size. 173
C.17 The impact of HD vaccine compared to SD on strain-specific heterologous seroconversion (H3N2 strains). The median and 89% equal-tailed credible interval (CI) of the overall effect (HD vs. SD) are shown. The numbers under each line show the sample size (HD/SD) for that specific strain or the overall effect size. 174
C.18 The impact of HD vaccine compared to SD on strain-specific heterologous seroconversion (B strains). The median and 89% equal-tailed credible interval (CI) of the overall effect (HD vs. SD) are shown. The numbers under each line show the sample size (HD/SD) for that specific strain or the overall effect size. 175
C.19 The impact of HD vaccine compared to SD on vaccine-specific heterologous seroprotection (H1N1 strains). The median and 89% equal-tailed credible interval (CI) of the overall effect (HD vs. SD) are shown. The numbers under each line show the sample size (HD/SD) for that specific strain or the overall effect size. 176

C.20 The impact of HD vaccine compared to SD on vaccine-specific heterologous seroprotection (H3N2 strains). The median and 89% equal-tailed credible interval (CI) of the overall effect (HD vs. SD) are shown. The numbers under each line show the sample size (HD/SD) for that specific strain or the overall effect size. 177
C.21 The impact of HD vaccine compared to SD on vaccine-specific heterologous seroprotection (B strains). The median and 89% equal-tailed credible interval (CI) of the overall effect (HD vs. SD) are shown. The numbers under each line show the sample size (HD/SD) for that specific strain or the overall effect size 178
C.22 The impact of HD vaccine compared to SD on strain-specific homologous responses. The median and 89% equal-tailed credible interval (CI) of the overall effect (HD vs. SD) are shown. The numbers under each line show the sample size (HD/SD) for that specific strain or the overall effect size. . 181
C.23 The impact of HD vaccine compared to SD on strain-specific heterologous titer increase (H1N1 strains). The median and 89% equal-tailed credible interval (CI) of the overall effect (HD vs. SD) are shown. The numbers under each line show the sample size (HD/SD) for that specific strain or the overall effect size. 182
C.24 The impact of HD vaccine compared to SD on strain-specific heterologous titer increase (H3N2 strains). The median and 89% equal-tailed credible interval (CI) of the overall effect (HD vs. SD) are shown. The numbers under each line show the sample size (HD/SD) for that specific strain or the overall effect size. 183

C.25 The impact of HD vaccine compared to SD on strain-specific heterologous titer increase (B strains). The median and 89% equal-tailed credible interval (CI) of the overall effect (HD vs. SD) are shown. The numbers under each line show the sample size (HD/SD) for that specific strain or the overall effect size. 184
C.26 The impact of HD vaccine compared to SD on strain-specific heterologous seroconversion (H1N1 strains). The median and 89% equal-tailed credible interval (CI) of the overall effect (HD vs. SD) are shown. The numbers under each line show the sample size (HD/SD) for that specific strain or the overall effect size. 185
C.27 The impact of HD vaccine compared to SD on strain-specific heterologous seroconversion (H3N2 strains). The median and 89% equal-tailed credible interval (CI) of the overall effect (HD vs. SD) are shown. The numbers under each line show the sample size (HD/SD) for that specific strain or the overall effect size. 186
C.28 The impact of HD vaccine compared to SD on strain-specific heterologous seroconversion (B strains). The median and 89% equal-tailed credible interval (CI) of the overall effect (HD vs. SD) are shown. The numbers under each line show the sample size (HD/SD) for that specific strain or the overall effect size. 187

C.29 The impact of HD vaccine compared to SD on strain-specific heterologous seroprotection (H1N1 strains). The median and 89% equal-tailed credible interval (CI) of the overall effect (HD vs. SD) are shown. The numbers under each line show the sample size (HD/SD) for that specific strain or the overall effect size. 188

C.30 The impact of HD vaccine compared to SD on strain-specific heterologous seroprotection (H3N2 strains). The median and 89% equal-tailed credible interval (CI) of the overall effect (HD vs. SD) are shown. The numbers under each line show the sample size (HD/SD) for that specific strain or the overall effect size. 189

C.31 The impact of HD vaccine compared to SD on strain-specific heterologous seroprotection (B strains). The median and 89% equal-tailed credible interval (CI) of the overall effect (HD vs. SD) are shown. The numbers under each line show the sample size (HD/SD) for that specific strain or the overall effect size. 190

C.32 The impact of HD vaccine compared to SD on vaccine-specific analyses. The median and 89% equal-tailed credible interval (CI) of the overall effect (HD vs. SD) are shown. The numbers under each line show the sample size (HD/SD) for that specific strain or the overall effect size. The top row shows homologous responses (A to C), the bottom row is heterologous (D to F). 191

C.33 The impact of HD vaccine compared to SD on strain-specific, homologous HAI titer increase. The median and 89% equal-tailed credible interval (CI) of the overall effect (HD vs. SD) are shown. The numbers under each line show the sample size (HD/SD) for that specific strain or the overall effect size. 192
C.34 The impact of HD vaccine compared to SD on strain-specific, heterologous HAI titer increase (H1N1 strains). The median and 89% equal-tailed credible interval (CI) of the overall effect (HD vs. SD) are shown. The numbers under each line show the sample size (HD/SD) for that specific strain or the overall effect size. 193
C.35 The impact of HD vaccine compared to SD on strain-specific, heterologous HAI titer increase (H3N2 strains). The median and 89% equal-tailed credible interval (CI) of the overall effect (HD vs. SD) are shown. The numbers under each line show the sample size (HD/SD) for that specific strain or the overall effect size. 194
C.36 The impact of HD vaccine compared to SD on strain-specific, heterologous HAI titer increase (B strains). The median and 89% equal-tailed credible interval (CI) of the overall effect (HD vs. SD) are shown. The numbers under each line show the sample size (HD/SD) for that specific strain or the overall effect size. 195

C.37 The impact of HD vaccine compared to SD on strain-specific heterologous seroconversion (H1N1 strains). The median and 89% equal-tailed credible interval (CI) of the overall effect (HD vs. SD) are shown. The numbers under each line show the sample size (HD/SD) for that specific strain or the overall effect size 196
C.38 The impact of HD vaccine compared to SD on strain-specific heterologous seroconversion (H3N2 strains). The median and 89% equal-tailed credible interval (CI) of the overall effect (HD vs. SD) are shown. The numbers under each line show the sample size (HD/SD) for that specific strain or the overall effect size. 197
C.39 The impact of HD vaccine compared to SD on strain-specific heterologous seroconversion (B strains). The median and 89% equal-tailed credible interval (CI) of the overall effect (HD vs. SD) are shown. The numbers under each line show the sample size (HD/SD) for that specific strain or the overall effect size. 198
C.40 The impact of HD vaccine compared to SD on strain-specific heterologous seroprotection (H1N1 strains). The median and 89% equal-tailed credible interval (CI) of the overall effect (HD vs. SD) are shown. The numbers under each line show the sample size (HD/SD) for that specific strain or the overall effect size. 199

C.41 The impact of HD vaccine compared to SD on strain-specific heterologous seroprotection (H3N2 strains). The median and 89% equal-tailed credible interval (CI) of the overall effect (HD vs. SD) are shown. The numbers under each line show the sample size (HD/SD) for that specific strain or the overall effect size. 200
C.42 The impact of HD vaccine compared to SD on strain-specific heterologous seroprotection (B strains). The median and 89% equal-tailed credible interval (CI) of the overall effect (HD vs. SD) are shown. The numbers under each line show the sample size (HD/SD) for that specific strain or the overall effect size. 201
C.43 The impact of HD vaccine compared to SD on vaccine-specific HAI responses. The median and 89% equal-tailed credible interval (CI) of the overall effect (HD vs. SD) are shown. The numbers under each line show the sample size (HD/SD) for that specific strain or the overall effect size. The top row shows homologous responses, the bottom row is heterologous. 202
C.44 The impact of HD vaccine compared to SD on strain-specific, homologous HAI titer increase. The median and 89% equal-tailed credible interval (CI) of the overall effect (HD vs. SD) are shown. The numbers under each line show the sample size (HD/SD) for that specific strain or the overall effect size. 204

C.45 The impact of HD vaccine compared to SD on strain-specific, heterologous HAI titer increase (H1N1 strains). The median and 89% equal-tailed credible interval (CI) of the overall effect (HD vs. SD) are shown. The numbers under each line show the sample size (HD/SD) for that specific strain or the overall effect size. 205
C.46 The impact of HD vaccine compared to SD on strain-specific, heterologous HAI titer increase (H3N2 strains). The median and 89% equal-tailed credible interval (CI) of the overall effect (HD vs. SD) are shown. The numbers under each line show the sample size (HD/SD) for that specific strain or the overall effect size. 206
C.47 The impact of HD vaccine compared to SD on strain-specific, heterologous HAI titer increase (B strains). The median and 89% equal-tailed credible interval (CI) of the overall effect (HD vs. SD) are shown. The numbers under each line show the sample size (HD/SD) for that specific strain or the overall effect size. 207
C.48 The impact of HD vaccine compared to SD on strain-specific heterologous seroconversion (H1N1 strains). The median and 89% equal-tailed credible interval (CI) of the overall effect (HD vs. SD) are shown. The numbers under each line show the sample size (HD/SD) for that specific strain or the overall effect size 208

C.49 The impact of HD vaccine compared to SD on strain-specific heterologous seroconversion (H3N2 strains). The median and 89% equal-tailed credible interval (CI) of the overall effect (HD vs. SD) are shown. The numbers under each line show the sample size (HD/SD) for that specific strain or the overall effect size. 209
C.50 The impact of HD vaccine compared to SD on strain-specific heterologous seroconversion (B strains). The median and 89% equal-tailed credible interval (CI) of the overall effect (HD vs. SD) are shown. The numbers under each line show the sample size (HD/SD) for that specific strain or the overall effect size. 210
C.51 The impact of HD vaccine compared to SD on strain-specific heterologous seroprotection (H1N1 strains). The median and 89% equal-tailed credible interval (CI) of the overall effect (HD vs. SD) are shown. The numbers under each line show the sample size (HD/SD) for that specific strain or the overall effect size. 211
C.52 The impact of HD vaccine compared to SD on strain-specific heterologous seroprotection (H3N2 strains). The median and 89% equal-tailed credible interval (CI) of the overall effect (HD vs. SD) are shown. The numbers under each line show the sample size (HD/SD) for that specific strain or the overall effect size. 212

C.53 The impact of HD vaccine compared to SD on strain-specific heterologous seroprotection (B strains). The median and 89% equal-tailed credible interval (CI) of the overall effect (HD vs. SD) are shown. The numbers under each line show the sample size (HD/SD) for that specific strain or the overall effect size. 213
C.54 The impact of HD vaccine compared to SD on vaccine-specific HAI responses. The median and 89% equal-tailed credible interval (CI) of the overall effect (HD vs. SD) are shown. The numbers under each line show the sample size (HD/SD) for that specific strain or the overall effect size. The top row shows homologous responses, the bottom row is heterologous. 214

LIST OF TABLES

2.1 Description of infected individuals 13

3.1 Antibody response in human challenge study (N-samples/N-patients, mean (IQR)) 30
3.2 Antibody response in human vaccination study (N-samples/N-patients, mean (IQR)), part I 31
3.3 Antibody response in human vaccination study (N-samples/N-patients, mean (IQR)), part II 31

4.1 Description of the study. 49

A.1 Modifi ed vesikari score components 90
A.2 Modifi ed vesikari score components 90
A.3 Modifi ed vesikari score components 92

C.1 The impact of gender in vaccine-specific analyses 179

CHAPTER 1

INTRODUCTION

This dissertation contains research topics related to virus infection control and prevention. Specifically, with data from norovirus trials and influenza vaccine population studies, the natural infection profiles, within host virus dynamics, the impact of inoculum dose for norovirus infections were investigated; the immunogenicity of high-dose and standard-dose influenza vaccine were studied and compared for homologous and heterologous responses.

1.1 Summary of Objectives

The primary goal of this dissertation is to explore associations between amount of virus or antigen exposure with disease and immunological responses. Research focuses were given to the pathogens of norovirus and influenza. Totally, there were three questions. First, what is the impact of norovirus inoculum dose on infection outcomes. Second, how homologous and heterologous responses of Fluzone high-dose vaccine different from the standard-dose vaccine. Third, the comparison of associated antibody decay half-life time between real infections and a novel bivalent norovirus vaccine candidate.

1.1.1 Chapter 2

Norovirus leads to millions of hospitalizations and hundreds of thousands of deaths globally (Bartsch et al., 2016; Lozano et al., 2012; Patel et al., 2008). A better understanding of the role dose might have on important quantities such as shedding and symptoms can provide useful information for better outbreak control.

In general, the amount of virus an individual is exposed to plays an important role in the probability of infection with norovirus. However, the possible impact of dose on the course of an infection, given that infection occurred, is relatively unclear.

With data from a human norovirus challenge study, we performed a secondary analysis using Bayesian mixed effects models. We found higher levels of norovirus infection dose were associated with more rapid shedding and symptom onset and increased symptom severity.

1.1.2 Chapter 3

Norovirus is a public health threat. Its high transmissibility (Atmar et al., 2008; Atmar et al., 2014) along with lack of norovirus-specific treatments and the vaccine is contributing its heavy health burden on populations (Atmar et al., 2011; Bitler et al., 2013; Carling et al., 2009; Isakbaeva et al., 2005; Johnston et al., 2007; Scallan et al., 2011; Wikswo et al., 2011).

Infections may provide immunity for future infections (Cannon et al., 2019), and vaccines are possible to mimic that (Bhurani et al., 2018). With data from a human norovirus challenge study and a vaccine candidate study, we performed a secondary analysis of kinetics of serum antibodies.

1.1.3 Chapter 4

Influenza vaccines are widely used to protect humans from influenza infections. However, the average effectiveness is only around 50% (Centers for Disease Control and Prevention, 2021).

The high-dose (HD) Fluzone influenza vaccine is provided to the elderly population because the standard-dose (SD) version had low immunogenicity and protective effect. Although increased dose may lead to improved immunogenicity (Couch et al., 2007; Hilleman, 1958), the role of vaccine dose toward induction of heterologous immunity (against other strains) is not well understood.

With data from human volunteers vaccinated with either the SD or HD Fluzone vaccine during influenza seasons spanning the years 2014-2018, we performed a secondary analysis using Bayesian hierarchical models. We found that the HD vaccine led to overall improvement for both homologous and heterologous immunity. Some exceptions were noted for heterologous immunity, where the increased dose led to reduced immunogenicity.

CHAPTER 2

ANALYZING THE ASSOCIATION BETWEEN INOCULUM DOSE AND NOROVIRUS INFECTION OUTCOMES

[1]

[1] Yang Ge, W. Zane Billings, Juan Leon, Katia Koelle, Antone R. Opekun, Mary K. Estes, David Y. Graham, Robert L. Atmar, Benjamin A. Lopman, Andreas Handel. To be submitted to *The Journal of Infectious Diseases*

2.1 Abstract

Background The amount of virus an individual is exposed to plays an important role in the probability of infection with norovirus. However, the possible impact of dose on the course of an infection, given that infection occurred, is less understood. A better understanding of the role dose might have on important quantities such as shedding and symptoms can provide useful information for better outbreak control.

Methods We performed a secondary analysis of data from a human norovirus challenge study in which individuals were infected with different doses of virus. Using Bayesian mixed effects models, we report posterior means and 89% equal-tailed credible intervals of the associations between dose and several shedding and infection severity outcomes.

Results As the dose increased from 4.8 to 4800 reverse transcription-polymerase chain reaction (RT-PCR) units, average fecal virus shedding onset time decreased from 1.4 to 0.8 days and day of virus peak decreased from 2.3 to 1.5 days. In contrast, duration and total amount of virus shedding did not show a noticeable association with dose. The incubation period decreased from 1.5 to 0.8 days as dose increased. Two different symptom scores (modified Modified Vesikari and comprehensive score) increased from 4.1 and 9.4 in the low dose group, to 5.1 and 17.5 in the high dose group, respectively.

Conclusions Higher levels of norovirus infection dose were associated with more rapid shedding and symptom onset and increased symptom severity. However, there was little association between dose and duration or amount of virus shedding in either feces or vomit.

2.2 Introduction

Every year, norovirus leads to millions of hospitalizations and hundreds of thousands of deaths globally (Bartsch et al., 2016; Lozano et al., 2012; Patel et al., 2008). In the USA, norovirus is a predominant cause of food-borne disease responsible for more than 20 million gastroenteritis cases annually (Scallan et al., 2011). Norovirus is highly infectious (Atmar et al., 2008; Atmar et al., 2014). Norovirus-specific treatments are unavailable to patients, and the vaccine for vulnerable populations is developing (Atmar et al., 2011; Scallan et al., 2011). Aggressive infection-control measures are needed to reduce disease burden (Bitler et al., 2013; Carling et al., 2009; Isakbaeva et al., 2005; Johnston et al., 2007; Wikswo et al., 2011).

As is generally the case for any infectious agent, an increase in norovirus exposure dose tends to increase the infection risk (P. F. Teunis et al., 2008). Therefore, infection control measures that reduce virus exposure levels can decrease infection risk. Less is known about the possible impact of dose on disease outcome, given that infection has occurred. Some evidence suggests that dose is associated with increased illness (Atmar et al., 2008; Atmar et al., 2014). To better understand the impact of dose on virus shedding and symptom severity, we performed a secondary analysis of data from a human norovirus challenge study (Atmar et al., 2011). We found that while severity of symptoms increases with dose, and onset of shedding and disease is more rapid, the total amount of shedding does not change noticeably.

2.3 Methods

The following sections provide brief descriptions of our methodology. Full modeling and analysis details, including all data and code needed to reproduce our results, are provided in the supplement.

2.3.1 Data

The data came from a human challenge study, which has been described in detail previously (Ajami et al., 2012; Atmar et al., 2008; Atmar et al., 2014; Czakó et al., 2012; Kavanagh et al., 2011). In the study, investigators randomly gave either placebo or norovirus (GI.1 NV) at 4 different doses (0.48, 4.8, 48, or 4800 RT-PCR units) to 57 healthy individuals (18 to 50 years of age). A total of 21 individuals were infected. One infected individual was lost to follow-up and thus excluded from our analysis. Only a single individual in the 0.48 unit dose group became infected. We thus removed that dose from our main analysis (N = 19). We conducted a sensitivity analysis including this individual, shown in the supplementary material.

All individuals stayed in the research center for at least four days (96 hours), and were followed up for at least five additional weeks (Atmar et al., 2008. The maximum follow-up was 91 days. The study collected samples of feces and vomit and measured clinical symptoms. As appropriate, for some of our analyses presented below, we focused on the 96 hours during which individuals were under clinical observation. For other analyses we included the full time-series, including data collected after individuals returned home. We state which data are used for each analysis.

2.3.2 Overall analysis approach and Implementation

Since this is a secondary data analysis, a strict hypothesis-testing framework using p-values is not suitable. We therefore decided to perform all analyses in a Bayesian framework. We report all our model results as posterior mean. To minimize the urge of readers to think about statistical significance or mis-interpret our reported uncertainty levels as confidence intervals, we report 89% (instead of 95%) equal-tailed credible intervals (McElreath, 2020). All analyses were completed using R (Team, 2017 and the brms package (Burkner, 2017).

For all analyses, we used Bayesian mixed effects models. For the results shown in the main text, we treated the dose as a continuous variable. In a sensitivity analysis, we repeated the fitting but treated dose as a categorical variable (supplementary materials). Detailed method descriptions, sensitivity analyses, and all data and code required to reproduce the results are provided in the supplementary materials.

2.3.3 Virus shedding

Virus shedding concentration in samples was measured by either an immunomagnetic capture (IMC) RT-PCR assay that provided a qualitative readout (positive or negative) or real-time quantitative RT-PCR (qRT-PCR), which provided a quantitative readout in genomic equivalent copies (GEC) (Atmar et al., 2008. These two methods had limits of detection at $<$ 15,000 GEC (termed LOD1 in the following) and $<$ 40,000,000 GEC (termed LOD2 in the following), respectively. Therefore, the virus shedding concentration could be between zero and LOD1 (negative IMC, negative qRT-PCR), between LOD1 and LOD2 (positive IMC, negative qRT-PCR), or a quantitative measurement above LOD2 (positive qRT-PCR). Vomit shed-

ding data was reported similarly, with either a numeric value, or a positive or negative readout. We accounted for this censored data structure in our models (see supplement for details).

The total virus contained in each sample was obtained by multiplying virus concentration with sample weight for feces (i.e., GEC/g * weight of feces) or sample volume for vomit (i.e., GEC/ml * volume of vomit). We calculated each participant's total amount of virus shedding in feces and vomit by summing up virus shedding in all samples per participant. We assessed associations between inoculum dose and total amount of virus shedding using Bayesian linear mixed effects models.

As an alternative approach to the analysis of the total amount of shedding, we modeled the longitudinal time-series of virus concentration in feces using a previously developed equation that has been shown to describe trajectories of acute viral infections well (Holder and Beauchemin, 2011; Li and Handel, 2014). We fitted the trajectories with a Bayesian non-linear mixed effects model. We sampled from the posterior distribution to obtain predicted trajectories of virus concentration kinetics. From these time-series, we computed several summary quantities, namely 1) virus shedding onset (time at which the trajectory crossed the lower limit of detection, LOD1); 2) time to peak virus shedding; 3) shedding duration, defined as the total amount of time at which virus concentration was above LOD1; and 4) total amount of virus shed, defined as area under the virus concentration curve.

Vomiting episodes were too few to allow for a time-series analysis similar to the one we performed for virus shedding in feces (see supplementary material for vomit event time-series data).

2.3.4 Symptoms

The study reported the following symptoms: body temperature, malaise, muscle aches, headache, nausea, chills, anorexia, cramps, unformed or liquid feces, and vomiting. Clinical symptoms (except feces and vomit) were reported as none, mild, moderate, or severe, which we coded as a score of 0 to 3. For feces, we used a scoring of solid = 0, unformed = 1 and liquid = 2. Vomit was reported as absent or present and scored as 0 or 1.

As outcomes of interest, we considered time to onset of symptoms (incubation period) and two versions of overall symptom scores. We defined onset of symptoms as the time between inoculation and the first reported symptom of any type. For the first overall symptom score, we used a modified Vesikari score (MVS) that was previously applied to measure norovirus severity (Atmar et al., 2011; Bierhoff et al., 2018; Freedman et al., 2010; Ruuska and Vesikari, 1990; Shim et al., 2016. The MVS is a clinical outcome measurement that focuses on fever, diarrhea, vomiting, doctor visit and treatment. For our study setup, doctor visit was not applicable, we thus removed it from the score, as done previously (Atmar et al., 2011). Since we did not have information on treatment, we also dropped that component.

For a second score, which we named the comprehensive symptom score (CSS), we looked at all symptoms that were reported. For each symptom, we recorded the highest value that was reported per day. These daily highest scores for each symptom were added up to produce a daily comprehensive symptom score. Those daily scores were then added again for a score covering the first four days (96 hours).

We assessed associations between dose and these symptom-related outcomes using Bayesian generalized linear mixed effects models. Details of score computation, scores for each individual, and model details are given in the supplement.

2.3.5 Sensitivity analyses

We performed two sensitivity analyses. In one analysis, we treated dose as categorical instead of as continuous. In the other analysis, we included an additional infected individual, the only individual who became infected after exposure to a dose of 0.48 RT-PCR units. Results from these sensitivity analyses show the same overall patterns as those shown in the main text, and are reported in the supplementary material.

2.4 Results

2.4.1 Data description

The overall dataset has been described in detail previously (Ajami et al., 2012; Atmar et al., 2008; Atmar et al., 2014; Czakó et al., 2012; Kavanagh et al., 2011. Of the 19 infected individuals included in the main analyses, 6, 7, and 6 individuals received norovirus doses of 4.8, 48, and 4800 RT-PCR units respectively. Age, sex, and ABO blood groups were generally similar across dose groups (Table 2.1).

Table 2.1: Description of infected individuals

Characteristics	Level	Dose 4.8 RT-PCR Units	Dose 48 RT-PCR Units	Dose 4800 RT-PCR Units
Sample size (N)		6	7	6
Age (Median, IQR)		29.50 [25.50, 34.25]	24.00 [23.00, 32.50]	27.50 [23.75, 29.00]
Sex (N, %)	Female	2 (33.3)	4 (57.1)	2 (33.3)
	Male	4 (66.7)	3 (42.9)	4 (66.7)
Blood Group (N, %)	A	2 (33.3)	2 (28.6)	3 (50.0)
	O	4 (66.7)	5 (71.4)	3 (50.0)

2.4.2 Assessing association of total virus shedding with dose

Total virus shedding in either feces or vomit was computed by summing values of all samples for each individual. Every infected individual shed virus in feces, but only a few individuals vomited in each dose group. Neither virus shedding in feces nor vomit showed any noticeable trend with dose (Figure 2.1).

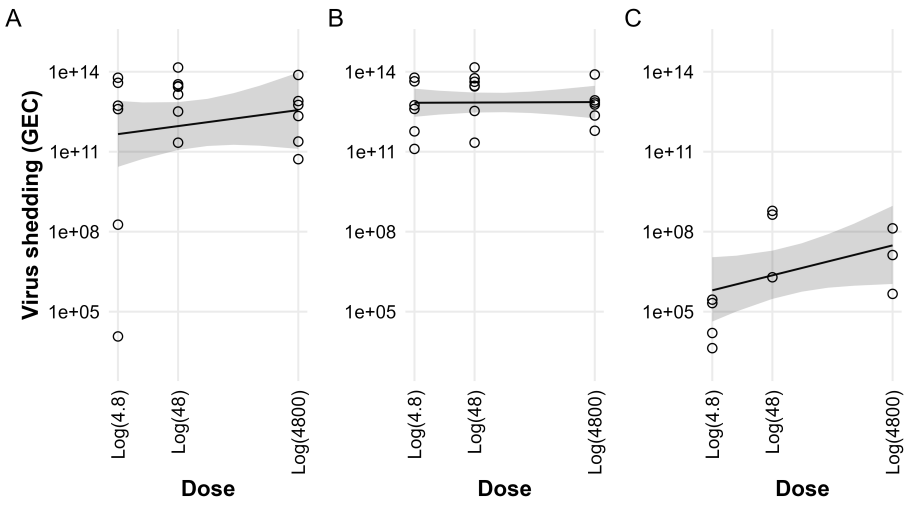

Figure 2.1: Virus shedding in feces or vomit. The straight lines and shaded regions indicate the mean and 89% credible intervals of the fitted Bayesian model. Points with circle shape are raw data. A) Cumulative virus shedding in feces during the first 96 hours. B) Cumulative virus shedding in feces during the full observation period (up to 91 days). C) Cumulative virus shedding in vomit. Only a few of the infected individuals had vomiting episodes, all within the first 96 hours.

2.4.3 Modeling of virus concentration in feces

The longitudinal virus shedding data in feces and fitted model results are shown in Figure 2.2 for each individual, and the population-level curves per dose group are shown in Figure 2.3. Figure 2.4 shows the model-predicted relationship between dose and 1) time at which virus became detectable, 2) time of virus peak, 3) shedding duration, and 4) total amount of virus shed. As the dose increased from 4.8 to 4800 RT-PCR units, average onset time decreased from 1.4 (89%CI, 1.2 - 1.7) to 0.8 (89%CI, 0.6 - 1) days; and the time of virus peak decreased from 2.3 (89%CI, 2 - 2.6) to 1.5 (89%CI, 1.3 - 1.8) days. There was a slight trend toward increasing duration of shedding, and no noticeable trend for the total virus load.

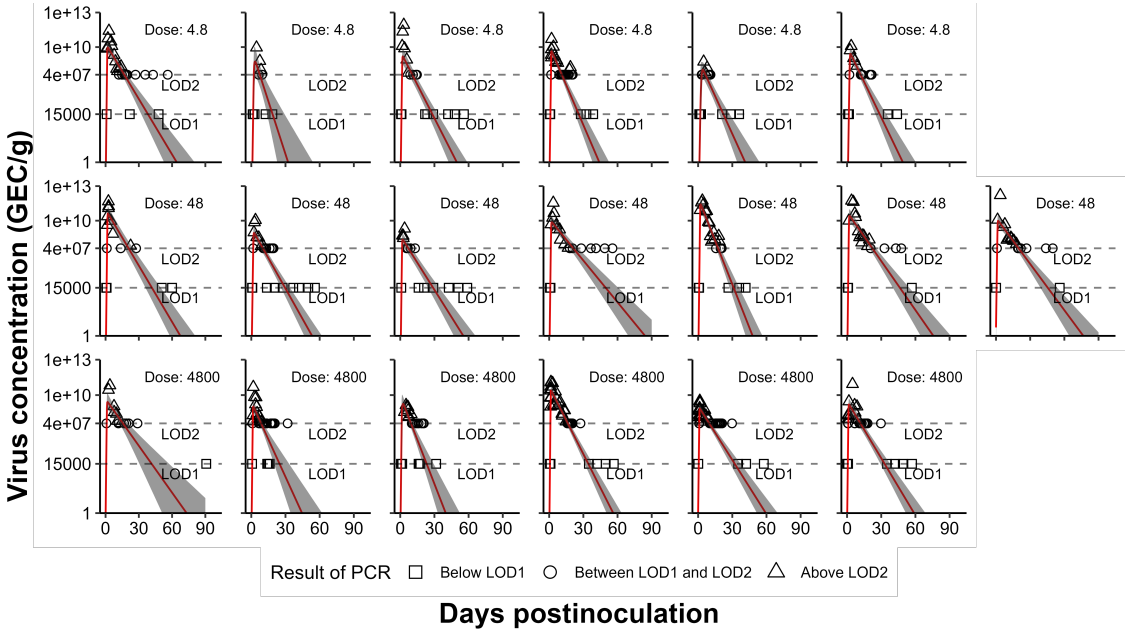

Figure 2.2: Fitted fecal virus concentration curves. The red lines show mean of estimations. The grey areas show 89% equal-tailed credible interval (CI). LOD1 and LOD2 indicate the two limits of detection. Points with triangle shape represented samples that are positive qRT-PCR. Points with circle shape represented samples that are positive IMC and negative qRT-PCR. Points with square shape represented samples that are negative IMC and negative qRT-PCR.

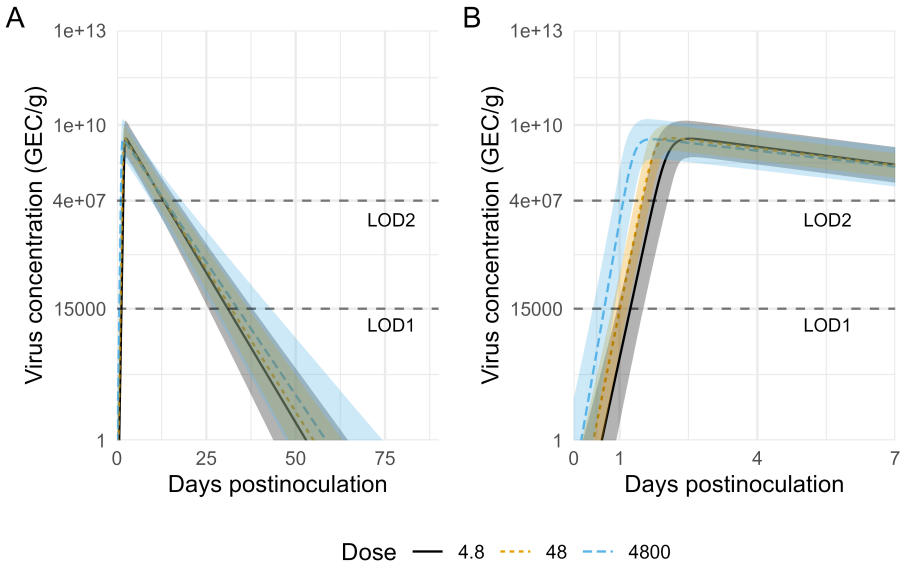

Figure 2.3: Fitted virus concentration (GEC/g) in feces. The lines show mean of estimations. The colored areas show 89% equal-tailed credible interval (CI). A) The fitted curves for 90 days. B) The fitted curves for the first 7 days.

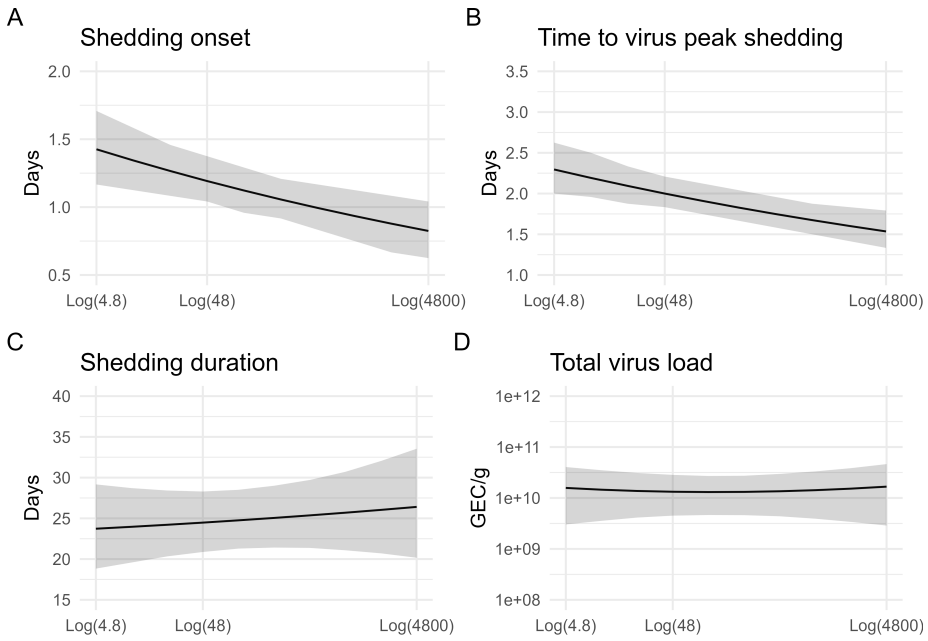

Figure 2.4: Model predictions for viral kinetics as a function of inoculum dose. The lines show mean of estimations. The colored areas show 89% equal-tailed credible interval (CI). A) Shedding onset (time at which virus load reaches LOD1). B) Time to virus peak shedding. C) Shedding duration (amount of time where virus load was above LOD1). D) Total virus load (area under virus concentration curve).

2.4.4 Assessing association of symptoms with dose

An increase in dose led to an earlier symptom onset and higher symptom scores, which was more noticeable for the comprehensive symptom score (2.5). The incubation period decreased from 1.5 (89%CI, 1 - 2.3) to 0.8 (89%CI, 0.5 - 1.2) days as dose increased. Two different symptom scores (modified Vesikari and comprehensive score) increased from 4.1 (89%CI, 2.7 - 5.8) and 9.4 (89%CI, 6.7 - 12.6) in the 4.8 RT-PCR unit dose group, to 5.1 (89%CI, 3.1 - 7.4) and 17.5 (89%CI, 12.2 - 23.9) respectively in the 4800 RT-PCR unit dose group.

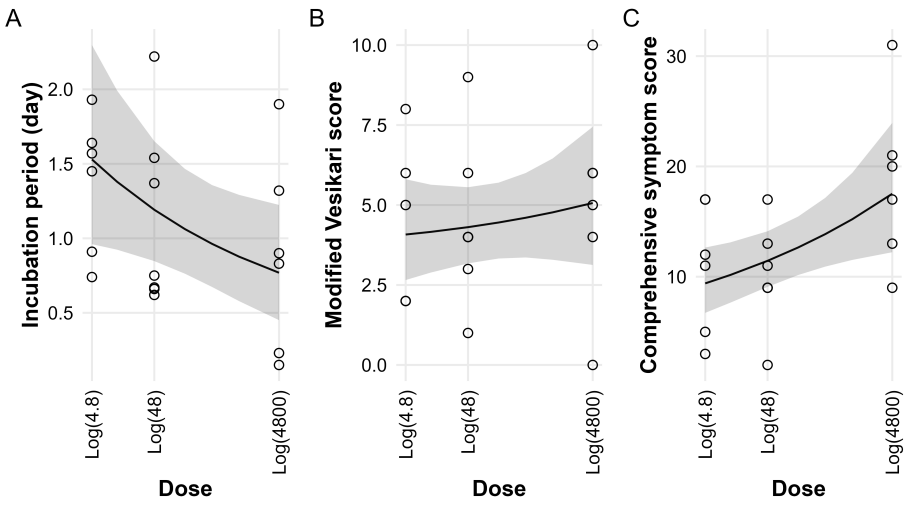

Figure 2.5: Association between dose and symptom scores. The lines show mean of estimations. The colored areas show 89% equal-tailed credible interval (CI). Points with circle shape are raw data. A) Incubation period, i.e., time between infection and onset of first symptoms. B) Severity using the modified Vesikari score. C) Severity using the comprehensive symptom score.

2.5 Discussion

Our analyses allowed us to explore the impact of norovirus inoculum dose on disease outcomes after infection, an important gap in the existing literature. We found that while increases in dose were associated with a faster onset and peak of virus shedding in feces (Figure 2.4 A and B), the total shedding duration and total amount of virus shedding showed little association (Figure 2.1 and Figure 2.4 C and D). Our analysis also showed a general pattern of accelerated onset of symptoms and increased symptom severity with higher inoculum dose (Figure 2.5).

While our study provides important insights into the role of dose for norovirus infections, there are clear limitations. First, the sample size is small. Second, this is a secondary data analysis, which means that the findings here are exploratory and need further confirmation, ideally using larger sample sizes. Larger sample sizes might also allow for stratification based on host characteristics, which could yield information regarding possible interactions between host characteristics and dose-outcome relationships.

If our findings hold, they suggest that inoculum dose has little impact on shedding (and thus transmission potential). Thus, while infection control measures that reduce the exposure levels can lower infection risk, those measures may have little impact on virus shedding after infection occurs.

However, dose seems to be associated with disease severity. This finding might help explain the mechanisms of several recent norovirus vaccine candidates. These vaccines have shown limited effectiveness at reducing infection, but do seem to reduce disease outcomes Atmar et al., 2011; Bernstein et al., 2015. Perhaps protection induced by current vaccine can-

didates (assumed to be mainly mediated by antibodies) is not enough to provide sterilizing immunity and thus prevent infection Handel et al., 2018 but can reduce the effective dose that starts an infection, and thus reduce symptoms – consistent with our findings here.

To summarize, our results suggest that norovirus infection dose seems clinically important but does not seem to have an epidemiological impact on transmission potential.

2.6 Acknowledgements

This work was partially supported by NIH grant R01 GM124280.

CHAPTER 3

NOROVIRUS ANTIBODY KINETICS COMPARISONS BETWEEN INFECTION AND VACCINATION

[2]

[2] Yang Ge, W. Zane Billings, Juan Leon, Katia Koelle, Benjamin A. Lopman, Andreas Handel. To be submitted to *The Journal of Infectious Diseases*

3.1 Abstract

Background Norovirus is a public health threat, causing innumerable hospitalizations and deaths. To assist the ongoing norovirus vaccine developments, we analyzed the dose-dependent kinetics of norovirus antibodies acquired from infection and vaccination.

Methods We collected antibodies' kinetics data from a human challenge study and a multisite randomized bivalent norovirus candidate vaccine study. In both studies, norovirus-specific immunoglobulin G (IgG) and immunoglobulin A (IgA), and histoblood group antigen (HBGA) blocking antibodies were measured. We used Bayesian mixed-effect models to study potential exponential and power-law decay patterns.

Results In the human challenge study, 19 individuals got infection. As the dose increased from 4.8 to 4800 RT-PCR units, the peak level of GI.1 HBGA titer decreased from 2380.7 to 620.5; the peak level of GI.1 IgA value decreased from 291.4 to 199.3 ug/ml; the peak level of GI.1 IgG value decreased from 859.3 to 395.1 ug/ml. For the half-life time, as the dose increased from 4.8 to 4800 RT-PCR units, GI.1 HBGA changed from 108.6 to 185.9 days; GI.1 IgA changed from 63.1 to 59.6 days; GI.1 IgG changed from 81.9 to 102.6 days. In the HV study, as the dose increased from 5-5 mcg to 150-150 mcg, the peak level of GI.1 HBGA titer decreased from 4635.7 to 720.6; the peak level of GI.1 IgA value decreased from 1342.2 to 10505.5 ug/ml; the peak level of GI.1 IgG value decreased from 525.1 to 5268.8 ug/ml; the peak level of GII.4 IgA value decreased from 536.3 to 50.2 ug/ml; the peak level of GII.4 IgG value decreased from 121.3 to 41.7 ug/ml. For the half-life time, as the dose increased from 5-5 mcg to 150-150 mcg, GI.1 HBGA changed from 11.5 to 33.3 days; GI.1 IgA changed from 11.5 to 3.5 days; GI.1 IgG changed from 26.8 to 16

days; GII.4 IgA changed from 13.6 to 111.7 days; GII.4 IgG changed from 222.3 to 356.6 days.

Conclusions We found a higher dose of antigen does not necessarily lead to a stronger and long-lasting immune response.

3.2 Introduction

Norovirus is a public health threat, causing innumerable hospitalizations and deaths globally every year (Bartsch et al., 2016; Lozano et al., 2012; Patel et al., 2008; Scallan et al., 2011). The high transmissibility (Atmar et al., 2008; Atmar et al., 2014), along with the lack of norovirus-specific treatments and the vaccine, is contributing to its heavy health burden on populations (Atmar et al., 2011; Bitler et al., 2013; Carling et al., 2009; Isakbaeva et al., 2005; Johnston et al., 2007; Scallan et al., 2011; Wikswo et al., 2011). Following the success of the rotavirus vaccine, norovirus vaccines are in development (Bucardo et al., 2014; O'Ryan, 2017; Scallan et al., 2011).

Human norovirus has three genogroups, I, II, and IV (GI, GII and GIV) (Glass et al., 2009). The GII.4 genotype caused the majority of human diseases, but other genotypes are also important (Hoa Tran et al., 2013; Vega et al., 2014). Therefore, a bivalent vaccine could provide much more benefits.

Norovirus infections may provide immunity for future infections (Cannon et al., 2019), and vaccines are possible to mimic that (Bhurani et al., 2018). Studies suggest that protection of infection may correlate with blocking antibodies (serum antibodies inhibiting norovirus virus-like particles binding to H type 1 or H type 3 synthetic carbohydrates), but not necessary with Immunoglobulin A and G (IgA, IgG) antibodies (Atmar and Estes, 2012; Johnson et al., 1990; Reeck et al., 2010).

To assist the ongoing norovirus vaccine developments, we collected serologic antibody data from two studies. One is a norovirus infections study, and the other is a norovirus candidate vaccine study. We analyzed

the dose impact of antigen on the kinetics of antibodies and the half-life time. The purpose of this study is to explore the dose-dependent kinetics of norovirus antibodies of these two ways of acquired immunity.

3.3 Methods

The following sections provide brief descriptions of our methodology. Full modeling and analysis details, including all data and code needed to reproduce our results, are provided in the supplement.

3.3.1 Study design

We collected antibodies' kinetics data from two studies. The first study is a human challenge study (ClinicalTrials.gov, NCT00138476) (Ajami et al., 2012; Atmar et al., 2008; Atmar et al., 2014; Czakó et al., 2012; Kavanagh et al., 2011; Reeck et al., 2010), which we named HC (human challenge study). In the HC study, 19 participants got infected with norovirus (GI.1 NV) who randomly received inoculum norovirus dose from one level of GI.1 NV, 0.48, 4.8, 48, 4800 reverse transcription-polymerase chain reaction (RT-PCR) units. We dropped data from the 0.48 RT-PCR dose group because only one sample size was available.

The second study is a multisite randomized bivalent norovirus candidate vaccine study (ClinialTrials.gov: NCT01168401) (Ramani et al., 2017; Treanor et al., 2014), which we named HV (human vaccination study). In the HV study, researchers prepared a bivalent virus-like particles (VLPs) vaccine candidate with genotype GI.1 and GII.4 noroviruses components with a dose-escalation design (5 ug, 15 ug, 50 ug, or 150 ug of each of the 2 VLP components) and randomly gave one dose to 39 participants twice (28 days apart).

For each study, blood samples were collected at different days for measurements of norovirus-specific immunoglobulin G (IgG), immunoglobulin A (IgA), and histoblood group antigen (HBGA) blocking antibodies

(Kavanagh et al., 2011; Reeck et al., 2010; P. F. M. Teunis et al., 2016). In the HC study, samples were taken on day 0, 2nd, 7th, 13th to 15th, 27th to 32th, and 163th to 188th. In the HV study, the samples were taken on day 0 (pre-vaccination), 7th, 21th, 28th, 35th, 56th, 180th, 393th post-vaccination.

In addition to the different sampling times, more importantly, study designs are also different. In the HC study, norovirus was given once at the beginning of the study. In the HV study, the candidate norovirus vaccine was given twice at day 0th and 28th.

We aimed to study the decay of antibodies based on the observed kinetics, and then compare the half-life time between norovirus infection and vaccines across different dose groups.

3.3.2 Immunological decay

In general, antibody decay can be measured by exponential and power-law models (Cohen et al., 2021; de Graaf et al., 2014; P. F. M. Teunis et al., 2016). Both models introduce explicit mathematical expressions for the kinetics of antibodies while preserving biological meaning (P. F. M. Teunis et al., 2016). The exponential models use the idea of a fixed decay rate to measure the average speed of waning immunity (de Graaf et al., 2014). However, heterogeneous antibody decay is possible (Cohen et al., 2021). Thus, the power-law model with a time dependent decay rate has been proposed (P. F. M. Teunis et al., 2016). power-law models produce better fitting results in several studies (Cohen et al., 2021; Zarnitsyna et al., 2021). In our study, we implemented both models and compared them with ELPD-WAIC (Vehtari et al., 2017).

We used Bayesian mixed-effect models to fit both models. We firstly computed the peak level of antibodies, and then further measured the half-life time after the peak. All results were summarized by mean and 89% Equal-tailed credible intervals (ETI). All analyses were completed using R (Team, 2017). We used brms package (Burkner, 2017) for the Bayesian multilevel analyses. Detailed method descriptions, and code required to reproduce the results are given in the supplementary materials.

3.4 Results

3.4.1 Data description

In the HC study, 19 infected individuals included in the main analyses, 6, 7, and 6 individuals received norovirus doses of 4.8, 48, and 4800 RT-PCR units, respectively. Data description was presented in Table 3.1. In the HV study, 39 individuals received candidate vaccines (Table 3.2 to 3.3).

Table 3.1: Antibody response in human challenge study (N-samples/N-patients, mean (IQR))

Antibody	Dose-group	Day 0	Day 2	Day 7	Day 13 - 15	Day 27 - 32	Day 163 - 188
GI.1 HBGA	RT-PCR 4.8	6/6, 152, (12,183)	N/A	N/A	6/6, 4562, (488,7444)	6/6, 4273, (588,3410)	6/6, 1578, (263,623)
	RT-PCR 48	7/7, 57, (12,82)	N/A	N/A	7/7, 2833, (444,1726)	7/7, 3609, (542,2064)	7/7, 1559, (366,818)
	RT-PCR 4800	6/6, 101, (12,61)	N/A	N/A	6/6, 850, (260,886)	6/6, 1113, (468,994)	6/6, 588, (406,676)
GI.1 IgA	RT-PCR 4.8	6/6, 9, (1,7)	6/6, 9, (1,8)	6/6, 33, (14,52)	6/6, 577, (276,754)	6/6, 292, (69,514)	6/6, 39, (9,38)
	RT-PCR 48	7/7, 8, (1,10)	7/7, 8, (1,9)	7/7, 56, (32,74)	7/7, 1153, (379,1645)	7/7, 330, (86,407)	7/7, 26, (9,29)
	RT-PCR 4800	6/6, 7, (1,1)	6/6, 7, (1,2)	6/6, 30, (9,39)	6/6, 288, (187,401)	6/6, 160, (111,220)	6/6, 18, (6,26)
GI.1 IgG	RT-PCR 4.8	6/6, 29, (4,41)	6/6, 26, (3,34)	6/6, 41, (22,56)	6/6, 756, (443,1108)	6/6, 1061, (430,1808)	6/6, 137, (81,202)
	RT-PCR 48	7/7, 18, (7,27)	7/7, 17, (6,24)	7/7, 41, (32,46)	7/7, 751, (432,1113)	7/7, 1082, (550,1255)	7/7, 185, (98,159)
	RT-PCR 4800	6/6, 14, (2,19)	6/6, 13, (2,17)	6/6, 23, (12,28)	6/6, 297, (130,338)	6/6, 412, (232,426)	6/6, 87, (59,102)

Table 3.2: Antibody response in human vaccination study (N-samples/N-patients, mean (IQR)), part I

Antibody	Dose-group	Day: 0	Day: 7	Day: 21	Day: 28
GI.1 HBGA	5-5mcg	20/10, 41, (12,46)	10/10, 1110, (570,1647)	10/10, 879, (605,979)	9/9, 670, (566,846)
	15-15mcg	19/10, 31, (12,33)	10/10, 879, (542,1325)	10/10, 853, (393,1021)	10/10, 600, (332,788)
	50-50mcg	19/10, 32, (12,21)	10/10, 993, (255,1655)	10/10, 665, (235,1093)	10/10, 512, (202,713)
	150-150mcg	17/9, 17, (12,12)	9/9, 401, (198,450)	9/9, 344, (185,409)	9/9, 286, (154,360)
GII.4 HBGA	5-5mcg	10/10, 59, (12,74)	10/10, 299, (123,390)	10/10, 306, (154,387)	9/9, 242, (103,332)
	15-15mcg	10/10, 32, (12,47)	10/10, 503, (145,299)	10/10, 294, (103,265)	10/10, 234, (82,200)
	50-50mcg	10/10, 49, (12,78)	10/10, 766, (354,746)	10/10, 454, (261,546)	10/10, 304, (173,326)
	150-150mcg	9/9, 95, (25,113)	9/9, 892, (369,1331)	9/9, 460, (274,671)	9/9, 353, (181,437)
GI.1 IgA	5-5mcg	20/10, 14, (3,6)	10/10, 226, (134,307)	10/10, 222, (99,163)	9/9, 214, (78,223)
	15-15mcg	19/10, 4, (3,5)	10/10, 492, (130,640)	10/10, 229, (100,164)	10/10, 159, (53,129)
	50-50mcg	19/10, 6, (3,3)	10/10, 1331, (239,1339)	10/10, 592, (120,958)	10/10, 414, (80,765)
	150-150mcg	17/9, 6, (3,3)	9/9, 1179, (93,1214)	9/9, 582, (125,565)	9/9, 294, (86,289)
GII.4 IgA	5-5mcg	20/10, 25, (4,22)	10/10, 157, (126,179)	10/10, 116, (106,127)	9/9, 125, (103,138)
	15-15mcg	19/10, 12, (3,15)	10/10, 246, (60,244)	10/10, 125, (34,182)	10/10, 78, (21,144)
	50-50mcg	19/10, 15, (3,3)	10/10, 92, (25,149)	10/10, 64, (4,108)	10/10, 44, (3,66)
	150-150mcg	17/9, 12, (3,13)	9/9, 51, (35,63)	9/9, 28, (15,43)	9/9, 21, (9,31)
GI.1 IgG	5-5mcg	20/10, 29, (2,21)	10/10, 282, (77,387)	10/10, 326, (117,471)	9/9, 330, (157,440)
	15-15mcg	19/10, 13, (2,19)	10/10, 254, (85,346)	10/10, 204, (75,300)	10/10, 175, (69,263)
	50-50mcg	19/10, 30, (4,31)	10/10, 2516, (1253,3250)	10/10, 1695, (1060,2625)	10/10, 1443, (686,2090)
	150-150mcg	17/9, 22, (2,24)	9/9, 1804, (233,2545)	9/9, 1580, (449,2500)	9/9, 1088, (378,1975)
GII.4 IgG	5-5mcg	20/10, 47, (10,51)	10/10, 122, (57,116)	10/10, 187, (64,337)	9/9, 191, (64,276)
	15-15mcg	19/10, 26, (5,52)	10/10, 158, (67,255)	10/10, 153, (67,253)	10/10, 129, (58,147)
	50-50mcg	19/10, 12, (2,12)	10/10, 47, (38,58)	10/10, 39, (28,53)	10/10, 35, (27,46)
	150-150mcg	17/9, 22, (4,29)	9/9, 41, (38,60)	9/9, 43, (40,50)	9/9, 40, (34,47)

Table 3.3: Antibody response in human vaccination study (N-samples/N-patients, mean (IQR)), part II

Antibody	Dose-group	Day: 35	Day: 56	Day: 180	Day: 393
GI.1 HBGA	5-5mcg	10/9, 621, (376,737)	18/9, 481, (322,635)	9/9, 196, (93,298)	7/7, 136, (82,171)
	15-15mcg	9/9, 637, (361,911)	18/9, 353, (180,386)	9/9, 232, (79,303)	9/9, 164, (48,186)
	50-50mcg	10/10, 426, (182,660)	18/9, 345, (120,523)	9/9, 168, (65,185)	8/8, 115, (56,151)
	150-150mcg	8/8, 351, (185,483)	16/8, 389, (260,441)	8/8, 187, (123,231)	7/7, 111, (67,150)
GII.4 HBGA	5-5mcg	9/9, 229, (120,268)	9/9, 268, (149,200)	N/A	N/A
	15-15mcg	9/9, 211, (94,176)	9/9, 142, (86,177)	N/A	N/A
	50-50mcg	10/10, 332, (162,395)	9/9, 181, (96,225)	N/A	N/A
	150-150mcg	8/8, 322, (154,344)	8/8, 225, (152,224)	N/A	N/A
GI.1 IgA	5-5mcg	10/9, 192, (47,252)	18/9, 129, (26,93)	9/9, 32, (6,26)	7/7, 37, (8,46)
	15-15mcg	9/9, 145, (58,113)	18/9, 67, (13,67)	9/9, 15, (9,20)	9/9, 13, (9,17)
	50-50mcg	10/10, 222, (77,322)	18/9, 67, (12,106)	9/9, 13, (8,13)	8/8, 9, (7,13)
	150-150mcg	8/8, 234, (82,306)	16/8, 102, (15,68)	8/8, 27, (8,35)	7/7, 25, (7,29)
GII.4 IgA	5-5mcg	10/9, 102, (57,131)	18/9, 83, (47,116)	9/9, 31, (9,45)	7/7, 19, (6,32)
	15-15mcg	9/9, 94, (29,171)	18/9, 56, (16,85)	9/9, 22, (8,28)	9/9, 17, (3,24)
	50-50mcg	10/10, 37, (4,43)	18/9, 33, (9,41)	9/9, 18, (3,19)	8/8, 16, (3,15)
	150-150mcg	8/8, 30, (16,42)	16/8, 23, (13,35)	8/8, 18, (10,23)	7/7, 19, (10,28)
GI.1 IgG	5-5mcg	10/9, 292, (77,498)	18/9, 237, (68,358)	9/9, 57, (24,65)	7/7, 64, (27,105)
	15-15mcg	9/9, 185, (72,311)	18/9, 146, (66,201)	9/9, 70, (47,84)	9/9, 56, (44,69)
	50-50mcg	10/10, 998, (571,1064)	18/9, 505, (89,700)	9/9, 62, (24,86)	8/8, 36, (21,39)
	150-150mcg	8/8, 1159, (633,1765)	16/8, 534, (125,508)	8/8, 81, (71,99)	7/7, 57, (24,80)
GII.4 IgG	5-5mcg	10/9, 162, (69,249)	18/9, 156, (60,161)	9/9, 56, (33,61)	7/7, 46, (14,72)
	15-15mcg	9/9, 141, (67,132)	18/9, 99, (59,113)	9/9, 46, (26,60)	9/9, 52, (38,77)
	50-50mcg	10/10, 36, (29,41)	18/9, 52, (28,52)	9/9, 31, (7,31)	8/8, 17, (8,28)
	150-150mcg	8/8, 43, (33,49)	16/8, 46, (28,57)	8/8, 27, (11,19)	7/7, 31, (15,48)

3.4.2 Kinetics of serum antibodies

Antibody results of the longitudinal model are shown in Figure 3.1 to 3.3. Models with the highest ELPD-WACI were best-fit models. In the HC study, exponential decay models had higher ELPD-WACI than power-law decay models. However, in the HV study, except for the antibody of GII.4 IgG, power-law decay models had higher ELPD-WACI than exponential decay models.

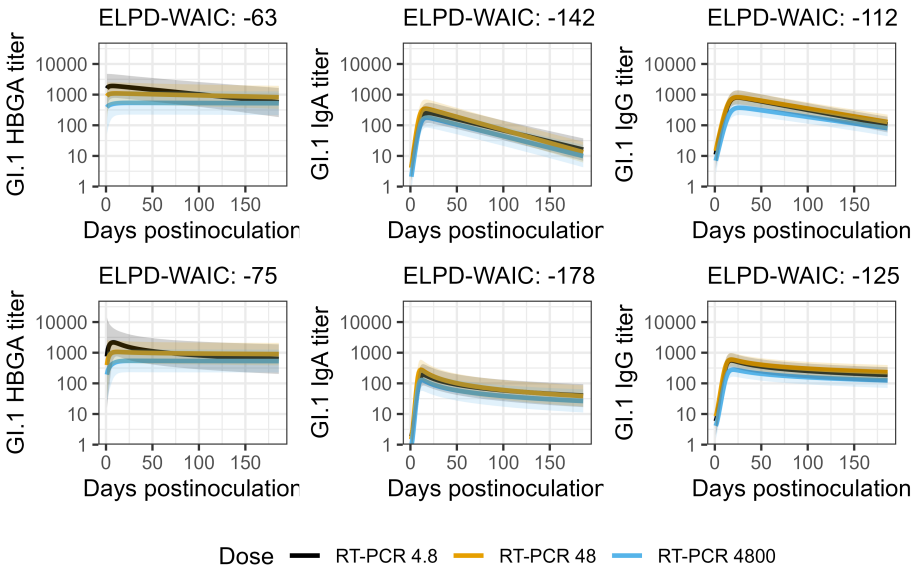

Figure 3.1: Fitted longitudinal antibody results in the HC study. The first row of the panel is the exponential decay model. The second row is the power-law decay model. The lines show the means of estimations. The colored areas show 89% equal-tailed credible intervals (CI).

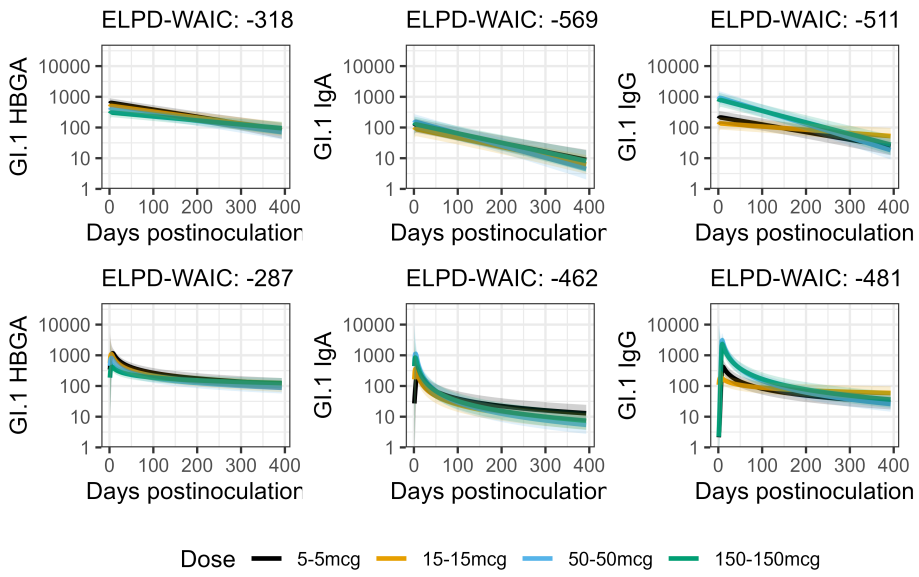

Figure 3.2: Fitted GI.1 longitudinal antibody results in the HV study. The first row of the panel is the exponential decay model. The second row is the power-law decay model. The lines show the means of estimations. The colored areas show 89% equal-tailed credible intervals (CI).

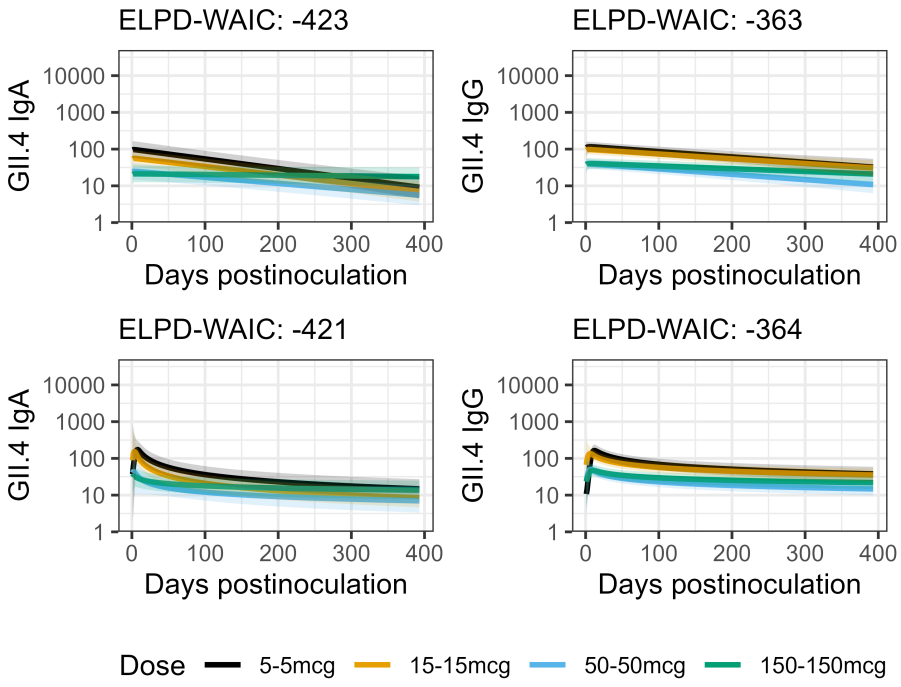

Figure 3.3: Fitted GII.4 longitudinal antibody results in the HV study. The first row of the panel is the exponential decay model. The second row is the power-law decay model. The lines show the means of estimations. The colored areas show 89% equal-tailed credible intervals (CI).

Based on the best fit models, peak level of antibodies, and half-list time were computed (Figure 3.4 to 3.5).

In the HC study, as the dose increased from 4.8 to 4800 RT-PCR units, the peak level of GI.1 HBGA titer decreased from 2380.7 (89%CI, 856.4 to 4952.2) to 620.5 (89%CI, 217.9 to 1242.7); the peak level of GI.1 IgA value decreased from 291.4 (89%CI, 125.2 to 558.6) to 199.3 (89%CI, 83.1 to 380.4) ug/ml; the peak level of GI.1 IgG value decreased from 859.3 (89%CI, 465.8 to 1410.7) to 395.1 (89%CI, 218.4 to 647.2) ug/ml.

For the half-life time, as the dose increased from 4.8 to 4800 RT-PCR units, GI.1 HBGA changed from 108.6 (89%CI, 64 to 186) to 185.9 (89%CI, 186 to 186) days; GI.1 IgA changed from 63.1 (89%CI, 54 to 74) to 59.6 (89%CI, 51 to 69) days; GI.1 IgG changed from 81.9 (89%CI, 69 to 99) to 102.6 (89%CI, 82 to 134) days.

In the HV study, as the dose increased from 5-5 mcg to 150-150 mcg, the peak level of GI.1 HBGA titer decreased from 4635.7 (89%CI, 922.5 to 12638.2) to 720.6 (89%CI, 346.5 to 1378.7); the peak level of GI.1 IgA value increased from 1342.2 (89%CI, 186.8 to 4805.7) to 10505.5 (89%CI, 549.7 to 37190.5) ug/ml; the peak level of GI.1 IgG value increased from 525.1 (89%CI, 263.6 to 830.9) to 5268.8 (89%CI, 1458.7 to 13554.5) ug/ml; the peak level of GII.4 IgA value decreased from 536.3 (89%CI, 124.8 to 1611.9) to 50.2 (89%CI, 18.6 to 101.8) ug/ml; the peak level of GII.4 IgG value decreased from 121.3 (89%CI, 87.9 to 160.3) to 41.7 (89%CI, 29.7 to 56.5) ug/ml.

For the half-life time, as the dose increased from 5-5 mcg to 150-150 mcg, GI.1 HBGA changed from 11.5 (89%CI, 0.5 to 32) to 33.3 (89%CI, 2 to 106.1) days; GI.1 IgA changed from 11.5 (89%CI, 0.4 to 24) to 3.5

(89%CI, 0.4 to 12) days; GI.1 IgG changed from 26.8 (89%CI, 22 to 34) to 16 (89%CI, 2.4 to 20) days; GII.4 IgA changed from 13.6 (89%CI, 0.7 to 31) to 111.7 (89%CI, 3 to 393) days; GII.4 IgG changed from 222.3 (89%CI, 151 to 336.1) to 356.6 (89%CI, 249 to 393) days.

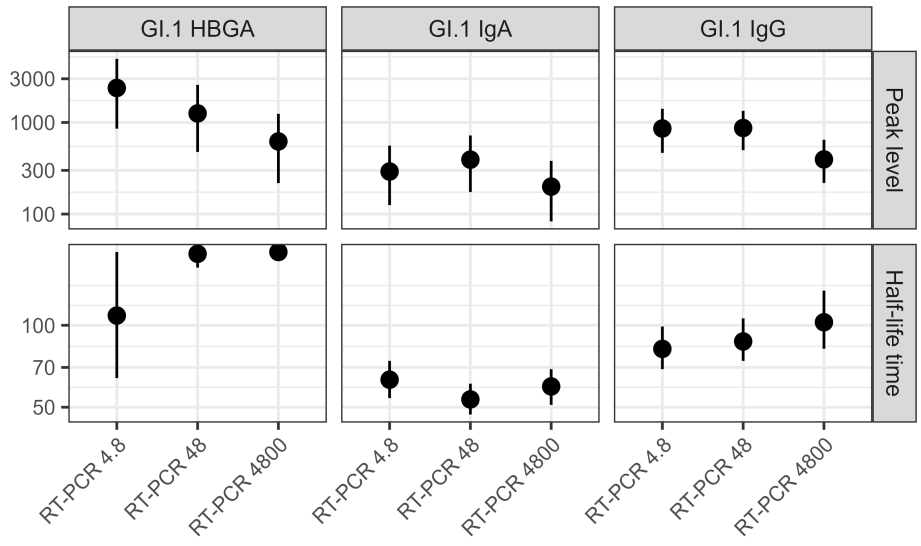

Figure 3.4: Fitted peak level of antibodies and half-list time in the HC study. The lines show means of estimations. The colored areas show 89% equal-tailed credible intervals (CI).

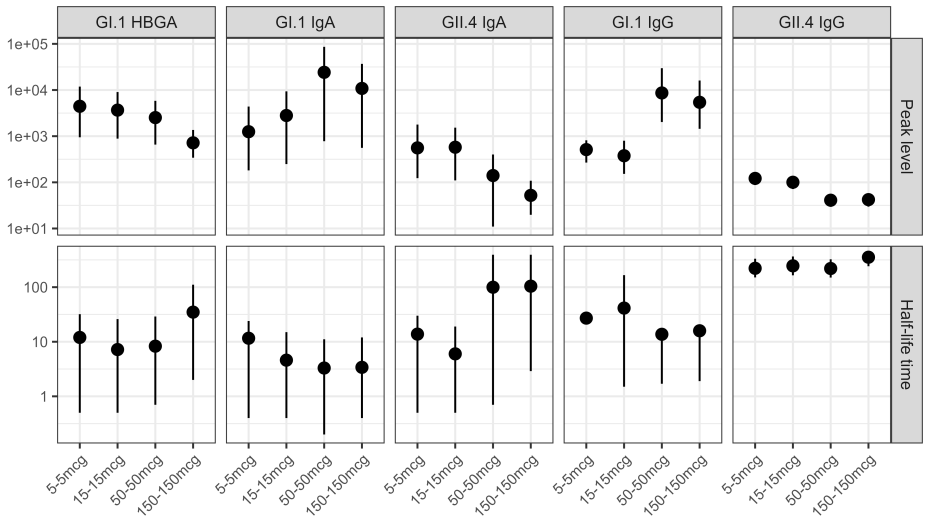

Figure 3.5: Fitted peak level of antibodies and half-list time in the HV study. The lines show means of estimations. The colored areas show 89% equal-tailed credible intervals (CI).

3.5 Discussion

We used data from a human challenge and a vaccine candidate study to explore the impact of norovirus antigen dose on the kinetics of serum antibodies. We found higher dose not necessary produce higher level of antibodies or longer half-life time (Figure 3.1 to 3.3). Our analyses also suggest that serum antibody responses acquired from the candidate vaccine was weaker than that acquired from infection.

The knowledge of the impact of antigen dose on immune responses is not explicit. An empirical understanding is that a higher level of antigen exposure associates with a stronger immune response (Handel et al., 2018). However, theoretically, observations might be different when the exposure level is above a threshold. Our study, along with a few previous modeling and observational studies, suggests that the association between antigen exposure and the strength of antibodies responses could be non-linear (de Menezes Martins et al., 2018; Handel et al., 2018).

It is not clear that how the antigen dose impacts the decay of serum antibodies. One study showed that a lower dose of yellow fever vaccine provided a similar percentage of seropositivity after eight years (de Menezes Martins et al., 2018). In our study, the half-life time of antibodies, acquired from either infection or vaccination, did not depend on the antigen dose.

This study compared the impact of antigen dose on different serum antibodies between infection-associated and vaccination-associated antibody responses, which had not well explored in previous studies. However, there are clear limitations. First, the total sample sizes of participants and serum samples are not large. Second, our study is a secondary data analysis. So findings here are exploratory and need further confirmation. More serum

samples, especially in the first month, might provide a more complete understanding of antibody kinetics.

To summarize, we analyzed the kinetics of serum antibodies induced by norovirus infection and candidate vaccines. We compared the peak level and half-life time of antibodies across different dose groups. Our results show that, for norovirus, a higher dose of antigen does not necessarily lead to a stronger and long-lasting immune response.

CHAPTER 4

IMPACT OF SEASONAL INFLUENZA VACCINE DOSE ON HOMOLOGOUS AND HETEROLOGOUS IMMUNITY

[3] Yang Ge, Amanda Skarlupta, W. Zane Billings, Ye Shen, Justin Bahl, Paul Thomas, Ted Ross, Andreas Handel.

To be submitted to *PLOS Medicine*

4.1 Abstract

Background The high-dose (HD) Fluzone influenza vaccine is provided to the elderly population because the standard-dose (SD) version had low immunogenicity and protective effect. Although the increased dose seems to improve homologous protection (against the vaccine strain), the heterologous protection (against other strains) is not well studied. We set out to perform a detailed investigation of the differences between SD and HD vaccines for several recent vaccine years both with respect to homologous and heterologous antibody immune responses.

Methods We used data from human volunteers vaccinated with either the SD or HD Fluzone vaccine during influenza seasons spanning the years 2014-2018. We used a Bayesian hierarchical modeling framework to explore the impact of dose on immune protection as quantified by hemagglutination inhibition titer (HAI). We estimated the additional benefits of HD compared to SD vaccine by strain-specific and vaccine-specific analyses, for both homologous and heterologous immunity.

Results We found that the HD vaccine led to overall improvement for both homologous and heterologous immunity. In the vaccine-strain specific analyses, across all strains the HD vaccine was associated with a (0.19 (89%CI, -0.1 - 0.44), CI: equal-tailed credible interval) log2 HAI units, stronger increase in HAI titer following vaccination, with the strongest impact noted for the H1N1 vaccine component. We also observed that the HD vaccine overall induced stronger heterologous responses, though there was noticeable variation across vaccine and test strains. In the per-vaccine analyses, HD vaccines showed stronger increases in HAI titer following vaccination against both homologous and heterologous strains, with the homologous response stronger and less variable (overall increase across 5

seasons of 0.21 (89%CI, -0.12 - 0.53) log2 HAI units and the heterologous response showing a reduced and more variable impact (overall increase -0.01 (89%CI, -0.35 - 0.33) log2 HAI units). These findings were robust across different ways of quantifying the vaccine response (seroconversion, post-vaccination titers, and seroprotection).

Conclusions Overall, the HD influenza vaccine was able to induce better homologous and heterologous antibody immunity. Some exceptions were noted for heterologous immunity, where the increased dose led to reduced immunogenicity. Based on these findings, considering extension of the HD vaccine to other age-groups, and further dose optimization studies seem warranted.

4.2 Introduction

Influenza vaccines are widely used to protect humans from influenza infections, but the average effectiveness is only around 50% (Centers for Disease Control and Prevention, 2021). In the elderly population, the licensed standard-dose (SD) split-inactivated virion vaccine, which includes 15 micrograms of HA antigen for each strain, had low immunogenicity and protective effect (Grohskopf, 2021). That led to the development of a high-dose (HD) influenza vaccine, Fluzone HD (Sanofi Pasteur), which has 60 micrograms of HA for each of the vaccine strains (Falsey et al., 2009). The increased dose led to better homologous protection (against the vaccine strain) (Couch et al., 2007; DiazGranados et al., 2013; Diaz-Granados et al., 2014; Falsey et al., 2009; J. K. H. Lee et al., 2021), thus was licensed in the US in 2009 and has since been offered to individuals 65+ years of age.

Although increased dose may lead to improved immunogenicity (Couch et al., 2007; Hilleman, 1958), the role of vaccine dose toward induction of heterologous immunity (against other strains) is not well understood. As non-monotone patterns have been reported for various antigens (Campi-Azevedo et al., 2014; Handel et al., 2018; Regules et al., 2016; Rhodes et al., 2019), it is for instance plausible that a higher dose might induce a broader B-cell or T-cell response, thus increasing both strength and breadth of protection. Alternatively, a higher dose might more strongly induce dominant B-cell or T-cell responses, which might target an epitope which may or may not be neutralizing. This immunodominant clones might outcompete other lineages and thus lead to a narrower response (Angeletti and Yewdell, 2018). Since there is often a mismatch between vaccine strains and circulating strains. The actual impact of HD influenza vaccine on

heterologous protection is a critical question but has not been thoroughly studied to date.

Maximizing both homologous and heterologous protection will significantly benefit the effectiveness of the influenza vaccine and has been identified as a critical objective in the development of a universal influenza vaccine (Erbelding et al., 2018; Paules et al., 2018). We considered the decision of vaccine dose is important to efficacy, side effects, costs and availability (Couch et al., 2007; Rhodes et al., 2019). To have a dose optimized vaccine, the impact of dose needs to be carefully determined.

Here, using data of volunteers receiving either SD or HD Fluzone vaccine across five vaccine seasons, 2014/15 - 2018/19, we compared HAI responses against 10 vaccine strains and 40 heterologous strains between HD and SD vaccine dose groups. We found that the HD induced better homologous and heterologous immunity, with some differences between H1N1, H3N2 and B strains.

4.3 Methods

4.3.1 Data source

Our dataset is collected from an ongoing vaccination study in which volunteers who had not yet received an influenza vaccine for the season were recruited each year before the start of the influenza season. Individuals 65+ years of age were offered a choice between the HD and SD vaccine. The data analyzed here spans the influenza seasons of 2014/15 - 2018/19. The HD vaccine was trivalent, while the SD vaccines were trivalent in year 2014 and quadrivalent in the remaining years. The quadrivalent formulation contains an additional B-strain. Biological samples were taken prior to vaccination and 21-28 days after vaccination. Demographic information of age, sex and race were also collected. Details of the study and data collection methodology have been described previously (Abreu et al., 2020; Carlock et al., 2019; Nuñez et al., 2017).

4.3.2 Data processing

The main quantity of interest for our analysis are hemagglutination-inhibition antibody titers (HAI) pre- and post-vaccination by strains. HAI titers were measured with the standard dilution assay. The limit of detection (LOD) in this study was 1:10, values below the LOD were coded as 1:5. Following (Beyer et al., 2004; Ranjeva et al., 2019), we transformed HAI titer measurements using the relation $\log 2(HAI/5)$, where HAI was the dilution level. This lead to a transformation of HAI values onto a range from zero (LOD) to 12 (maximum reported dilution of 1:20480). Because the HD vaccine was only available to 65+ years old participants, for our main analyses we only included SD vaccine recipients 65+ years old. A sensitivity analysis allowing that includes all age SD recipients (with a

multivariable model adjusting for age) is shown in the supplement. Since the trivalent HD vaccine only contained a single B strain, we only retained the matching B strain information for the quadrivalent SD recipients and removed the B strain that was not present in both SD and HD formulations for each season.

4.3.3 Outcome definitions

We quantified the impact of the SD and HD vaccine on HAI titers using 4 different but related outcomes (Beyer et al., 2004; Falsey et al., 2009). The first two outcomes are on an integer scale (after transformation of titer as described above), namely 1) titer increase, defined as the difference between post-vaccination and pre-vaccination titer and 2) post-vaccination titer. The other two outcomes are categorical versions of the first two outcomes, namely 3) seroconversion, defined as either a pre-vaccination titer of 0 (=LOD) with a post-vaccination titer of at least 3 (after transformation of titer values as described above), or a pre-vaccination titer above the LOD and a post-vaccination titer that is at least 2 units higher (corresponding to a dilution measurement of $<$ 1:10 pre-vaccination and $\geq$ 1:40 post-vaccination or a $\geq$ 4-fold increase from pre- to post-vaccination in dilution units) (Falsey et al., 2009), and 4) seroprotection, defined as a post-vaccination HAI titer of 3 or greater (i.e., an equal or greater 1:40 dilution in the original units), which is generally considered a threshold for protection (Coudeville et al., 2010).

4.3.4 Statistical analyses

In the descriptive analyses, we report mean and standard deviation for the continuous outcomes of titer increase and post-vaccination titer and counts and percentages for the binary outcomes of seroconversion and seroprotec-

tion. We used a Bayesian hierarchical modeling approach to estimate the impact of vaccine dose with the recognition of study hierarchical features (Supplementary material). We additionally included sex, race, age, and pre-vaccination titer as covariates in our models. We estimated the overall strain-specific or vaccine-specific impact of vaccine dose and its variations by multilevel models (Faraway, 2016). For continuous outcomes, we used a linear model, and for the categorical outcomes we used a logistic model. The inclusion of pre-vaccination titer as a covariate means that the models for titer increase and post-vaccination titer as outcomes lead to mathematically identical dose coefficient estimations and thus we did not fit the multivariable models for the outcome of post-vaccination titer. The impact of HD vaccine relative to SD was summarized with median and 89% equal-tailed credible interval (CI) (McElreath, 2020). Detailed descriptions of all models, as well as code to run the analyses are provided in the supplementary material.

In addition to our main analyses, we performed a sensitivity analysis by adjusting modeling approaches and data. In one analysis, we included SD recipients of any age with the same multilevel models. We also used Bayesian generalized linear models for 65+ years old population and 1:1 dose group propensity score matched data (using the nearest neighbor matching algorithm (Ho et al., 2007/ed)). Results from these sensitivity analyses are reported in the supplementary material.

4.3.5 Implementation

All analyses were completed using R (R Core Team, 2020). The package of brms v2.15 (Bürkner, 2018) was used for the Bayesian analysis. R scripts for all analyses are provided as supplementary materials.

4.4 Results

4.4.1 Data Description

Our samples span the 2014-2018 influenza seasons. During that time the HD vaccine was given 197 times, the remaining 157 samples were from individuals 65+ years who received SD vaccine (Table 4.1). In both dose groups, most participants were white with similar other demographic characteristics. Over the duration of the study, two H1N1 vaccine strains (H1N1-California-2009 in seasons 2014/15, 2015/16 and H1N1-Michigan-2015 in 2017/18, 2018/19), four H3N2 strains (H3N2-Texas-2012 in 2014/15, H3N2-Switzerland-2013 in 2015/16, H3N2-Hong Kong-2014 in 2016/17 and 2017/18, H3N2-Singapore-2016 in 2018/19) and four type B strains (B-Brisbane-2008 2015/16, 2016/17, 2017/18, B-Massachusetts-2012 in 2014/15, B-Phuket-2013 in 2015/16, 2016/17, 2017/18, 2018/19, B-Colorado-2017 in 2018/19) were included in the vaccines.

The mean titer increase following vaccination ranged from 0.5 to 3 units, and the post-vaccination titer ranged from 2.4 to 5.6 units. The percentage of individuals who seroconverted ranged from 9.1% to 78.9%, and seroprotection ranged from 50% to 100%.

Table 4.1: Description of the study.

Variables	Standard-dose vaccine	High-dose vaccine
Sample size (N)	157	197
Age (median, IQR)	68.00 [66.00, 74.00]	70.00 [68.00, 75.00]
Sex, n (%)		
- Female	97 (61.8)	137 (69.5)
- Male	60 (38.2)	60 (30.5)
Race, n (%)		
- White	123 (78.3)	140 (71.1)
- Black	30 (19.1)	54 (27.4)
- Hispanic	3 (1.9)	3 (1.5)
- Other	1 (0.6)	0 (0.0)
H1N1-Michigan-2015	N = 25 (2017, 2018)	N = 19 (2017, 2018)
H1N1-California-2009	N = 88 (2014, 2015, 2016)	N = 93 (2014, 2015, 2016)
H3N2-Singapore-2016	N = 11 (2018)	N = 8 (2018)
H3N2-Hong Kong-2014	N = 47 (2016, 2017)	N = 91 (2016, 2017)
H3N2-Switzerland-2013	N = 38 (2015)	N = 58 (2015)
H3N2-Texas-2012	N = 53 (2014)	N = 39 (2014)
B-Colorado-2017	N = 11 (2018)	N = 8 (2018)
B-Phuket-2013	N = 77 (2015, 2016, 2017, 2018)	N = 58 (2015)
B-Massachusetts-2012	N = 53 (2014)	N = 39 (2014)
B-Brisbane-2008	N = 76 (2015, 2016, 2017)	N = 91 (2016, 2017)

The comparison between HD and SD for each seasons on titer increase had variabilities. HD vaccine overall had higher homologous titer increase, but lower heterologous responses in 2016 and 2018 seasons.

4.4.2 HD vaccines led to increased strain-specific homologous responses

Vaccine-strain specific homologous HAI responses following vaccination with the HD vaccine was stronger compared to the SD vaccine (Figure 4.1). For both of the H1N1 vaccine strains, HD led to a robustly increased response, indicated in Figure 4.1 by results that are strongly to the right of the no-effect line. The impact of HD on H3N2 vaccine strains was more

variable, with the titer increase outcome for the Texas-2012 vaccine even showing a slightly reduced impact of the HD vaccine, though very close to the no-effect line. For type B strains, the impact of HD was again robustly beneficial.

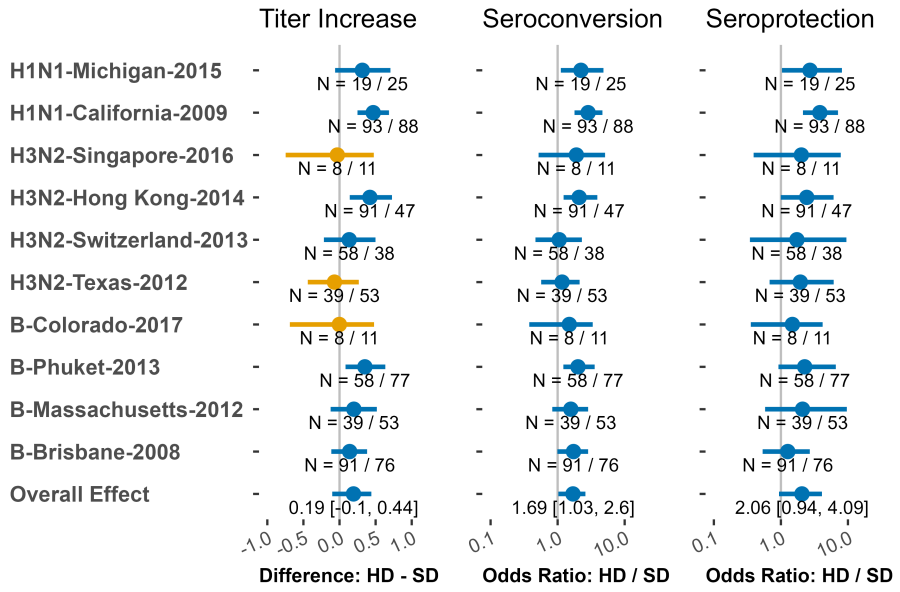

Figure 4.1: The impact of HD vaccine compared to SD on strain-specific, homologous HAI responses. The median and 89% equal-tailed credible interval (CI) of the overall effect (HD vs. SD) are shown. The numbers under each line show the sample size (HD/SD) for that specific strain or the overall effect size.

4.4.3 HD vaccines led to increased strain-specific heterologous responses

Heterologous HAI responses also showed a generally stronger impact of the HD vaccines compared to the SD vaccine excepted H1N1-California-2009 and H3N2-Singapore-2016 (Figures 4.2 - 4.4). Heterologous responses had more variabilities, and some strains indicated a negative effect of the HD. The H1N1-California-2009 HD vaccine had a notice-

able negative impact on multiple strains. This was very pronounced for H3N2-Singapore-2016, however the sample size for this vaccine strain is too small to draw useful conclusions. HD vaccine of H3N2-Texas-2012 had a negative impact against H3N2-HongKong-1968, HD vaccine of Massachusetts-2012 had a negative impact against B-Yamagata-1988. The overall heterologous effect of HD was positive. No trend (e.g., more or less impact of HD for older strains) was observed.

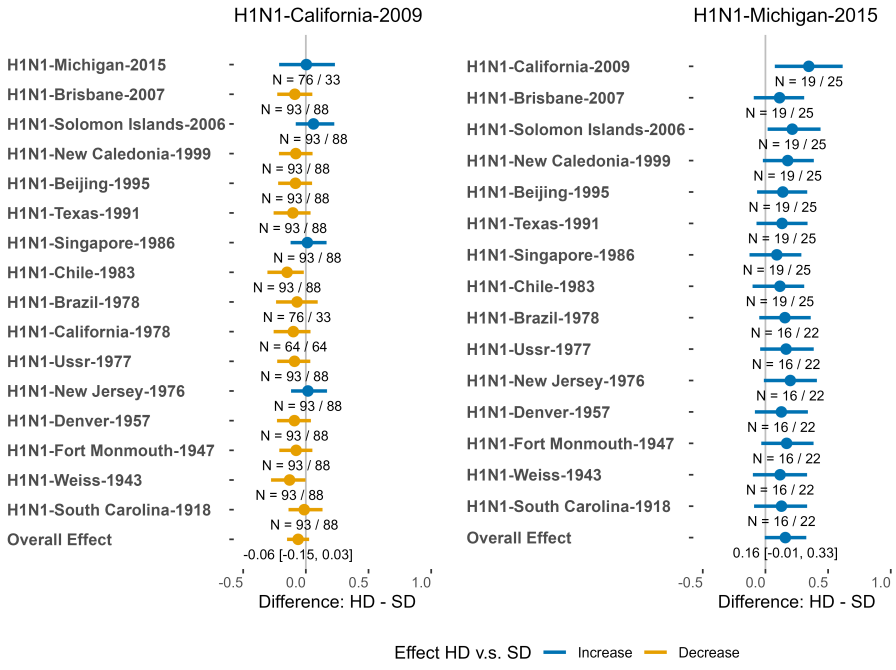

Figure 4.2: The impact of HD vaccine compared to SD on strain-specific, heterologous HAI responses. The median and 89% equal-tailed credible interval (CI) of the overall effect (HD vs. SD) are shown. The numbers under each line show the sample size (HD/SD) for that specific strain or the overall effect size. Figures for seroconversion and seroprotection outcomes show similar results (see supplementary material).

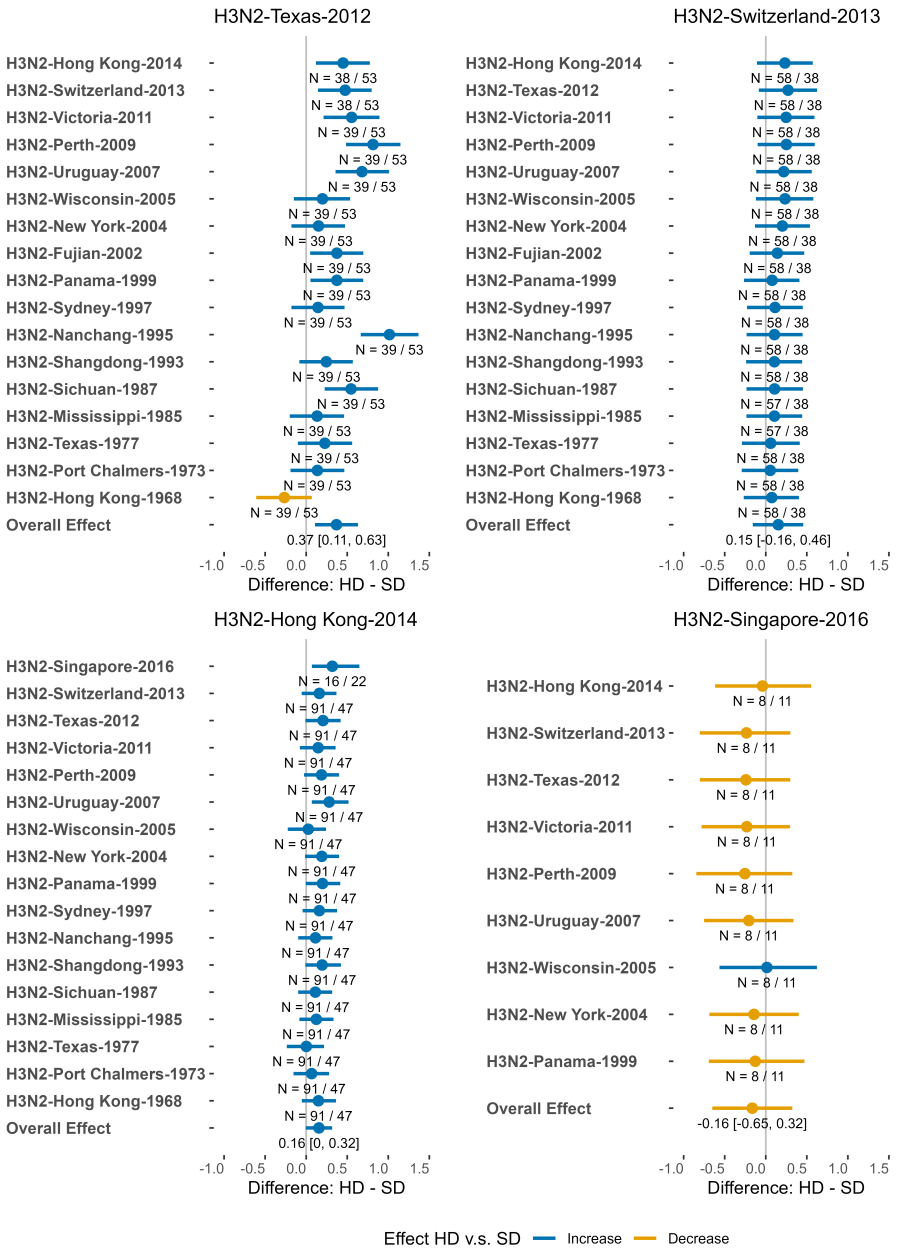

Figure 4.3: The impact of HD vaccine compared to SD on strain-specific, heterologous HAI responses. The median and 89% equal-tailed credible interval (CI) of the overall effect (HD vs. SD) are shown. The numbers under each line show the sample size (HD/SD) for that specific strain or the overall effect size.

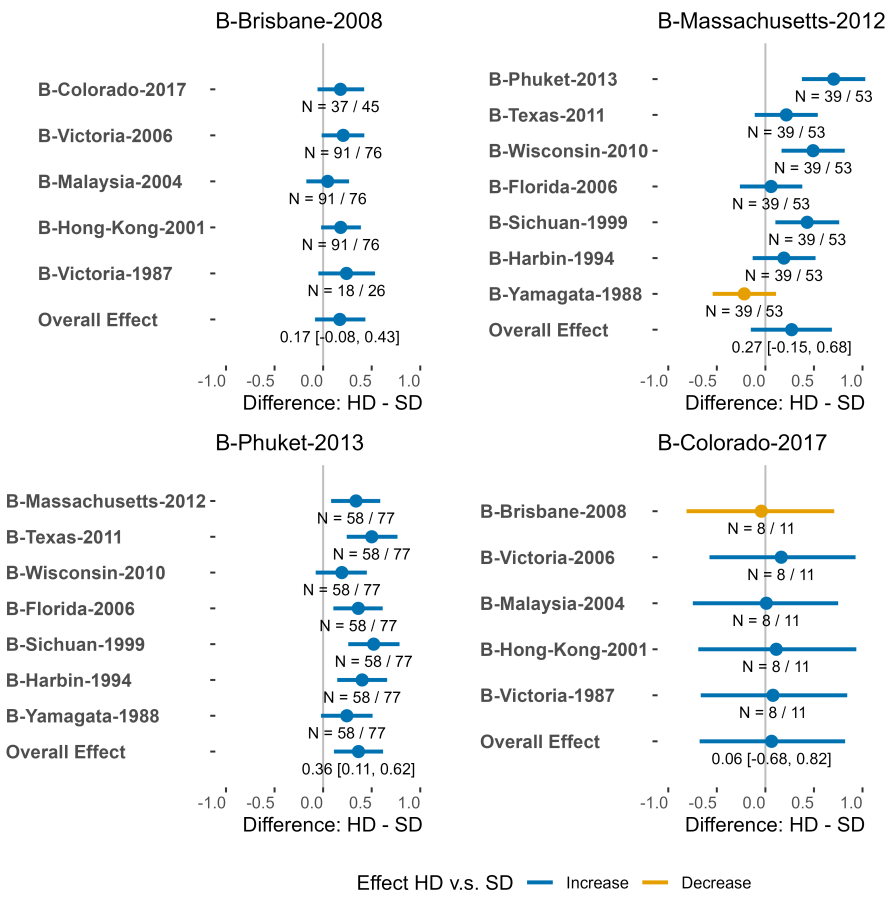

Figure 4.4: The impact of HD vaccine compared to SD on strain-specific, heterologous HAI responses. The median and 89% equal-tailed credible interval (CI) of the overall effect (HD vs. SD) are shown. The numbers under each line show the sample size (HD/SD) for that specific strain or the overall effect size.

4.4.4 HD vaccines led to increased vaccine-specific homologous responses

Vaccine-specific analyses provided a summarized comparison between HD and SD for each seasonal vaccine, showing the average impact of dose across all vaccine strains for a given vaccine. As Figure 4.5 shows, for

all seasons the HD vaccine led to a robust improved homologous HAI response against the strains contained in the vaccine.

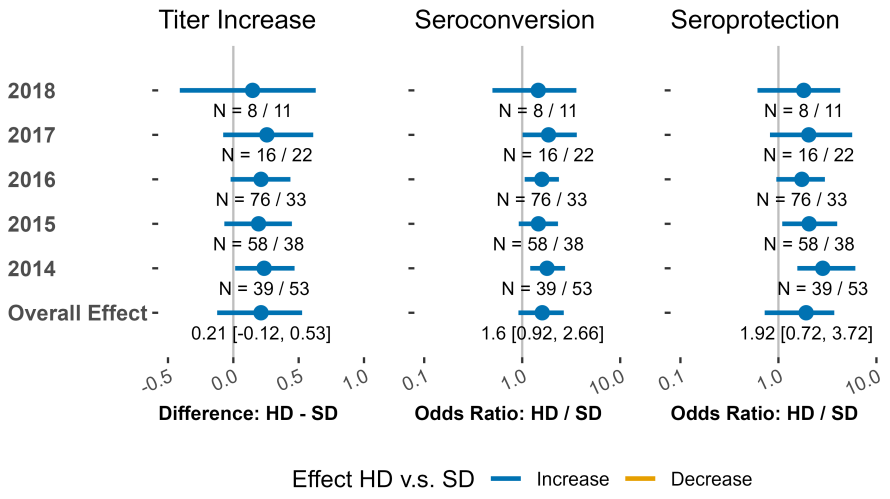

Figure 4.5: The impact of HD vaccine compared to SD on vaccine-specific, homologous HAI responses. The median and 89% equal-tailed credible interval (CI) of the overall effect (HD vs. SD) are shown. The numbers under each line show the sample size (HD/SD) for that specific strain or the overall effect size.

4.4.5 HD vaccines led to increased vaccine-specific heterologous responses

To determine an overall heterologous response, we considered all heterologous responses for each strain contained in the vaccine as a whole were a cluster in the multilevel model. As Figure 4.6) shows, there were more variabilities benefit in HD vaccines. In 2016 and 2018, the HD vaccine had lower heterologous responses compared to the SD vaccine.

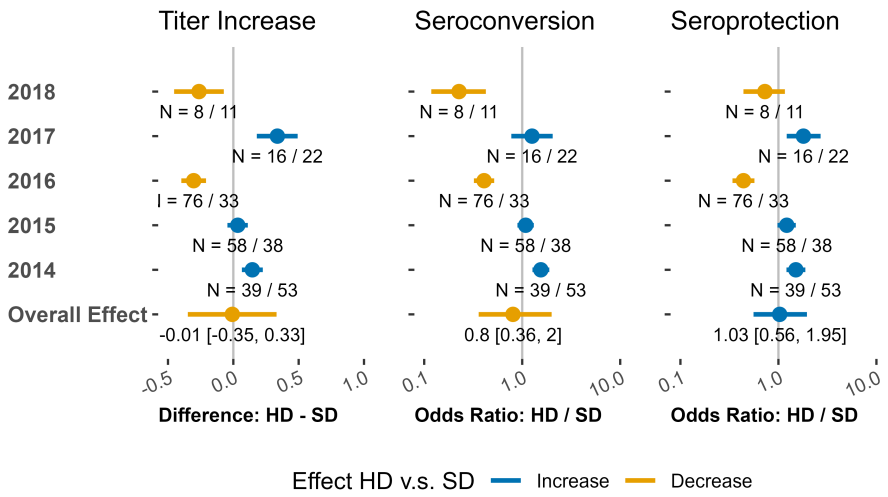

Figure 4.6: The impact of HD vaccine compared to SD on vaccine-specific, heterologous HAI responses. The median and 89% equal-tailed credible interval (CI) of the overall effect (HD vs. SD) are shown. The numbers under each line show the sample size (HD/SD) for that specific strain or the overall effect size.

4.4.6 Further analyses

We performed additional analyses to explore the sensitivity of our results to variants of model and data. This section provides a brief description, the full details are provided in the supplementary materials.

Data variant exploration. In the analyses of multilevel models with data including all age groups, we found similar results. The only major difference was that no inferior impact of HD in 2018 was found.

Model variant exploration. We conducted non-hierarchical generalized linear models. Such models ignore the fact that strains within a given vaccine are shared, and thus consider the response to each strain as fully independent. It also ignore that some volunteers had repeated vaccinations across different seasons. As shown in the supplement, we found overall patterns of HD leading to a stronger HAI response. In strain-specific

analyses, the credible intervals and the variations between strains were much wider and stronger, respectively. In vaccine-specific analyses, the HD vaccine had lower heterologous responses compared to the SD vaccine in 2018 but not in 2016.

Model and data variant exploration. We conducted non-hierarchical generalized linear models with 1:1 1:1 dose group propensity score matched data. The overall benefit of HD vaccines were also observed, and similar to non-hierarchical generalized linear models with all 65+ years old data.

Interactions between sex and dose. We extracted coefficients of the variable of sex from models. In parts of strain-specific and vaccine-specific analyses, we found male had lower titer increase, ORs of seroconversion and seroprotection than female.

4.5 Discussion

While vaccines are one of our best tools against infectious diseases, most vaccines are far from perfect and could be further improved. This is definitely the case for influenza, where effectiveness rarely goes above 50% (Doyle et al., 2021). The hope is that in the not-too-distant future, one or several universal influenza vaccines will become available that have induced immunity that is strongly protective and long-lasting, against a broad range of current and future circulating strains. Optimization of dose is an important component of overall optimization of such future vaccines.

The HD Fluzone vaccine has previously shown to induce stronger homologous immunity and protection (Couch et al., 2007; DiazGranados et al., 2013; DiazGranados et al., 2014; Falsey et al., 2009; J. K. H. Lee et al., 2021). Here, we set out to analyze this in more detail for multiple vaccine seasons, and to also determine the impact of dose on heterologous responses.

We found that overall, HD vaccine induced a stronger HAI response against both homologous and heterologous strains. Of note, the increase in titer for the HD was fairly small (less than 0.5. log2 units). Also worth noting is that for the vaccine-specific analyses, the (categorical) seroconversion outcome showed a pattern different from the (continuous) titer increase outcome. This is perhaps not surprising but suggests that in studies that assess the impact of influenza (or other) vaccines, using only a single way of defining and measuring vaccine response is not ideal. If feasible, the use of multiple outcomes, as we have done here, could provide more robust conclusions.

The overall impact of HD on heterologous responses was similar to the results of homologous, but the effect size was small and variations across strains were obvious. In vaccine-specific analyses, we found HD vaccines failed to provide additional benefits compared to SD vaccines in 2016 and 2018. Raw data description shown titer increase of HD vaccines in 2016 and 2018 were inferior to SD vaccines. However, sensitivity analyses only found similar results in 2018. The discrepancies could be partly explained by the ignorance of repeated measurements in the generalized linear models. In general, we found that HD may also benefit heterologous responses, cautions are needed for extrapolating because of the variances.

Our findings come with some caveats. First, this was a secondary data analysis. Thus our analyses is exploratory, and future confirmatory studies might be useful. Another important consideration is the fact that our data comes from an observational cohort, not a clinical trial. Participants 65+ years old were not randomized to receive either HD or SD vaccine, instead they were allowed to choose. This could have introduced some biases. We tried to correct for some of them in our multivariable models by adjusting for factors such as age and pre-existing antibody levels. However, we did not have information on other possibly important factors, e.g., overall participant health and pre-existing conditions.

We found that overall, Fluzone HD induces both better homologous and heterologous HAI responses compared to SD. However, HD might negatively impact the broad of heterologous HAI responses for individuals 65+ years old.

CHAPTER 5

CONCLUSION

In this chapter, a summary of all research topics in the dissertation is provided. Specifically, major contributions and future work is highlighted.

5.0.1 Chapter 2: Analyzing the association between inoculum dose and norovirus infection outcomes

We analyzed the impact of norovirus inoculum dose on disease outcomes after infection with the data from a human challenge study. The dose dependent norovirus infection outcomes is not well explored before. We found that while increases in dose were associated with a faster onset and peak of virus shedding in feces, the total shedding duration and total amount of virus shedding showed little association. Our analysis also showed a general pattern of accelerated onset of symptoms and increased symptom severity with higher inoculum dose.

Our findings suggest that inoculum dose has little impact on norovirus shedding. Thus, while a strong infection control intervention could reduce the viruses in the external environment. This effort may only reduce the norovirus infection risk but have limited impact on transmission potential.

Future large sample size studies are needed to confirm our results. Explorations on the interactions between host characteristics and dose-outcome relationships is warranted.

5.0.2 Chapter 3: Norovirus antibody kinetics comparisons between infection and vaccination

We explored the impact of norovirus antigen dose on the kinetics of serum antibodies with data from a norovirus human challenge study and a norovirus candidate vaccine study. We found higher dose not necessary produce higher level of antibodies or longer half-life time. Our analyses also suggest that serum antibody responses acquired from the candidate vaccine may weaker than that acquired from infection.

The knowledge of the impact of antigen dose on immune responses is not explicit. We are also not aware of a conclusion of how the antigen dose impacts the decay of serum antibodies. Our findings may benefit the development of norovirus vaccines.

To better explore the kinetics of serum antibodies, future studies could collected samples more frequently to avoid the missing of potential turning points.

5.0.3 Chapter 4: Impact of seasonal influenza vaccine dose on homologous and heterologous immunity

We compared the high-dose (HD) Fluzone influenza vaccine and the standard-dose (SD) Fluzone influenza vaccine on homologous and heterologous immune responses with hemagglutination inhibition titer (HAI) data from a cohort influenza study. We found that the HD vaccine overall led to improvement for both homologous and heterologous immunity. However, for homologous immunity, the HD only provided a small increase on titer increase. Inferior results of HD also were observed on heterologous immunity.

Most vaccines are far from perfect and could be further improved including influenza vaccines. A universal influenza vaccine is one of the ultimate purposes on influenza outbreak control. Optimization of dose is an important component in the development of universal influenza vaccines.

Future studies should generate better study designs to better control the interactions between multiple strains contained in the vaccine for explicite conclusions.

BIBLIOGRAPHY

Abreu, R. B., Clutter, E. F., Attari, S., Sautto, G. A., & Ross, T. M. (2020). IgA Responses Following Recurrent Influenza Virus Vaccination. *Frontiers in Immunology*, *11*, 902. https://doi.org/10.3389/fimmu.2020.00902

Ajami, N. J., Barry, M. A., Carrillo, B., Muhaxhiri, Z., Neill, F. H., Prasad, B. V. V., Opekun, A. R., Gilger, M. A., Graham, D. Y., Atmar, R. L., & Estes, M. K. (2012). Antibody Responses to Norovirus Genogroup GI.1 and GII.4 Proteases in Volunteers Administered Norwalk Virus. *Clinical and Vaccine Immunology*, *19*(12), 1980–1983. https://doi.org/10.1128/CVI.00411-12
ZSCC: 0000012

Angeletti, D., & Yewdell, J. W. (2018). Understanding and Manipulating Viral Immunity: Antibody Immunodominance Enters Center Stage. *Trends in Immunology*, *39*(7), 549–561. https://doi.org/10.1016/j.it.2018.04.008

Atmar, R. L., Bernstein, D. I., Harro, C. D., Al-Ibrahim, M. S., Chen, W. H., Ferreira, J., Estes, M. K., Graham, D. Y., Opekun, A. R., Richardson, C., & Mendelman, P. M. (2011). Norovirus Vaccine against Experimental Human Norwalk Virus Illness. *New England Journal of Medicine*, *365*(23), 2178–2187. https://doi.org/10.1056/NEJMoa1101245
ZSCC: 0000389

Atmar, R. L., & Estes, M. K. (2012). Norovirus vaccine development: Next steps. *Expert Review of Vaccines*, *11*(9), 1023–1025. https://doi.org/10.1586/erv.12.78

Atmar, R. L., Opekun, A. R., Gilger, M. A., Estes, M. K., Crawford, S. E., Neill, F. H., & Graham, D. Y. (2008). Norwalk Virus Shedding after Experimental Human Infection. *Emerging Infectious Diseases*, *14*(10), 1553–1557. https://doi.org/10.3201/eid1410.080117
ZSCC: 0000625

Atmar, R. L., Opekun, A. R., Gilger, M. A., Estes, M. K., Crawford, S. E., Neill, F. H., Ramani, S., Hill, H., Ferreira, J., & Graham, D. Y. (2014). Determination of the 50% Human Infectious Dose for Norwalk Virus. *The Journal of Infectious Diseases*, *209*(7), 1016–1022. https://doi.org/10.1093/infdis/jit620
ZSCC: 0000227

Bacaër, N. (2011). Verhulst and the logistic equation (1838). In N. Bacaër (Ed.), *A Short History of Mathematical Population Dynamics* (pp. 35–39). Springer. https://doi.org/10.1007/978-0-85729-115-8_6

Bartsch, S. M., Lopman, B. A., Ozawa, S., Hall, A. J., & Lee, B. Y. (2016). Global Economic Burden of Norovirus Gastroenteritis. *PloS One*, *11*(4), e0151219. https://doi.org/10.1371/journal.pone.0151219

Bernstein, D. I., Atmar, R. L., Lyon, G. M., Treanor, J. J., Chen, W. H., Jiang, X., Vinjé, J., Gregoricus, N., Frenck, R. W., Jr, Moe, C. L., Al-Ibrahim, M. S., Barrett, J., Ferreira, J., Estes, M. K., Graham, D. Y., Goodwin, R., Borkowski, A., Clemens, R., & Mendelman, P. M. (2015). Norovirus Vaccine Against Experimental Human GII.4 Virus Illness: A Challenge Study in Healthy Adults. *The Journal of Infectious Diseases*, *211*(6), 870–878. https://doi.org/10.1093/infdis/jiu497

Beyer, W. E. P., Palache, A. M., Lüchters, G., Nauta, J., & Osterhaus, A. D. M. E. (2004). Seroprotection rate, mean fold increase, seroconversion rate: Which parameter adequately expresses seroresponse to influenza vaccination? *Virus Research*, *103*(1), 125–132. https://doi.org/10.1016/j.virusres.2004.02.024

Bhurani, V., Mohankrishnan, A., Morrot, A., & Dalai, S. K. (2018). Developing effective vaccines: Cues from natural infection. *International Reviews of Immunology*, *37*(5), 249–265. https://doi.org/10.1080/08830185.2018.1471479
_eprint: https://doi.org/10.1080/08830185.2018.1471479

Bierhoff, M., Arvelo, W., Estevez, A., Bryan, J., McCracken, J. P., López, M. R., López, B., Parashar, U. D., Lindblade, K. A., & Hall, A. J. (2018). Incidence and Clinical Profile of Norovirus Disease in Guatemala, 2008–2013. *Clinical Infectious Diseases*, *67*(3), 430–436. https://doi.org/10.1093/cid/ciy091

Bitler, E. J., Matthews, J. E., Dickey, B. W., Eisenberg, J. N. S., & Leon, J. S. (2013). Norovirus outbreaks: A systematic review of commonly implicated transmission routes and vehicles. *Epidemiology & Infection*, *141*(8), 1563–1571. https://doi.org/10.1017/S095026881300006X

Bucardo, F., Reyes, Y., Svensson, L., & Nordgren, J. (2014). Predominance of norovirus and sapovirus in Nicaragua after implementation of universal rotavirus vaccination. *PloS One*, *9*(5), e98201. https://doi.org/10.1371/journal.pone.0098201

Burkner, P.-C. (2017). Brms An R Package for Bayesian Multilevel Models Using Stan. *Journal of Statistical Software*, *80*(1). https://doi.org/10.18637/jss.v080.i01
ZSCC: 0000687

Bürkner, P.-C. (2018). Advanced Bayesian Multilevel Modeling with the R Package brms. *The R Journal*, *10*(1), 395. https://doi.org/10.32614/RJ-2018-017
ZSCC: 0000002

Campi-Azevedo, A. C., de Almeida Estevam, P., Coelho-dos-Reis, J. G., Peruhype-Magalhães, V., Villela-Rezende, G., Quaresma, P. F., Maia, M. d. L. S., Farias, R. H. G., Camacho, L. A. B., Freire, M. d. S., Galler, R., Yamamura, A. M. Y., Almeida, L. F. C., Lima, S. M. B., Nogueira, R. M. R., Silva Sá, G. R., Hokama, D. A., de Carvalho, R., Freire, R. A. V., … Martins-Filho, O. A. (2014). Subdoses of 17DD yellow fever vaccine elicit equivalent virological/immunological kinetics timeline. *BMC Infectious Diseases*, *14*, 391. https://doi.org/10.1186/1471-2334-14-391

Cannon, J. L., Lopman, B. A., Payne, D. C., & Vinjé, J. (2019). Birth Cohort Studies Assessing Norovirus Infection and Immunity in Young Children: A Review. *Clinical Infectious Diseases*, *69*(2), 357–365. https://doi.org/10.1093/cid/ciy985

Carling, P. C., Bruno-Murtha, L. A., & Griffiths, J. K. (2009). Cruise Ship Environmental Hygiene and the Risk of Norovirus Infection Outbreaks: An Objective Assessment of 56 Vessels over 3 Years. *Clinical Infectious Diseases*, *49*(9), 1312–1317. https://doi.org/10.1086/606058

Carlock, M. A., Ingram, J. G., Clutter, E. F., Cecil, N. C., Ramgopal, M., Zimmerman, R. K., Warren, W., Kleanthous, H., & Ross, T. M. (2019). Impact of age and pre-existing immunity on the induction of human antibody responses against influenza B viruses. *Human Vaccines & Immunotherapeutics*, *15*(9), 2030–2043. https://doi.org/10.1080/21645515.2019.1642056

Centers for Disease Control and Prevention. (2021). Past Seasons Vaccine Effectiveness Estimates.

Cohen, K. W., Linderman, S. L., Moodie, Z., Czartoski, J., Lai, L., Mantus, G., Norwood, C., Nyhoff, L. E., Edara, V. V., Floyd, K., De Rosa, S. C., Ahmed, H., Whaley, R., Patel, S. N., Prigmore, B., Lemos, M. P., Davis, C. W., Furth, S., O'Keefe, J. B., ... McElrath, M. J. (2021). Longitudinal analysis shows durable and broad immune memory after SARS-CoV-2 infection with persisting antibody responses and memory B and T cells. *Cell Reports Medicine*, *2*(7), 100354. https://doi.org/10.1016/j.xcrm.2021.100354

Couch, R. B., Winokur, P., Brady, R., Belshe, R., Chen, W. H., Cate, T. R., Sigurdardottir, B., Hoeper, A., Graham, I. L., Edelman, R., He, F., Nino, D., Capellan, J., & Ruben, F. L. (2007). Safety and immunogenicity of a high dosage trivalent influenza vaccine among elderly subjects. *Vaccine*, *25*(44), 7656–7663. https://doi.org/10.1016/j.vaccine.2007.08.042

Coudeville, L., Bailleux, F., Riche, B., Megas, F., Andre, P., & Ecochard, R. (2010). Relationship between haemagglutination-inhibiting antibody titres and clinical protection against influenza: Development and application of a bayesian random-effects model. *BMC medical research methodology*, *10*, 18. https://doi.org/10.1186/1471-2288-10-18

Czakó, R., Atmar, R. L., Opekun, A. R., Gilger, M. A., Graham, D. Y., & Estes, M. K. (2012). Serum Hemagglutination Inhibition Activity Correlates with Protection from Gastroenteritis in Persons Infected with Norwalk Virus. *Clinical and Vaccine Immunology*, *19*(2), 284–287. https://doi.org/10.1128/CVI.05592-11
ZSCC: 0000040

de Graaf, W. F., Kretzschmar, M. E. E., Teunis, P. F. M., & Diekmann, O. (2014). A two-phase within-host model for immune response and its application to serological profiles of pertussis. *Epidemics*, *9*, 1–7. https://doi.org/10.1016/j.epidem.2014.08.002

de Menezes Martins, R., Maia, M. d. L. S., de Lima, S. M. B., de Noronha, T. G., Xavier, J. R., Camacho, L. A. B., de Albuquerque, E. M., Farias, R. H. G., da Matta de Castro, T., & Homma, A. (2018). Duration of post-vaccination immunity to yellow fever in volunteers eight years after a dose-response study. *Vaccine*, *36*(28), 4112–4117. https://doi.org/10.1016/j.vaccine.2018.05.041

DiazGranados, C. A., Dunning, A. J., Jordanov, E., Landolfi, V., Denis, M., & Talbot, H. K. (2013). High-dose trivalent influenza vaccine compared to standard dose vaccine in elderly adults: Safety, immunogenicity and relative efficacy during the 2009–2010 season. *Vaccine*, *31*(6), 861–866. https://doi.org/10.1016/j.vaccine.2012.12.013

DiazGranados, C. A., Dunning, A. J., Kimmel, M., Kirby, D., Treanor, J., Collins, A., Pollak, R., Christoff, J., Earl, J., Landolfi, V., Martin, E., Gurunathan, S., Nathan, R., Greenberg, D. P., Tornieporth, N. G., Decker, M. D., & Talbot, H. K. (2014). Efficacy of High-Dose versus Standard-Dose Influenza Vaccine in Older Adults. *New England Journal of Medicine*, *371*(7), 635–645. https://doi.org/10.1056/NEJMoa1315727

Doyle, J. D., Beacham, L., Martin, E. T., Talbot, H. K., Monto, A., Gaglani, M., Middleton, D. B., Silveira, F. P., Zimmerman, R. K., Alyanak, E., Smith, E. R., Flannery, B. L., Rolfes, M., & Ferdinands, J. M. (2021). Relative and Absolute Effectiveness of High-Dose and Standard-Dose Influenza Vaccine Against Influenza-Related Hospitalization Among Older Adults—United States, 2015–2017. *Clini-*

cal Infectious Diseases, *72*(6), 995–1003. https://doi.org/10.1093/cid/ciaa160

Erbelding, E. J., Post, D. J., Stemmy, E. J., Roberts, P. C., Augustine, A. D., Ferguson, S., Paules, C. I., Graham, B. S., & Fauci, A. S. (2018). A Universal Influenza Vaccine: The Strategic Plan for the National Institute of Allergy and Infectious Diseases. *The Journal of Infectious Diseases*, *218*(3), 347–354. https://doi.org/10.1093/infdis/jiy103

Falsey, A. R., Treanor, J. J., Tornieporth, N., Capellan, J., & Gorse, G. J. (2009). Randomized, Double-Blind Controlled Phase 3 Trial Comparing the Immunogenicity of High-Dose and Standard-Dose Influenza Vaccine in Adults 65 Years of Age and Older. *The Journal of Infectious Diseases*, *200*(2), 172–180. https://doi.org/10.1086/599790

Faraway, J. J. (2016). *Extending the Linear Model with R: Generalized Linear, Mixed Effects and Nonparametric Regression Models, Second Edition*
OCLC: 1100506358.

Freedman, S. B., Eltorky, M., Gorelick, M., & Group, t. P. E. R. C. G. S. (2010). Evaluation of a Gastroenteritis Severity Score for Use in Outpatient Settings. *Pediatrics*, *125*(6), e1278–e1285. https://doi.org/10.1542/peds.2009-3270

Gelman, A., Carlin, J. B., Stern, H. S., Dunson, D. B., Vehtari, A., & Rubin, D. B. (2013). *Bayesian Data Analysis, Third Edition*. CRC Press.

Gilpatrick, S. G., Schwab, K. J., Estes, M. K., & Atmar, R. L. (2000). Development of an immunomagnetic capture reverse transcription-PCR assay for the detection of Norwalk virus. *Journal of Viro-*

logical Methods, *90*(1), 69–78. https://doi.org/10.1016/s0166-0934(00)00220-2

Glass, R. I., Parashar, U. D., & Estes, M. K. (2009). Norovirus Gastroenteritis. *New England Journal of Medicine*, *361*(18), 1776–1785. https://doi.org/10.1056/NEJMra0804575
_eprint: https://doi.org/10.1056/NEJMra0804575

Grohskopf, L. A. (2021). Prevention and Control of Seasonal Influenza with Vaccines: Recommendations of the Advisory Committee on Immunization Practices, United States, 2021–22 Influenza Season. *MMWR. Recommendations and Reports*, *70*. https://doi.org/10.15585/mmwr.rr7005a1

Handel, A., Li, Y., McKay, B., Pawelek, K. A., Zarnitsyna, V., & Antia, R. (2018). Exploring the impact of inoculum dose on host immunity and morbidity to inform model-based vaccine design (M. P. Davenport, Ed.). *PLOS Computational Biology*, *14*(10), e1006505. https://doi.org/10.1371/journal.pcbi.1006505

Hilleman, M. R. (1958). Antibody response in volunteers to Asian influenza vaccine. *Journal of the American Medical Association*, *166*(10), 1134. https://doi.org/10.1001/jama.1958.02990100022005

Ho, D. E., Imai, K., King, G., & Stuart, E. A. (2007/ed). Matching as Nonparametric Preprocessing for Reducing Model Dependence in Parametric Causal Inference. *Political Analysis*, *15*(3), 199–236. https://doi.org/10.1093/pan/mpl013

Hoa Tran, T. N., Trainor, E., Nakagomi, T., Cunliffe, N. A., & Nakagomi, O. (2013). Molecular epidemiology of noroviruses associated with acute sporadic gastroenteritis in children: Global distribution of genogroups, genotypes and GII.4 variants. *Journal of Clinical Virology: The Official Publication of the Pan American Society for Clinical Virology*, *56*(3), 185–193. https://doi.org/10.1016/j.jcv.

2012.11.011

ZSCC: NoCitationData[s0]

Holder, B. P., & Beauchemin, C. A. (2011). Exploring the effect of biological delays in kinetic models of influenza within a host or cell culture. *BMC Public Health*, *11*(Suppl 1), S10. https://doi.org/10.1186/1471-2458-11-S1-S10

Isakbaeva, E. T., Widdowson, M.-A., Beard, R. S., Bulens, S. N., Mullins, J., Monroe, S. S., Bresee, J., Sassano, P., Cramer, E. H., & Glass, R. I. (2005). Norovirus Transmission on Cruise Ship. *Emerging Infectious Diseases*, *11*(1), 154–157. https://doi.org/10.3201/eid1101.040434

Johnson, P. C., Mathewson, J. J., DuPont, H. L., & Greenberg, H. B. (1990). Multiple-challenge study of host susceptibility to Norwalk gastroenteritis in US adults. *The Journal of Infectious Diseases*, *161*(1), 18–21. https://doi.org/10.1093/infdis/161.1.18

Johnston, C. P., Qiu, H., Ticehurst, J. R., Dickson, C., Rosenbaum, P., Lawson, P., Stokes, A. B., Lowenstein, C. J., Kaminsky, M., Cosgrove, S. E., Green, K. Y., & Perl, T. M. (2007). Outbreak Management and Implications of a Nosocomial Norovirus Outbreak. *Clinical Infectious Diseases*, *45*(5), 534–540. https://doi.org/10.1086/520666

Kavanagh, O., Estes, M. K., Reeck, A., Raju, R. M., Opekun, A. R., Gilger, M. A., Graham, D. Y., & Atmar, R. L. (2011). Serological Responses to Experimental Norwalk Virus Infection Measured Using a Quantitative Duplex Time-Resolved Fluorescence Immunoassay. *Clinical and Vaccine Immunology*, *18*(7), 1187–1190. https://doi.org/10.1128/CVI.00039-11

ZSCC: NoCitationData[s1]

Kirby, A. E., Streby, A., & Moe, C. L. (2016). Vomiting as a Symptom and Transmission Risk in Norovirus Illness: Evidence from Human

Challenge Studies. *PLOS ONE*, *11*(4), e0143759. https://doi.org/10.1371/journal.pone.0143759

Lee, J. K. H., Lam, G. K. L., Shin, T., Samson, S. I., Greenberg, D. P., & Chit, A. (2021). Efficacy and effectiveness of high-dose influenza vaccine in older adults by circulating strain and antigenic match: An updated systematic review and meta-analysis. *Vaccine*, *39*, A24–A35. https://doi.org/10.1016/j.vaccine.2020.09.004

Lee, N., Chan, M. C., Wong, B., Choi, K., Sin, W., Lui, G., Chan, P. K., Lai, R. W., Cockram, C., Sung, J. J., & Leung, W. K. (2007). Fecal Viral Concentration and Diarrhea in Norovirus Gastroenteritis. *Emerging Infectious Diseases*, *13*(9), 1399–1401. https://doi.org/10.3201/eid1309.061535

Li, Y., & Handel, A. (2014). Modeling inoculum dose dependent patterns of acute virus infections. *Journal of Theoretical Biology*, *347*, 63–73. https://doi.org/10.1016/j.jtbi.2014.01.008

Lozano, R., Naghavi, M., Foreman, K., Lim, S., Shibuya, K., Aboyans, V., Abraham, J., Adair, T., Aggarwal, R., Ahn, S. Y., AlMazroa, M. A., Alvarado, M., Anderson, H. R., Anderson, L. M., Andrews, K. G., Atkinson, C., Baddour, L. M., Barker-Collo, S., Bartels, D. H., … Murray, C. J. (2012). Global and regional mortality from 235 causes of death for 20 age groups in 1990 and 2010: A systematic analysis for the Global Burden of Disease Study 2010. *The Lancet*, *380*(9859), 2095–2128. https://doi.org/10.1016/S0140-6736(12)61728-0

ZSCC: NoCitationData[s1]

Matthews, J. E., Dickey, B. W., Miller, R. D., Felzer, J. R., Dawson, B. P., Lee, A. S., Rocks, J. J., Kiel, J., Montes, J. S., Moe, C. L., Eisenberg, J. N. S., & Leon, J. S. (2012). The epidemiology of published norovirus outbreaks: A review of risk factors associated with attack

rate and genogroup. *Epidemiology and Infection*, *140*(7), 1161–1172. https://doi.org/10.1017/S0950268812000234
ZSCC: NoCitationData[s2]

McElreath, R. (2020). *Statistical rethinking: A Bayesian course with examples in R and Stan* (Second). Taylor and Francis, CRC Press.

Nuñez, I. A., Carlock, M. A., Allen, J. D., Owino, S. O., Moehling, K. K., Nowalk, P., Susick, M., Diagle, K., Sweeney, K., Mundle, S., Vogel, T. U., Delagrave, S., Ramgopal, M., Zimmerman, R. K., Kleanthous, H., & Ross, T. M. (2017). Impact of age and pre-existing influenza immune responses in humans receiving split inactivated influenza vaccine on the induction of the breadth of antibodies to influenza A strains (V. C. Huber, Ed.). *PLOS ONE*, *12*(11), e0185666. https://doi.org/10.1371/journal.pone.0185666

O'Ryan, M. (2017). Rotavirus Vaccines: A story of success with challenges ahead. *F1000Research*, *6*, 1517. https://doi.org/10.12688/f1000research.11912.1

Patel, M. M., Widdowson, M.-A., Glass, R. I., Akazawa, K., Vinjé, J., & Parashar, U. D. (2008). Systematic literature review of role of noroviruses in sporadic gastroenteritis. *Emerging Infectious Diseases*, *14*(8), 1224–1231. https://doi.org/10.3201/eid1408.071114
ZSCC: 0001008

Paules, C. I., Sullivan, S. G., Subbarao, K., & Fauci, A. S. (2018). Chasing Seasonal Influenza — The Need for a Universal Influenza Vaccine. *New England Journal of Medicine*, *378*(1), 7–9. https://doi.org/10.1056/NEJMp1714916

Prior Choice Recommendations · stan-dev/stan Wiki. (n.d.).

R Core Team. (2020). *R: A language and environment for statistical computing*. Manual. R Foundation for Statistical Computing. Vienna, Austria.

Ramani, S., Neill, F. H., Ferreira, J., Treanor, J. J., Frey, S. E., Topham, D. J., Goodwin, R. R., Borkowski, A., Baehner, F., Mendelman, P. M., Estes, M. K., & Atmar, R. L. (2017). B-Cell Responses to Intramuscular Administration of a Bivalent Virus-Like Particle Human Norovirus Vaccine. *Clinical and Vaccine Immunology : CVI*, *24*(5), e00571–16. https://doi.org/10.1128/CVI.00571-16

Ranjeva, S., Subramanian, R., Fang, V. J., Leung, G. M., Ip, D. K. M., Perera, R. A. P. M., Peiris, J. S. M., Cowling, B. J., & Cobey, S. (2019). Age-specific differences in the dynamics of protective immunity to influenza. *Nature Communications*, *10*(1), 1660. https://doi.org/10.1038/s41467-019-09652-6

Reeck, A., Kavanagh, O., Estes, M. K., Opekun, A. R., Gilger, M. A., Graham, D. Y., & Atmar, R. L. (2010). Serological correlate of protection against norovirus-induced gastroenteritis. *The Journal of Infectious Diseases*, *202*(8), 1212–1218. https://doi.org/10.1086/656364

Regules, J. A., Cicatelli, S. B., Bennett, J. W., Paolino, K. M., Twomey, P. S., Moon, J. E., Kathcart, A. K., Hauns, K. D., Komisar, J. L., Qabar, A. N., Davidson, S. A., Dutta, S., Griffith, M. E., Magee, C. D., Wojnarski, M., Livezey, J. R., Kress, A. T., Waterman, P. E., Jongert, E., ... Vekemans, J. (2016). Fractional Third and Fourth Dose of RTS,S/AS01 Malaria Candidate Vaccine: A Phase 2a Controlled Human Malaria Parasite Infection and Immunogenicity Study. *The Journal of Infectious Diseases*, *214*(5), 762–771. https://doi.org/10.1093/infdis/jiw237

Rhodes, S. J., Knight, G. M., Kirschner, D. E., White, R. G., & Evans, T. G. (2019). Dose finding for new vaccines: The role for immunostimulation/immunodynamic modelling. *Journal of Theoretical Biology*, *465*, 51–55. https://doi.org/10.1016/j.jtbi.2019.01.017

Ruuska, T., & Vesikari, T. (1990). Rotavirus disease in Finnish children: Use of numerical scores for clinical severity of diarrhoeal episodes. *Scandinavian Journal of Infectious Diseases*, *22*(3), 259–267. https://doi.org/10.3109/00365549009027046

Scallan, E., Hoekstra, R. M., Angulo, F. J., Tauxe, R. V., Widdowson, M.-A., Roy, S. L., Jones, J. L., & Griffin, P. M. (2011). Foodborne Illness Acquired in the United States—Major Pathogens. *Emerging Infectious Diseases*, *17*(1), 7–15. https://doi.org/10.3201/eid1701.P11101
ZSCC: 0006210

Shim, D. H., Kim, D. Y., & Cho, K. Y. (2016). Diagnostic value of the Vesikari Scoring System for predicting the viral or bacterial pathogens in pediatric gastroenteritis. *Korean Journal of Pediatrics*, *59*(3), 126–131. https://doi.org/10.3345/kjp.2016.59.3.126

Team, R. C. (2017). R Core Team (2017). R: A language and environment for statistical computing. *R Found. Stat. Comput. Vienna, Austria. URL http://www. R-project. org/., page R Foundation for Statistical Computing*.

Teunis, P. F. M., Sukhrie, F. H. A., Vennema, H., Bogerman, J., Beersma, M. F. C., & Koopmans, M. P. G. (2015). Shedding of norovirus in symptomatic and asymptomatic infections. *Epidemiology and Infection*, *143*(8), 1710–1717. https://doi.org/10.1017/S095026881400274X
ZSCC: 0000124

Teunis, P. F. M., van Eijkeren, J. C. H., de Graaf, W. F., Marinović, A. B., & Kretzschmar, M. E. E. (2016). Linking the seroresponse to

infection to within-host heterogeneity in antibody production. *Epidemics*, *16*, 33–39. https://doi.org/10.1016/j.epidem.2016.04.001

Teunis, P. F., Moe, C. L., Liu, P., E. Miller, S., Lindesmith, L., Baric, R. S., Le Pendu, J., & Calderon, R. L. (2008). Norwalk virus: How infectious is it? *Journal of Medical Virology*, *80*(8), 1468–1476. https://doi.org/10.1002/jmv.21237
ZSCC: 0001020

Treanor, J. J., Atmar, R. L., Frey, S. E., Gormley, R., Chen, W. H., Ferreira, J., Goodwin, R., Borkowski, A., Clemens, R., & Mendelman, P. M. (2014). A novel intramuscular bivalent norovirus virus-like particle vaccine candidate–reactogenicity, safety, and immunogenicity in a phase 1 trial in healthy adults. *The Journal of Infectious Diseases*, *210*(11), 1763–1771. https://doi.org/10.1093/infdis/jiu337

Vega, E., Barclay, L., Gregoricus, N., Shirley, S. H., Lee, D., & Vinjé, J. (2014). Genotypic and epidemiologic trends of norovirus outbreaks in the United States, 2009 to 2013. *Journal of Clinical Microbiology*, *52*(1), 147–155. https://doi.org/10.1128/JCM.02680-13

Vehtari, A., Gelman, A., & Gabry, J. (2017). Practical Bayesian model evaluation using leave-one-out cross-validation and WAIC. *Statistics and Computing*, *27*(5), 1413–1432. https://doi.org/10.1007/s11222-016-9696-4

Wikswo, M. E., Cortes, J., Hall, A. J., Vaughan, G., Howard, C., Gregoricus, N., & Cramer, E. H. (2011). Disease Transmission and Passenger Behaviors during a High Morbidity Norovirus Outbreak on a Cruise Ship, January 2009. *Clinical Infectious Diseases*, *52*(9), 1116–1122. https://doi.org/10.1093/cid/cir144

YIN, X., GOUDRIAAN, J., LANTINGA, E. A., VOS, J., & SPIERTZ, H. J. (2003). A Flexible Sigmoid Function of Determinate Growth.

Annals of Botany, *91*(3), 361–371. https://doi.org/10.1093/aob/mcg029

Zarnitsyna, V. I., Akondy, R. S., Ahmed, H., McGuire, D. J., Zarnitsyn, V. G., Moore, M., Johnson, P. L. F., Ahmed, R., Li, K. W., Hellerstein, M. K., & Antia, R. (2021). Dynamics and turnover of memory CD8 T cell responses following yellow fever vaccination. *PLOS Computational Biology*, *17*(10), e1009468. https://doi.org/10.1371/journal.pcbi.1009468

APPENDIX A

APPENDIX: ANALYZING THE ASSOCIATION BETWEEN INOCULUM DOSE AND NOROVIRUS INFECTION OUTCOMES

A.1 Overview

This document contains detailed model description and additional results from our uncertainty analysis. It also describes how to reproduce all figures and tables shown in the main text and in this supplement.

A.2 Analysis of virus shedding

The following sections provide additional details and further results related to our analyses of virus shedding.

A.2.1 Accounting for limits of detection in virus shedding

The study that produced the data used two different methods to determine virus concentration in feces (Atmar et al., 2008). The first method was a quantitative real-time RT-PCR (qRT-PCR) method. This method was able to detect virus up to a limit of detection of 40×10^6 genomic equivalent copies (GEC). If a sample was below this level (negative qPCR reading), the sample was retested using an immunomagnetic capture (IMC) RT-PCR assay. IMC RT-PCR is more sensitive, with a lower limit of detection of 15×10^3 GEC, but only produces a qualitative positive or negative readout. We labeled the limit of 15×10^3 GEC as LOD1, and 40×10^6 as LOD2. Thus, virus samples have a numeric value if they are above LOD2, are labeled as positive if they are below LOD2 but above LOD1, and are labeled as negative if they are below LOD1.

We dealt with these detection limits as follows. If a sample had a quantitative concentration above 40×10^6 GEC, we used the numeric value. If a sample was reported as positive (concentration between 40×10^6 GEC and 15×10^3 GEC), we used the geometric mean of those two values ($\approx 7.75 \times 10^5$ GEC). Similarly, if a sample was recorded as negative (concentration below 15×10^3 GEC), we used the geometric mean of 15×10^3 GEC and 1 GEC (≈ 122 GEC).

To compute the total amount of virus shed per shedding event, we multiplied the virus concentration with the weight of the shed feces (i.e.,

GEC/g $\times$ weight of feces). Finally, for each individual, we summed values for all shedding events.

Data for vomiting had similar limits of detection. These data were recorded as either a numeric value above $2,200$ GEC, a positive readout below $2,200$ GEC or a negative readout. For the vomiting data, we did not have information on the limit of detection for the qualitative assay. Based on a comparison of the two methods (Gilpatrick et al., 2000), we made the assumption that the LOD for the qualitative assay was a factor of 10 lower, thus 220 GEC. We then again took the geometric mean of 2,200 GEC and 220 GEC for the positive values ($\approx$ 696 GEC), and 220 GEC and 1 GEC for the negative values ($\approx$ 15 GEC). All virus concentrations were then multiplied with total vomit volume (i.e., virus particles/ml $\times$ volume of vomit)), then summed those for each individual. This included making the additional assumption that 1 gram of vomit equated to 1 milliliter (Kirby et al., 2016).

To fit the time-series data of fecal virus shedding in our Bayesian non-linear mixed effects model, we used the built-in approach of 'brms' to handle censored values and deal with the limits of detection (Bürkner, 2018). In 'brms', the likelihood function uses a cumulative distribution function for censored data (Gelman et al., 2013).

A.2.2 Modeling total virus shedding

We computed total virus shedding by multiplying virus concentration with sample weight (feces) or volume (vomit) for each shedding event, and summing all values for each individual.

We applied a mixed effects model that investigated associations between the outcomes (total shedding amount) and inoculum dose. For the analysis shown in the main text, we assumed a linear relationship between the log of the dose (x_i) and the log of the outcome (y_i).

We fitted the same model to each of the 3 outcomes. Those are 1) fecal shedding during the 96 hours under clinical observation, 2) fecal shedding including the time at which individuals recorded shedding events at home, and 3) vomit shedding (which occurred only during the first 96 hours).

The mathematical definition of the model is as follows:

$$
\begin{aligned}
&\text{Likelihood:} \\
&\qquad y_i \sim \text{Normal}\,(\mu_i, \sigma) \\
&\text{Linear model:} \\
&\qquad \mu_i = \alpha_i + \beta\,(x_i - x^*) \\
&\text{Adaptive priors:} \\
&\qquad \alpha_i \sim \text{Normal}\,(\delta, \gamma) \\
&\text{Fixed priors:} \\
&\qquad \delta \sim \text{Normal}\,(25, 5) \\
&\qquad \gamma \sim \text{Half-Cauchy}\,(0, 2) \\
&\qquad \beta \sim \text{Normal}\,(0, 1) \\
&\qquad \sigma \sim \text{Half-Cauchy}\,(0, 2)
\end{aligned}
$$

The outcome of interest, y_i, is the total amount of virus shedding (in log units) of individual i. We assumed this value to be normally distributed with mean, μ_i, and an overall standard deviation, σ. The mean was assumed to have an individual-specific component and a dose-

dependent component. The parameter α_i describes the individual-level, dose-independent expected mean of the outcome for each individual, the parameter β encodes the potential impact of the dose, x_i, that the individual i received. To make priors easier to define and interpret, we subtracted the intermediate dose from the dose values, i.e. we set $x^* = \log(48)$. This adjustment implies that the parameter α_i represents the expected total amount of virus shedding when the inoculum dose is at this intermediate value. (Without subtraction of x^*, α_i would represent total shedding if the dose was zero, which is biologically not meaningful and makes assigning reasonable priors more difficult (McElreath, 2020).

Priors are chosen based on what we know about the virus kinetics, and to ensure prior predictive simulations produce flexible but reasonable outcomes (McElreath, 2020). Since vomit outcome values were lower than those for feces, we adjusted the α_i prior for this model to have a mean around 20.

As part of our sensitivity analyses, presented below, we also explored a model which treats dose as categorical. The following lines in the model are adjusted accordingly:

Linear model:

$$\mu_i = \alpha_i + \beta_{dose_i}$$

Adaptive priors:

$$\alpha_i \sim \text{Normal}\,(0, \gamma)$$

Fixed priors:

$$\gamma \sim \text{Half-Cauchy}\,(0, 2)$$

$$\beta_{dose_i} \sim \text{Normal}\,(25, 5)\,,$$

In this notation, the parameter β_{dose_i} takes on discrete values based on the dose level of each individual, i. Specifically, the 3 categories are low, medium, or high dose, corresponding to 4.8, 48, or 4800 RT-PCR units.

A.2.3 Modeling longitudinal virus concentration kinetics

To model the longitudinal time-series of virus concentration in feces, we used a previously developed equation that was shown to describe virus time-course in acute viral infections well (Holder and Beauchemin, 2011). This equation provides a good empirical function to fit the increase, then decrease of viral load seen in many acute viral infections. The equation has four parameters and is given by:

$$V(t) = \frac{2p}{e^{-g(t-T)} + e^{d(t-T)}}.$$

The outcome of interest is virus load as a function of time, $V(t)$. The model parameters approximately represent the peak virus load (p), the initial exponential growth rate (g), the time of virus peak (T) and the eventual rate of virus decline (d). (The parameters only approximately map to those biological quantities, see (Holder and Beauchemin, 2011) for details.)

Since all parameters in the model above need to be positive to achieve biologically reasonable trajectories for $V(t)$, we rewrote the equation for our purpose with exponentiated parameters. That is, we assume that the deterministic portion of the virus load data (on a log scale, denoted below as $\mu_{i,t}$), is described for each individual, i, by

$$\mu_{i,t} = \log\left(\frac{2\exp(p_i)}{e^{-\exp(g_i)(t_i-\exp(T_i))} + e^{\exp(d_i)(t_i-\exp(T_i))}}\right).$$

Since there was a fair amount of variability in the virus load data, we modeled the outcome using a non-standardized Student-t distribution instead of a Normal distribution, which provides more robust estimates in the presence of strong variability (Bürkner, 2018; McElreath, 2020). Specifically, we model the virus load data as

$$y_{i,t} \sim \text{Student-t}\left(k, \mu_{i,t}, \sigma\right),$$

where the standard deviation (σ) is modeled with a Half-Cauchy distribution, and the degrees of freedom (k) are modeled with a Gamma distribution with priors as shown in the equations below. We assumed that each of the four model parameters of the $\mu_{i,t}$ equation follow normal distributions, and can be described by linear models, each with an individual-level intercept parameter and a parameter quantifying the potential impact of dose. We again modeled the latter for our main analysis as being a linear function of the log of the dose. As described above, we again subtracted the intermediate dose to make the intercept parameters biologically meaningful. The model equations are given by:

Likelihood:

$$y_{i,t} \sim \text{Student}\,(k, \mu_{i,t}, \sigma)$$

Overall time-series equation:

$$\mu_{i,t} = \log\left(\frac{2\exp(p_i)}{e^{-\exp(g_i)(t_i-\exp(T_i))} + e^{\exp(d_i)(t_i-\exp(T_i))}}\right)$$

Parameter equations:

$$p_i = p_{0,i} + p_1 \cdot (x_i - x^*)$$

$$g_i = g_{0,i} + g_1 \cdot (x_i - x^*)$$

$$T_i = T_{0,i} + T_1 \cdot (x_i - x^*)$$

$$d_i = d_{0,i} + d_1 \cdot (x_i - x^*)$$

Adaptive priors:

$$p_{0,i} \sim \text{Normal}(\mu_p, \sigma_p)$$

$$g_{0,i} \sim \text{Normal}(\mu_g, \sigma_g)$$

$$T_{0,i} \sim \text{Normal}(\mu_T, \sigma_T)$$

$$d_{0,i} \sim \text{Normal}(\mu_d, \sigma_d)$$

Fixed priors:

$$\mu_p \sim \text{Normal}(25, 5)$$

$$\sigma_p \sim \text{Half-Cauchy}(0, 1)$$

$$\mu_g \sim \text{Normal}(3, 1)$$

$$\sigma_g \sim \text{Half-Cauchy}(0, 1)$$

$$\mu_T \sim \text{Normal}(0, 1)$$

$$\sigma_T \sim \text{Half-Cauchy}(0, 1)$$

$$\mu_d \sim \text{Normal}(-1, 0.5)$$

$$\sigma_d \sim \text{Half-Cauchy}(0, 1)$$

$$p_1 \sim \text{Normal}(0, 1)$$

$$g_1 \sim \text{Normal}(0, 0.5)$$

$$T_1 \sim \text{Normal}(0, 0.5)$$

$$d_1 \sim \text{Normal}(0, 0.5)$$

$$k \sim \text{Gamma}(2, 0.1)$$

$$\sigma \sim \text{Half-Cauchy}(0, 1)$$

Values for priors were chosen to be weakly informative, such that prior predictive simulations produced virus-load trajectories that made biological sense, while still allowing for a wide variety of possible trajectories to be informed by fitting to the data. The peak level of virus concentration for norovirus in our data and previous studies is broadly in the range of 10^{10} to 10^{14} (Atmar et al., 2008; N. Lee et al., 2007; P. F. M. Teunis et al., 2015) (around 23-35 in log units). We approximately centered our prior around those values, while allowing for a broad standard deviation so that the data will dominate the posterior results. Similarly, the growth rate, μ_g, will have a value such that the peak is reached within the first several days following infection. A Normal distribution with a mean of 3 (in log units) can produce the necessary range of value. Virus is expected to peak a few days following infection. Thus we chose μ_T and T_1 to have normal distributions with a spread such that the range of values for $\exp(T)$ is centered around the first few days. The decay rate, μ_d, needs to allow for a decline of virus to undetectable levels that can be as fast as a week or longer than a month. A Normal distribution with log-transformed mean of -1 can produce such outcomes.

We performed prior predictive simulations to ensure that our priors led to biologically reasonable time-series trajectories, while also being broad and flexible enough to let the data dominate the posterior distribution.

For the sensitivity analysis, where we treated dose as a categorical variable, the dose-associated parameters change and now are assigned distinct values based on dose category. The following components of the above model changed, with the rest remaining the same:

Parameter equations:

$$p_i = p_{0,i} + p_{1,dose_i}$$

$$g_i = g_{0,i} + g_{1,dose_i}$$

$$T_i = T_{0,i} + T_{1,dose_i}$$

$$d_i = d_{0,i} + d_{1,dose_i}$$

Adaptive priors:

$$p_{0,i} \sim \text{Cauchy}\,(0, \gamma_p)$$

$$p_{0,i} \sim \text{Cauchy}\,(0, \gamma_g)$$

$$p_{0,i} \sim \text{Cauchy}\,(0, \gamma_T)$$

$$p_{0,i} \sim \text{Cauchy}\,(0, \gamma_d)$$

Fixed priors:

$$\gamma_p \sim \text{Half-Cauchy}\,(0, 1)$$

$$\gamma_g \sim \text{Half-Cauchy}\,(0, 1)$$

$$\gamma_T \sim \text{Half-Cauchy}\,(0, 1)$$

$$\gamma_d \sim \text{Half-Cauchy}\,(0, 1)$$

$$p_{1,dose_i} \sim \text{Normal}(25, 5)$$

$$g_{1,dose_i} \sim \text{Normal}(3, 1)$$

$$T_{1,dose_i} \sim \text{Normal}(0, 1)$$

$$d_{1,dose_i} \sim \text{Normal}(-1, 0.5)$$

As before, in this categorical analysis, x_i is the dose category for individual i, and is either low, medium or high.

A.3 Analysis of symptom outcomes

The following sections provide additional details and further results related to our analyses of infection symptoms.

We considered three different symptom-related outcomes, namely time to first symptom onset (incubation period) and two versions of scores that quantify overall infection severity.

Since individuals were allowed to leave the study center after 96 hours and average illness duration primarily in the first a few days (Matthews et al., 2012), we calculated the scores based on records in the first 4 days.

A.3.1 Incubation period

Incubation period, i.e., the time between infection and onset of symptoms, was directly computed from the data as the time-span between reported time at which the infection challenge was administered, and the time at which the first symptom was reported.

A.3.2 Modified Vesikari score (MVS)

The modified Vesikari score (MVS) is a previously defined quantity that has been used in a modified form by several studies to measure norovirus severity (Atmar et al., 2011; Bierhoff et al., 2018; Freedman et al., 2010; Ruuska and Vesikari, 1990). The score has the seven components shown in Table A.1. For our data set, since volunteers were housed in a healthcare setting, the health care provider visit component was not applicable, and we thus removed it from the score calculation (Atmar et al., 2011). Since we did not have information on treatment, we also dropped that component.

This left us with a five-component score, which was computed for each individual following the rules shown in Table A.1.

Table A.1: Modifi ed vesikari score components

Components	Score = 0	Score = 1	Score = 2	Score = 3
C1: Diarrhea duration, days	0	1-4	5	≥ 6
C2: Maximum number of daily diarrheal stools	0	1-3	4-5	≥ 6
C3: Vomiting duration, days	0	1	2	≥ 3
C4: Maximum number of daily vomiting episodes	0	1	2-4	≥ 5
C5: Maximum recorded fever	Not Elevated	Moderate	Mild	Severe
Health care provider visits	N/A	N/A	N/A	N/A
Treatment	N/A	N/A	N/A	N/A

Table A.3 shows the scores for all 20 volunteers in the study that were part of our analyses.

Table A.2: Modifi ed vesikari score components

ID	Dose	C1	C2	C3	C4	C5	Total
1	0.48	0	3	1	1	1	6
2	4.8	0	1	1	1	2	5
3	4.8	0	0	0	1	1	2
4	4.8	1	3	1	1	2	8
5	4.8	0	1	2	1	2	6
6	4.8	0	1	1	0	0	2
7	4.8	0	1	1	0	0	2
8	48	0	1	2	0	0	3
9	48	0	3	1	0	0	4
10	48	1	0	0	0	0	1
11	48	2	1	1	1	1	6
12	48	1	3	1	1	3	9
13	48	0	1	1	1	1	4
14	48	0	3	1	0	0	4
15	4800	0	0	0	0	0	0
16	4800	0	3	1	0	0	4
17	4800	1	3	1	0	0	5
18	4800	0	1	3	1	1	6
19	4800	2	1	3	1	3	10
20	4800	0	1	2	1	2	6

A.3.3 Comprehensive symptom score (CSS)

In addition to the modified Vesikari score, we defined and computed a comprehensive symptom score which took all recorded symptoms into account.

The study reported the following symptoms: body temperature, malaise, muscle aches, headache, nausea, chills, anorexia, cramps, unformed or liquid feces, and vomiting. Clinical symptoms (except feces and vomiting) were reported as none, mild, moderate, or severe, which we coded as a score of 0 to 3. For feces, we used a scoring of solid = 0, unformed = 1, and liquid = 2. Vomit was reported as absent or present and scored as 0 or 1.

Individuals had their symptoms recorded at different times and frequencies throughout the day. Thus, summing up the recorded scores would have introduced bias due to different recording frequencies. Thus, we instead determined the highest score per symptom for each individual per day, and summed those. This produced a daily total symptom score for each individual. We then summed those to obtain our comprehensive symptom score. For example, if one individual had daily total symptom score values of 5 (1st day), 10 (2nd day), 2 (3rd day), and 0 (4th day), the final total symptom scores would be 17.

Table A.3 shows the daily and total comprehensive score values for the 20 individuals, Figure A.1 shows the same information in graphical form, stratified by dose.

Table A.3: Modifi ed vesikari score components

ID	Dose	Day1	Day2	Day3	Day4	Total
1	0.48	2	7	2	0	11
2	4.8	0	9	2	0	11
3	4.8	1	1	12	3	17
4	4.8	0	8	4	0	12
5	4.8	4	6	7	0	17
6	4.8	0	1	1	1	3
7	4.8	0	2	3	0	5
8	48	1	6	2	0	9
9	48	1	2	7	3	13
10	48	0	0	2	0	2
11	48	1	14	2	0	17
12	48	1	8	2	0	11
13	48	0	9	0	0	9
14	48	0	9	0	0	9
15	4800	1	6	2	0	9
16	4800	1	7	5	0	13
17	4800	0	6	13	2	21
18	4800	0	10	7	0	17
19	4800	1	14	13	3	31
20	4800	7	8	5	0	20

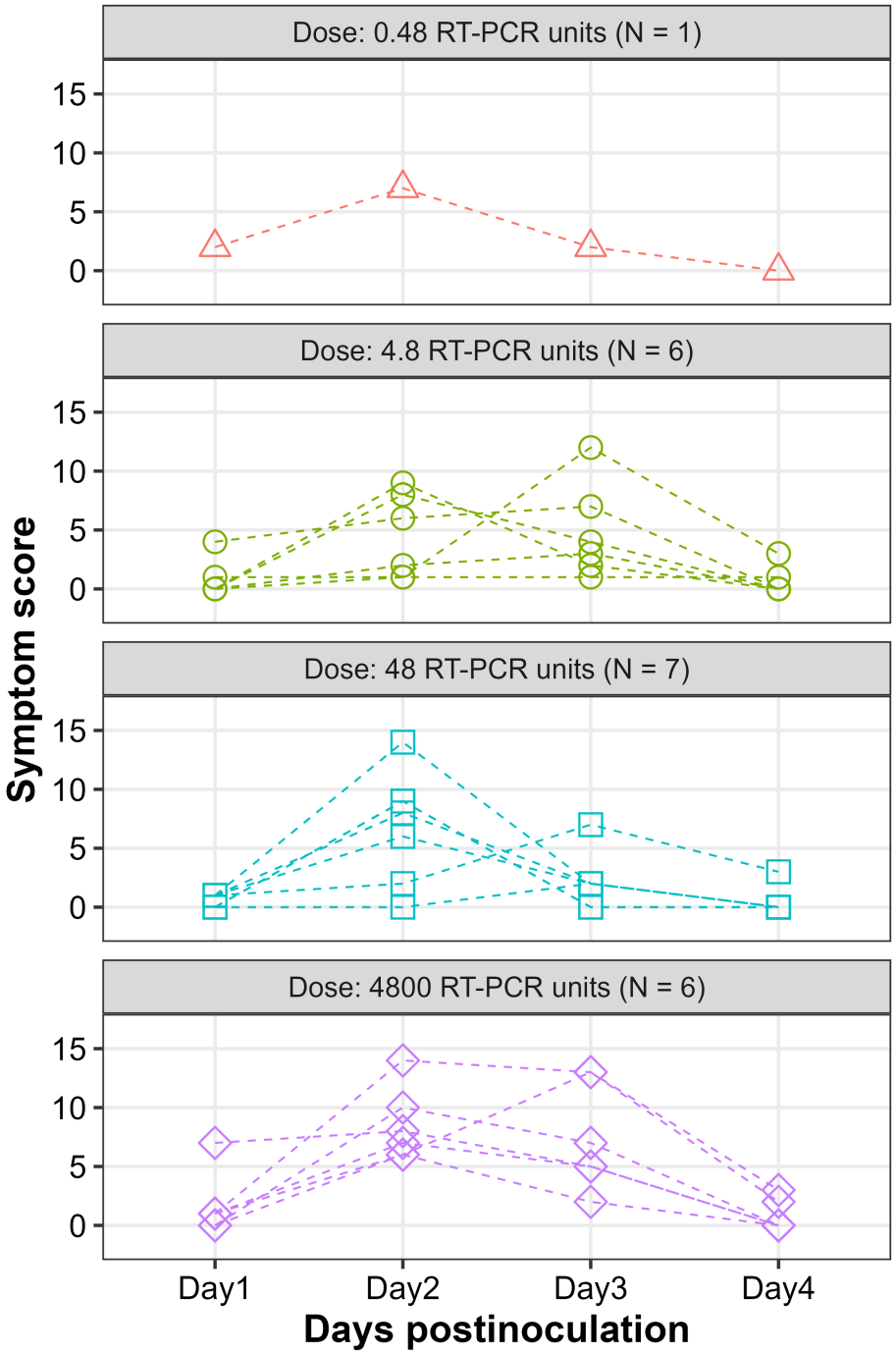

Figure A.1: Daily comprehensive symptom score stratified by inoculum dose group.

A.3.4 Modeling symptom outcomes

The incubation period is positive and not too far from zero (as measured in days). Thus, to prevent any possible negative outcomes, we assumed it followed a log-normal distribution. The rest of the model is similar to those implemented for the total shedding outcomes, with the full model is given below.

$$
\begin{aligned}
\text{Likelihood:} \\
Y_i &\sim \text{Log-Normal}\left(\mu_i, \sigma\right) \\
\text{Linear model:} \\
\exp(\mu_i) &= \alpha_i + \beta\left(x_i - x^*\right) \\
\text{Adaptive priors:} \\
\alpha_i &\sim \text{Normal}\left(\delta, \gamma\right) \\
\text{Fixed priors:} \\
\delta &\sim \text{Normal}\left(1, 5\right) \\
\gamma &\sim \text{Half-Cauchy}\left(0, 2\right) \\
\beta &\sim \text{Normal}\left(0, 1\right) \\
\sigma &\sim \text{Half-Cauchy}\left(0, 2\right),
\end{aligned}
$$

As we did for the total shedding outcomes, the model was adjusted for the categorical dose sensitivity analysis as follows.

Linear model:

$$\exp(\mu_i) = \alpha_i + \beta_{dose_i}$$

Adaptive priors:

α prior: $\alpha_i \sim \text{Normal}(0, \gamma)$

Fixed priors:

$$\gamma \sim \text{Half-Cauchy}(0, 2)$$

$$\beta_{dose_i} \sim \text{Normal}(1, 5)$$

We used the same overall model structure for the MSV and CSS outcomes. However, we modeled these outcomes using a Gamma-Poisson distribution (also called negative binomial distribution) for the likelihood, since both scores are non-negative integer-valued. The Gamma-Poisson model allows for additional variance (also called overdispersion) compared to a Poisson distribution. The variance is determined by the ϕ parameter, and the rate λ is similar to the rate of an ordinary Poisson distribution. We use the customary log-link for λ, and model its functional relationship with dose as above with an individual-level intercept and a dose-specific component, linearly dependent on the log of the dose. The model is given by the following set of equations.

Likelihood:

$$y_i \sim \text{Gamma-Poisson}\,(\lambda_i, \phi)$$

Linear model:

$$\log(\lambda_i) = \alpha_i + \beta\,(x_i - x^*)$$

Adaptive priors:

$$\alpha_i \sim \text{Normal}\,(\delta, \gamma)$$

Fixed priors:

$$\delta \sim \text{Normal}\,(1, 5)$$

$$\gamma \sim \text{Half-Cauchy}\,(0, 2)$$

$$\beta \sim \text{Normal}\,(0, 1)$$

$$\phi \sim \text{Half-Cauchy}\,(0, 2)$$

Values for the prior distributions were again chosen to ensure reasonable prior predictive results for the outcomes. To model dose as a categorial variable, we changed the following parts of the model.

Linear model:

$$\log(\lambda_i) = \alpha_i + \beta_{dose_i}$$

Adaptive priors:

$$\alpha_i \sim \text{Normal}\,(0, \gamma)$$

Fixed priors:

$$\gamma \sim \text{Half-Cauchy}\,(0, 2)$$

$$\beta_{dose_i} \sim \text{Normal}\,(1, 5)$$

A.4 Results from additional analyses

A.4.1 Vomit events

In each dose group, only a few individuals had vomiting events. Some of these individuals had multiple vomiting events. Figure A.2 graphically displays the vomiting event data. The recorded vomiting events were not sufficient to allow for a time-series analysis similar to the model we applied to the fecal shedding data.

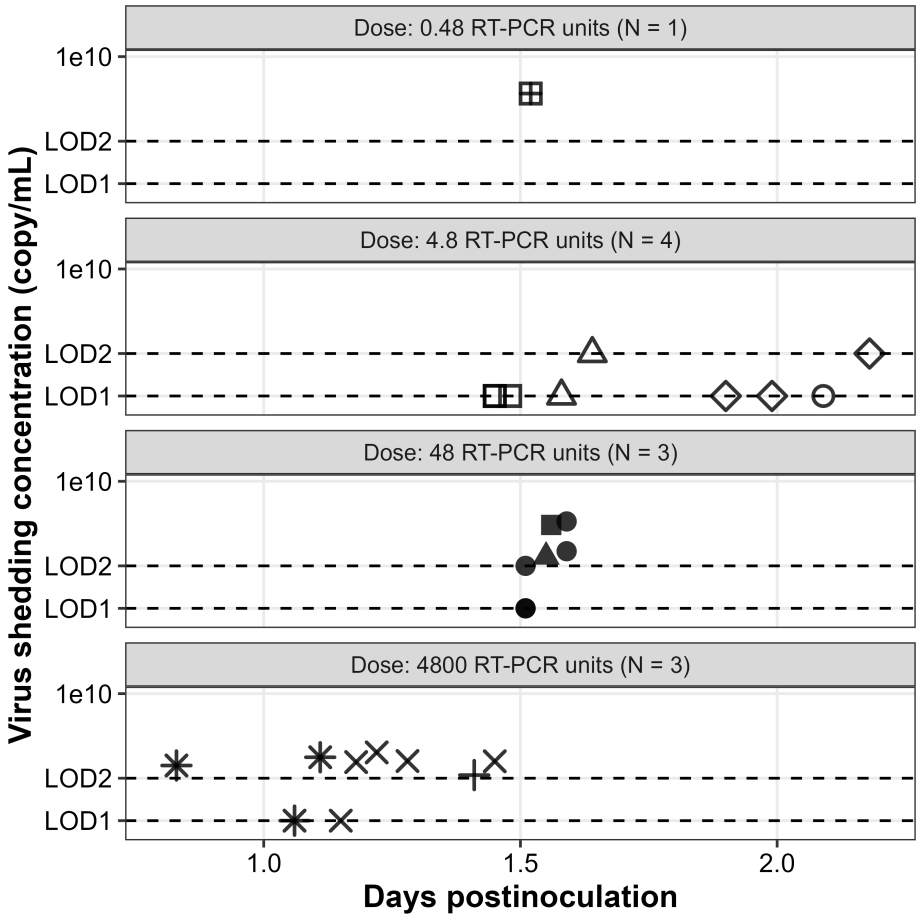

Figure A.2: Daily comprehensive symptom score stratified by inoculum dose group.

A.4.2 Analyses with dose as a categorical variable

The following figures repeat the analyses and results shown in the main text, but now with dose treated as categorical.

Assessing association of total virus shedding with dose

Figure A.3 shows data and model estimates for total shedding for each dose category, where low/medium/high indicate dose levels of 4.8, 48, and 4800 RT-PCR units. The overall pattern is similar to the one we found for the continuous analysis presented in the main text.

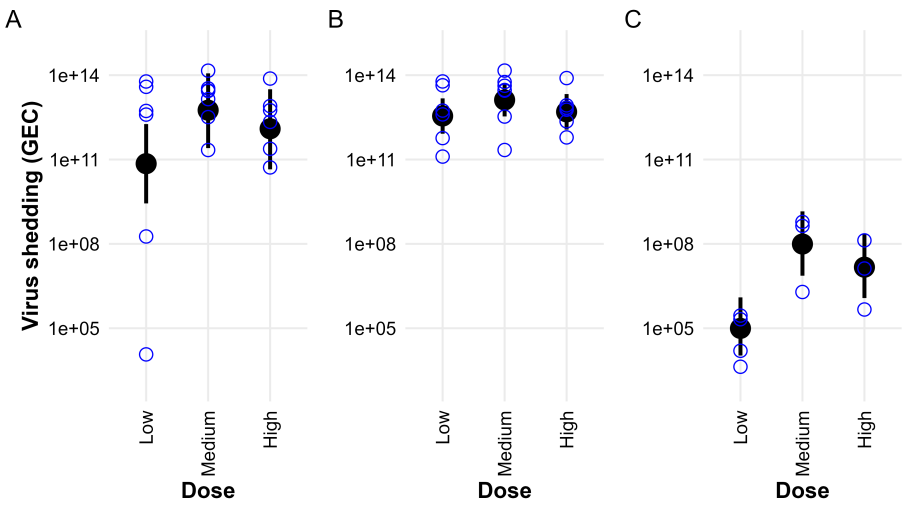

Figure A.3: Virus shedding in feces or vomit. The bars show 89% equal-tailed credible intervals (CI). Points with circle shape are raw data. A) Fecal virus shedding in the first 96 hours. B) Fecal virus shedding with all data. C) Vomit virus shedding. The points show mean of estimations.

Modeling of virus concentration in feces

Figures A.4 - A.6 show data and model estimates for the longitudinal time-series analysis of the virus concentration in feces, with dose now treated as

categorical (low, medium, or high). Again, the overall observed patterns are similar to the ones we found for the continuous analysis presented in the main text.

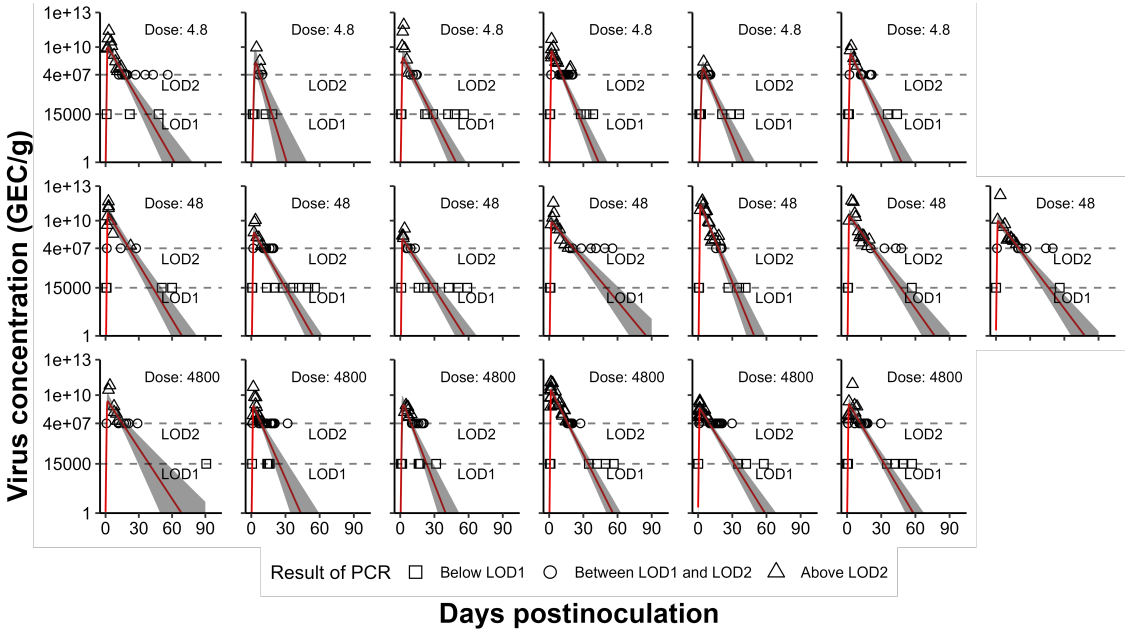

Figure A.4: Fitted fecal virus concentration curves. The red lines show means of estimations. The grey areas show 89% equal-tailed credible intervals (CI). LOD1 and LOD2 indicate the two limits of detection. Points with triangle shape represented samples that with positive qRT-PCR results. Points with circle shape represented samples with positive IMC and negative qRT-PCR results. Points with square shape represented samples with negative IMC and negative qRT-PCR results.

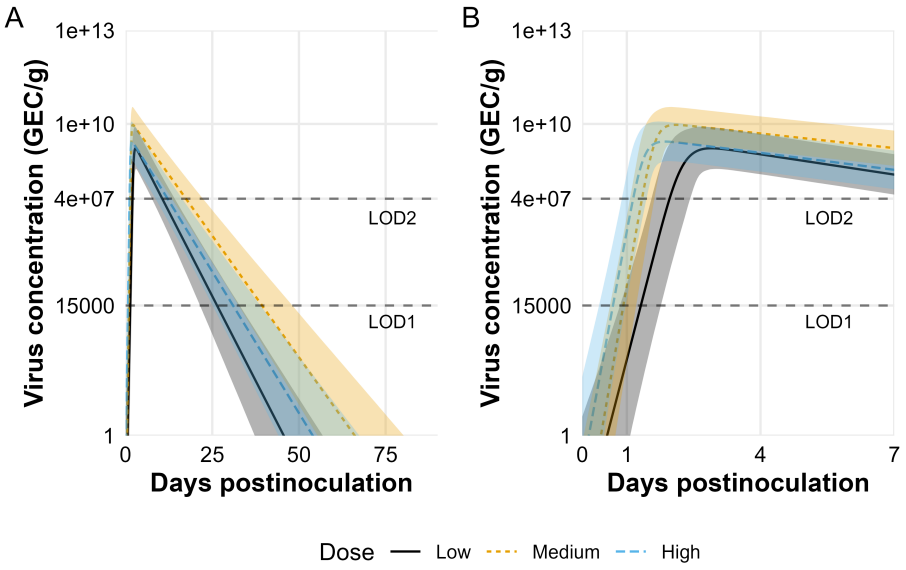

Figure A.5: Fitted virus concentration (GEC/g) in feces. The lines show means of estimations. The colored areas show 89% equal-tailed credible intervals (CI). LOD1 and LOD2 represent the two limits of detection. A) The fitted curves for 90 days. B) The fitted curves for the first 7 days.

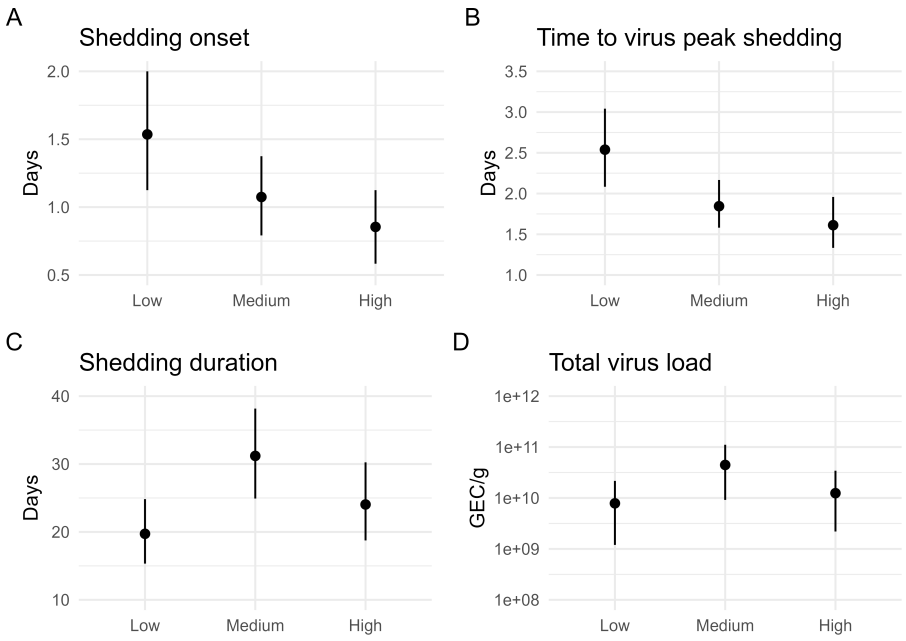

Figure A.6: Model predictions for viral kinetics as a function of inoculum dose. The points show means of estimations. The bars show 89% equal-tailed credible intervals (CI). A) Time to detection (above 15,000 GEC). B) Time to peak. C) Shedding duration (period that virus concentration above 15,000 GEC). D) Total virus load (area under concentration curve).

Assessing association of symptoms with dose

Figure A.7 shows data and model estimates for the different symptom outcomes for each dose category. Again, the patterns seen are similar to those shown in the main text. One difference is that the comprehensive score only increases for the highest dose group, while the two lower groups are similar.

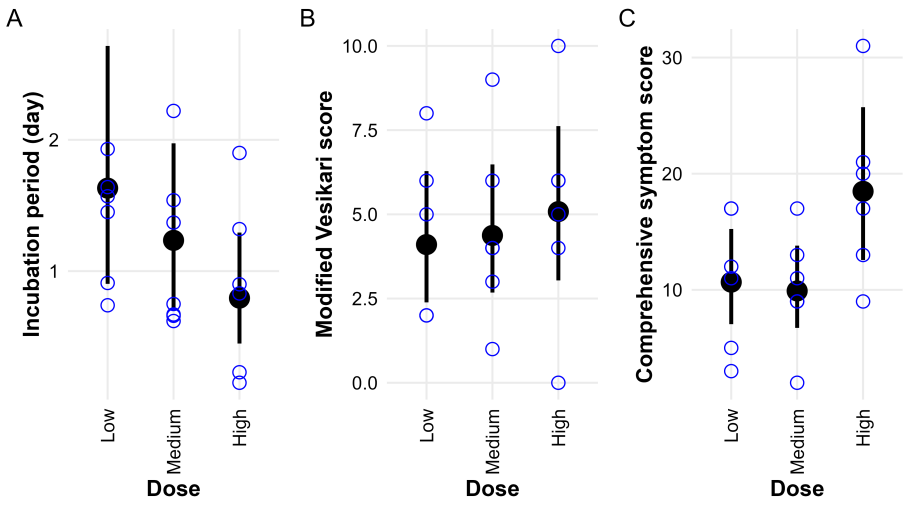

Figure A.7: Estimated dose impact on symptoms. The points show means of estimations. The bars show 89% equal-tailed credible intervals (CI). Points with circle shape are raw data.

A.4.3 Analyses that includes additional very-low dose infected individual

As explained in the main text, the original study also administered a dose of 0.48 RT-PCR units. At that dose level, only a single challenged individual became infected. We removed this person for the analysis presented in the main text. However, we also decided to conduct a sensitivity analysis that re-computes all results shown in the main text, now with the additional individual included.

Assessing association of total virus shedding with dose

Comparison of this figure with the one shown in the main text shows overall similar results.

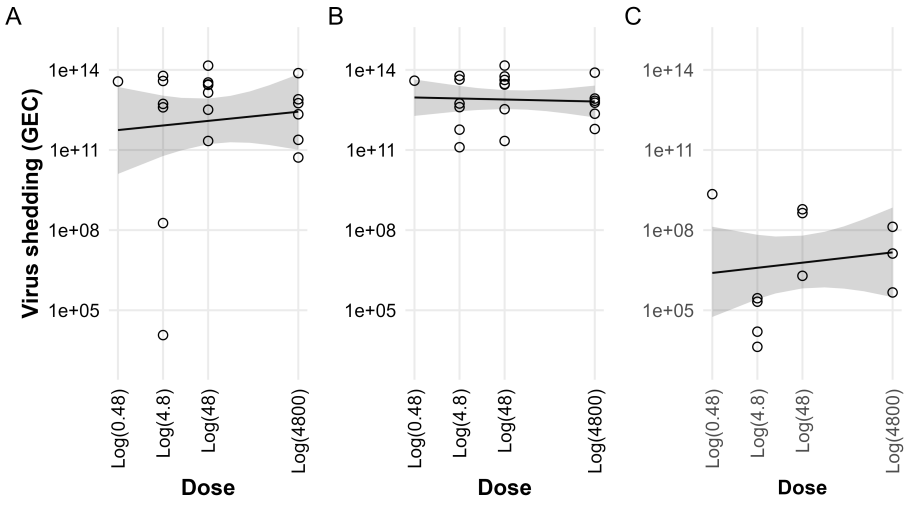

Figure A.8: Virus shedding in feces or vomit. A) Total fecal virus shedding in the first 96 hours. B) Total fecal virus shedding with all data. C) Total vomit virus shedding. The lines show means of estimations. The grey areas show 89% equal-tailed credible intervals (CI). Points with circle shape are raw data.

Modeling of virus concentration in feces

As Figures A.9 - A.11 show, the findings remain essentially unchanged for these outcomes compared to what is shown in the main text.

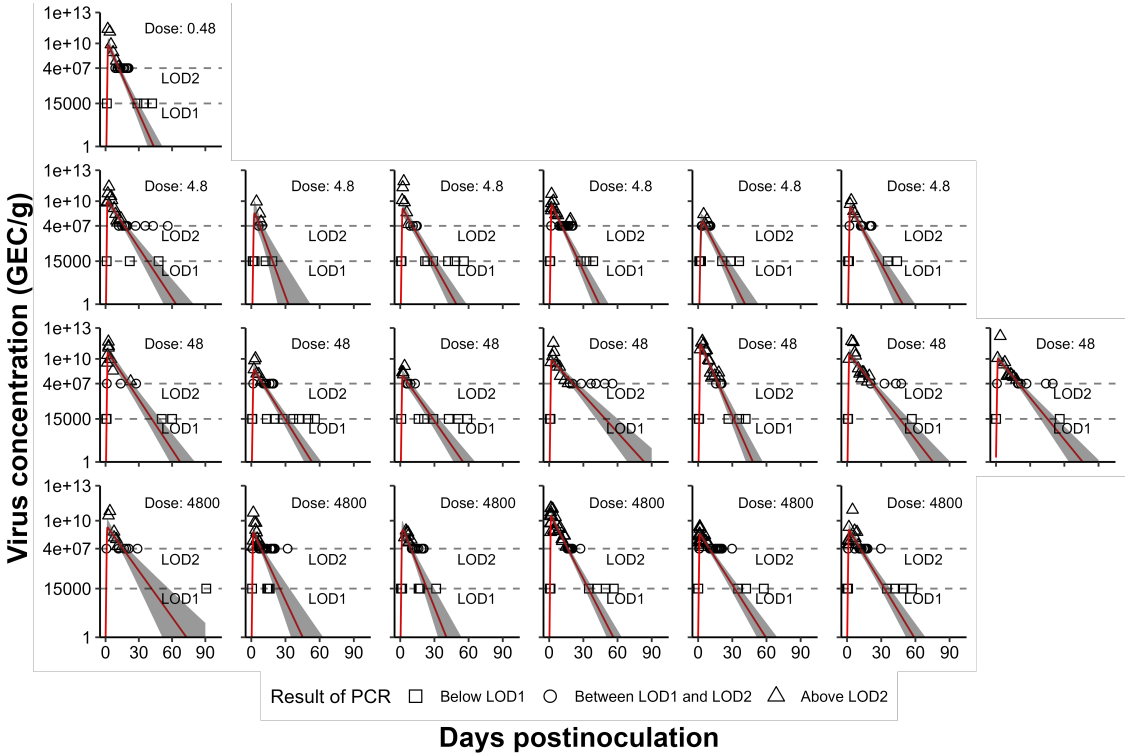

Figure A.9: Fitted fecal virus concentration curves. The red lines show means of estimations. The grey areas show 89% equal-tailed credible intervals (CI). LOD1 and LOD2 indicate the two limits of detection. Points with triangle shape represent samples that are positive for qRT-PCR. Points with circle shape represented samples that are positive for IMC and negative for qRT-PCR. Points with square shape represented samples that are negative for IMC and negative for qRT-PCR.

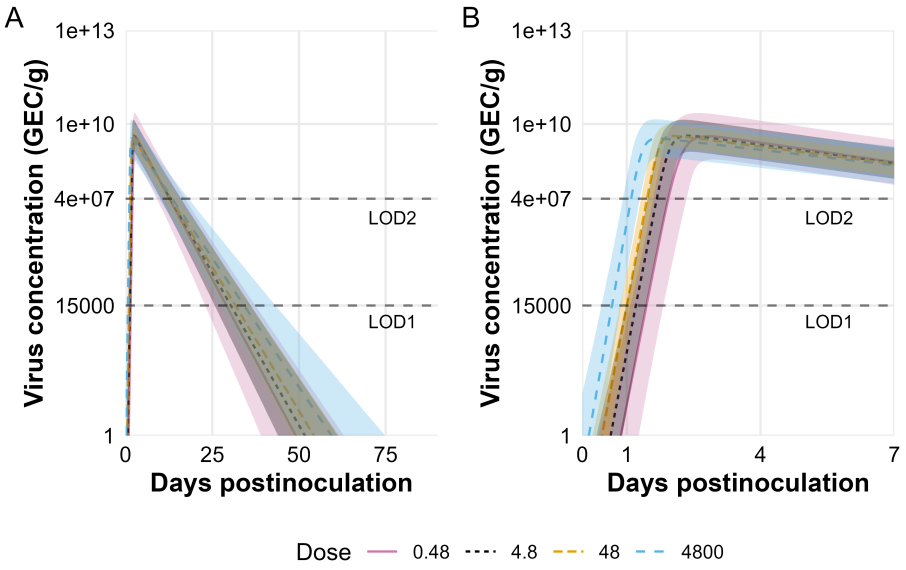

Figure A.10: Fitted virus concentration (GEC/g) in feces. The lines show means of estimations. The colored areas show 89% equal-tailed credible intervals (CI). LOD1 and LOD2 represent the two limits of detection. A) The fitted curves for 90 days. B) The fitted curves for the first 7 days.

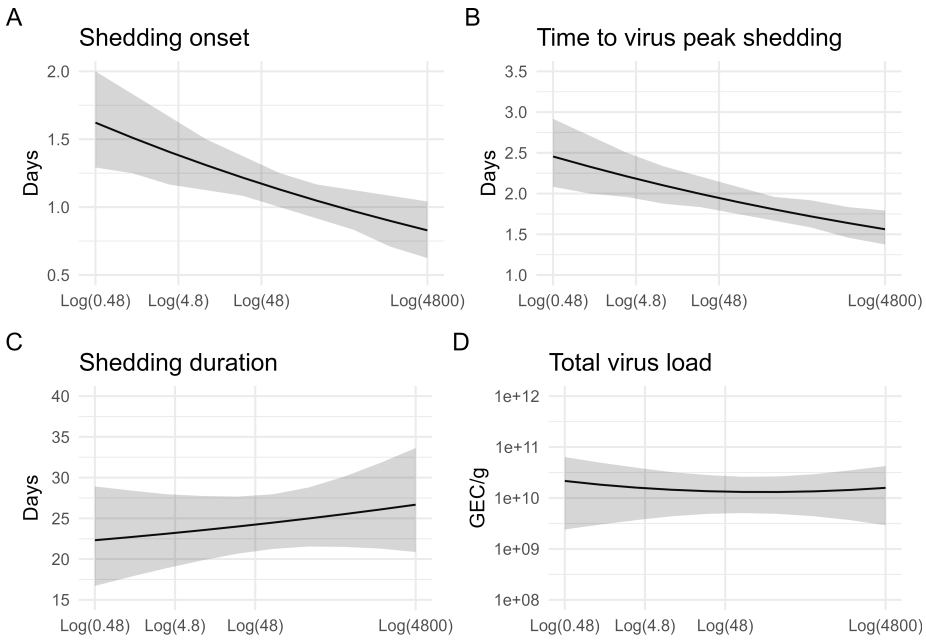

Figure A.11: Model predictions for viral kinetics as a function of inoculum dose. The lines show means of estimations. The grey areas show 89% equal-tailed credible intervals (CI). A) Time to detection (above $15,000$ GEC). B) Time to peak. C) Shedding duration (period that virus concentration above $15,000$ GEC). D) Total virus load (area under curve).

Assessing association of symptoms with dose

As figure A.12 shows, the association between dose and symptom outcomes also remains essentially unchanged when including the additional individual in the analysis.

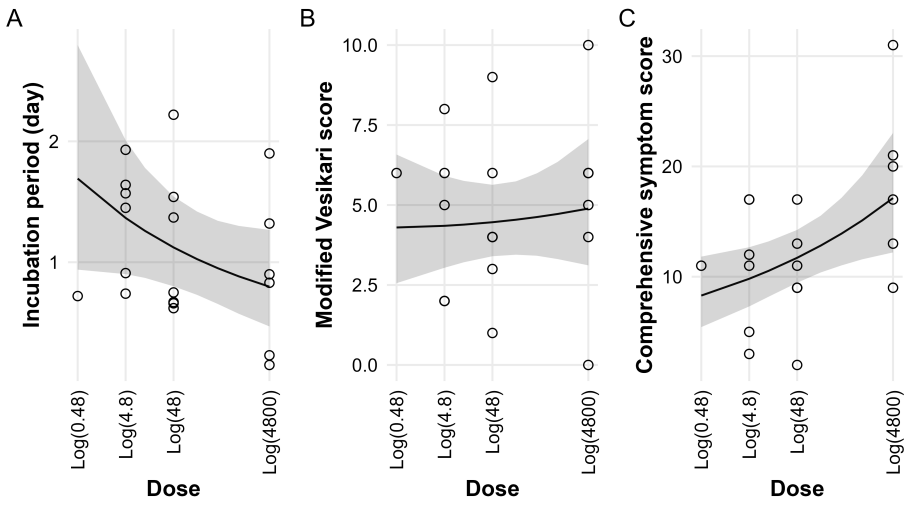

Figure A.12: Estimated dose impact on symptoms. The lines show means of estimations. The grey areas show 89% equal-tailed credible intervals (CI). Points with circle shape are raw data.

A.4.4 Categorical analyses that includes additional very-low dose infected individual

Neither the sensitivity analysis treating dose as categorical, nor the sensitivity analysis including the additional individual in the continuous analysis showed any discernible differences from the analyses shown in the main text. We thus decided to omit what would be yet one more sensitivity analysis of all 20 individuals with categorical dose.

APPENDIX B

APPENDIX: NOROVIRUS ANTIBODY KINETICS COMPARISONS BETWEEN INFECTION AND VACCINATION

B.1 Overview

This document contains detailed model description. It also describes all additional supplementary material needed to reproduce all figures and tables shown in the main text and in this supplement.

B.2 Accounting for limits of detection

In the human challenge study, the HBGA antibody had a limit of detection (< 25), and the IgA and IgG had limits of detection with 1.6 ug/ml and 1.4 ug/ml, respectively (Atmar et al., 2014; Kavanagh et al., 2011; Reeck et al., 2010). We found similar settings of limits of detection in the vaccine candidate study because of the same antibody assays to the human challenge study (Ramani et al., 2017; Treanor et al., 2014). Follow the setting in previous studies, we coded these values as 12.5, 0.8 ug/ml, and 0.7 ug/ml for analyses (Atmar et al., 2014; Kavanagh et al., 2011; Reeck et al., 2010).

B.3 Modeling antibodies kinetics

To model the longitudinal time-series of serum antibodies, we used a empirical equation contains two parts. The first part was used to model the increase of antibody. The second part was used to model the decay.

The equation for the increase of antibody is given by

$$\frac{P}{1+\exp\Big(G\cdot(t-T)\Big)}.$$

It is similar to a Sigmoid function (Bacaër, 2011; YIN et al., 2003). The outcome of interest is the level of antibody as a function of time, $y(t)$. The model parameters approximately represent the peak level (P), the speed of growth (G), the timing of middle point of the curve (T).

All parameters in the model above need to be positive to achieve biologically reasonable trajectories for $y(t)$, we rewrote the equation with

exponentiated parameters and assumed that the antibody data (on a log scale, denoted below as $\mu_{i,t}$), is described for each individual, i, by

$$\mu_{i,t} = \frac{\exp(p_i)}{1+\exp\Big(\exp(g_i)\cdot(t-\exp(T_i))\Big)}.$$

Since our limited sample size, to account for variability, we modeled the outcome using a Student-t distribution, which provides more robust estimates (Bürkner, 2018; McElreath, 2020).

$$y_{i,t} \sim \text{Student-t}\,(k, \mu_{i,t}, \sigma)\,,$$

where the standard deviation (σ) is modeled with a Half-Cauchy distribution, and the degrees of freedom (k) are modeled with a Gamma distribution with priors as shown in the equations below.

For the decay part, we implemented two methods, Exponential and Power-law (Cohen et al., 2021; de Graaf et al., 2014; P. F. M. Teunis et al., 2016). Both methods were used to study antibody kinetic (P. F. M. Teunis et al., 2016). The exponential models used a fixed decay rate to measure the average speed of waning immunity (de Graaf et al., 2014). The Power-law models has a time depended decay rate (Cohen et al., 2021; P. F. M. Teunis et al., 2016; Zarnitsyna et al., 2021). The equations of two methods are given by

$$\text{Exponential decay: } \exp\Big(D\cdot t\Big),$$

$$\text{Power-law decay: } t^{-\exp(D)},$$

where the decay rate (D) controls the speed of antibody decay by time (t).

We also implemented exponentiated parameters and assumed that the antibody decay is described for each individual, i, by

$$\exp\Big(-exp(d_i)\cdot t\Big),$$

$$t^{-\exp(d_i)},$$

Exponential decay model

Likelihood:

$$y_{i,t} \sim \text{Student}\,(k, \mu_{i,t}, \sigma)$$

Ttime-series:

$$\mu_{i,t} = \log\left(\frac{\exp(p_i)}{1+\exp\Big(-\exp(g_i)\cdot(t-\exp(T_i))\Big)}\cdot\exp\Big(-exp(d_i)\cdot t\Big)\right)$$

Parameter:

$$p_i = p_{0,i} + p_{1,dose_i}$$

$$g_i = g_{0,i} + g_{1,dose_i}$$

$$T_i = T_{0,i} + T_{1,dose_i}$$

$$d_i = d_{0,i} + d_{1,dose_i}$$

Adaptive priors:

$$p_{0,i} \text{ prior: } \; p_{0,i} \sim \text{Cauchy}\,(0, \gamma_p)$$

$$g_{0,i} \text{ prior: } \; g_{0,i} \sim \text{Cauchy}\,(0, \gamma_g)$$

$$T_{0,i} \text{ prior: } \; T_{0,i} \sim \text{Cauchy}\,(0, \gamma_T)$$

$$d_{0,i} \text{ prior: } \; d_{0,i} \sim \text{Cauchy}\,(0, \gamma_d)$$

Fixed priors:

$$\gamma_p \text{ prior: } \; \gamma_p \sim \text{Half-Cauchy}\,(0, 1)$$

$$\gamma_g \text{ prior: } \; \gamma_g \sim \text{Half-Cauchy}\,(0, 1)$$

$$\gamma_T \text{ prior: } \; \gamma_T \sim \text{Half-Cauchy}\,(0, 1)$$

$$\gamma_d \text{ prior: } \; \gamma_d \sim \text{Half-Cauchy}\,(0, 1)$$

$$p_{1,dose_i} \text{ prior: } \; p_{1,dose_i} \sim \text{Normal}(0, 10)$$

$$g_{1,dose_i} \text{ prior: } \; g_{1,dose_i} \sim \text{Normal}(0, 10)$$

$$T_{1,dose_i} \text{ prior: } \; T_{1,dose_i} \sim \text{Normal}(0, 10)$$

$$d_{1,dose_i} \text{ prior: } \; d_{1,dose_i} \sim \text{Normal}(0, 10)$$

$$k \text{ prior: } \; k \sim \text{Gamma}(\text{shape} = 2, \text{rate} = 0.1)$$

$$\sigma \text{ prior: } \; \sigma \sim \text{Half-Cauchy}(0, 1),$$

Values for priors were chosen to be weakly informative. The peak level of antibody values in the range of 10^1 to 10^5 (Kavanagh et al., 2011; Reeck et al., 2010; Treanor et al., 2014) (around 2-12 in log units). The growth rate will have a value such that the peak is reached within the first several weeks. The half of peak value also should within the first several weeks. The decay speed needs to allow for a slow decline. Therefore, we used wide normal distributions for these parameters, with a mean of 0 and a deviation of 10 (in log units).

Power-law decay model

Likelihood:

$$y_{i,t} \sim \text{Student}\,(k, \mu_{i,t}, \sigma)$$

Time-series:

$$\mu_{i,t} = \log\left(\frac{\exp(p_i)}{1+\exp\Big(-\exp(g_i)\cdot(t-\exp(T_i))\Big)}\cdot t^{-\exp(d_i)}\right)$$

Parameter:

$$p_i = p_{0,i} + p_{1,dose_i}$$

$$g_i = g_{0,i} + g_{1,dose_i}$$

$$T_i = T_{0,i} + T_{1,dose_i}$$

$$d_i = d_{0,i} + d_{1,dose_i}$$

Adaptive priors:

$$p_{0,i} \text{ prior: } \; p_{0,i} \sim \text{Cauchy}\,(0, \gamma_p)$$

$$g_{0,i} \text{ prior: } \; g_{0,i} \sim \text{Cauchy}\,(0, \gamma_g)$$

$$T_{0,i} \text{ prior: } \; T_{0,i} \sim \text{Cauchy}\,(0, \gamma_T)$$

$$d_{0,i} \text{ prior: } \; d_{0,i} \sim \text{Cauchy}\,(0, \gamma_d)$$

Fixed priors:

$$\gamma_p \text{ prior: } \; \gamma_p \sim \text{Half-Cauchy}\,(0, 1)$$

$$\gamma_g \text{ prior: } \; \gamma_g \sim \text{Half-Cauchy}\,(0, 1)$$

$$\gamma_T \text{ prior: } \; \gamma_T \sim \text{Half-Cauchy}\,(0, 1)$$

$$\gamma_d \text{ prior: } \; \gamma_d \sim \text{Half-Cauchy}\,(0, 1)$$

$$p_{1,dose_i} \text{ prior: } \; p_{1,dose_i} \sim \text{Normal}(0, 10)$$

$$g_{1,dose_i} \text{ prior: } \; g_{1,dose_i} \sim \text{Normal}(0, 10)$$

$$T_{1,dose_i} \text{ prior: } \; T_{1,dose_i} \sim \text{Normal}(0, 10)$$

$$d_{1,dose_i} \text{ prior: } \; d_{1,dose_i} \sim \text{Normal}(0, 10)$$

$$k \text{ prior: } \; k \sim \text{Gamma}(\text{shape} = 2, \text{rate} = 0.1)$$

$$\sigma \text{ prior: } \; \sigma \sim \text{Half-Cauchy}(0, 1),$$

Values for priors were chosen similar to the model with exponential decay.

B.3.1 Additional results

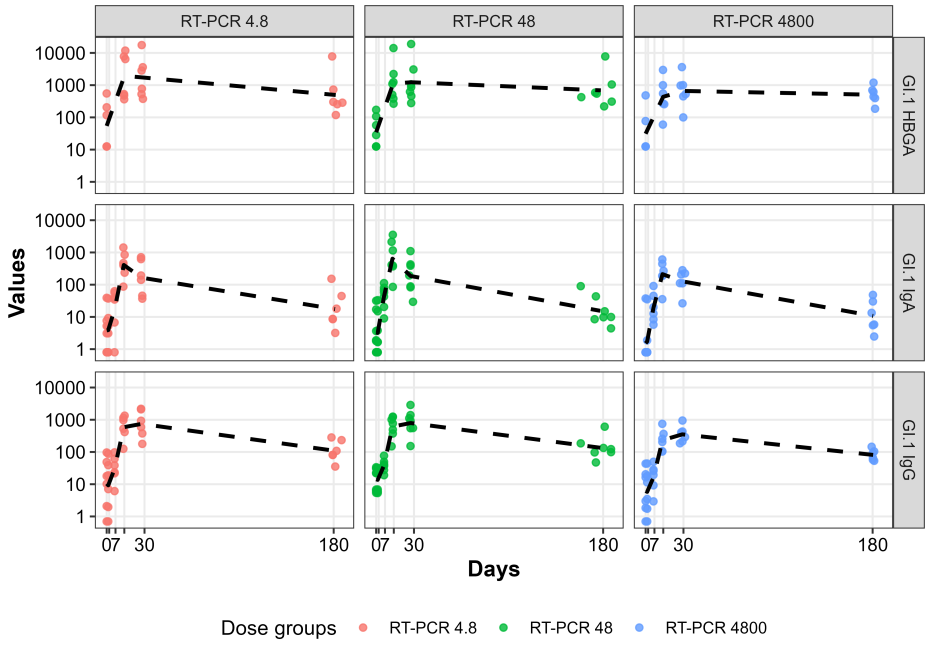

Figure B.1: Description of serum antibodies in the HC study.

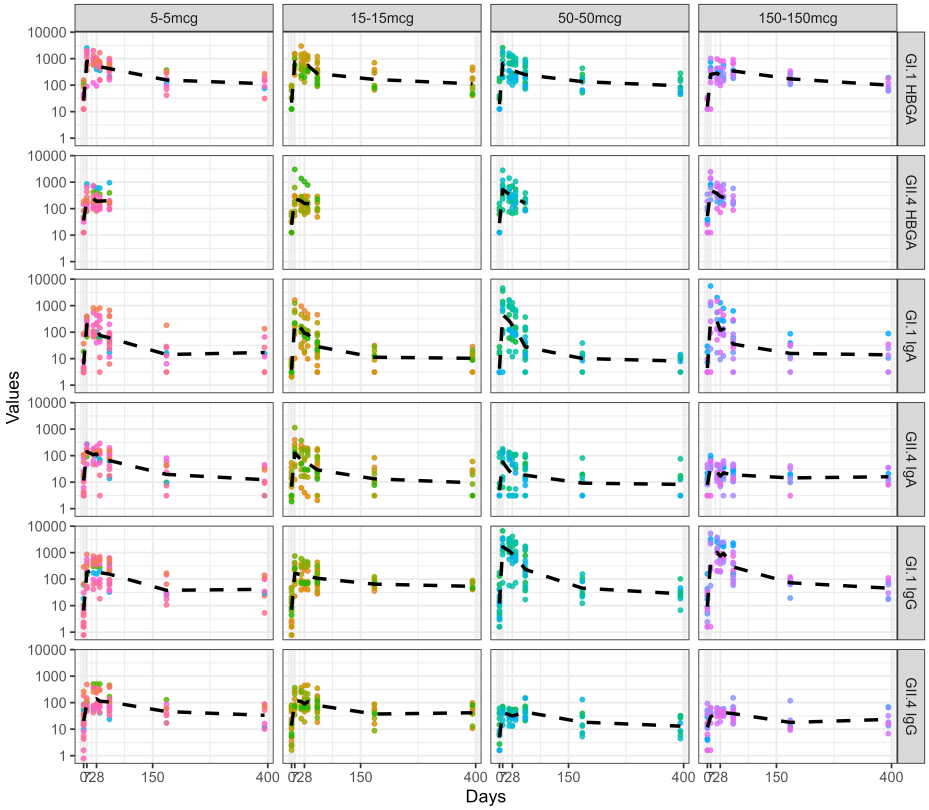

Figure B.2: Description of serum antibodies in the HV study.

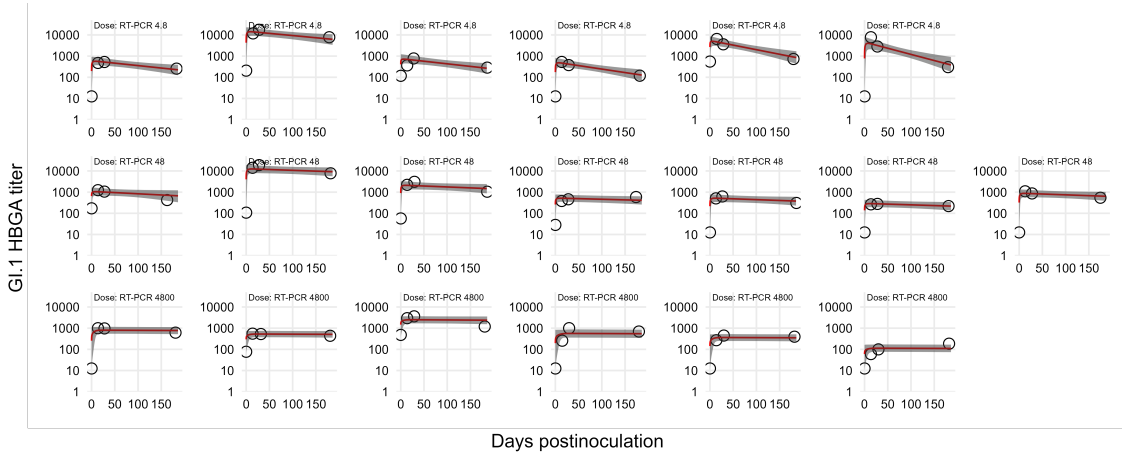

Figure B.3: Fitted individual kinetics of GI.1 HBGA antibody in the HC study (Exponential decay). The lines show means of estimations. The colored areas show 89% equal-tailed credible intervals (CI).

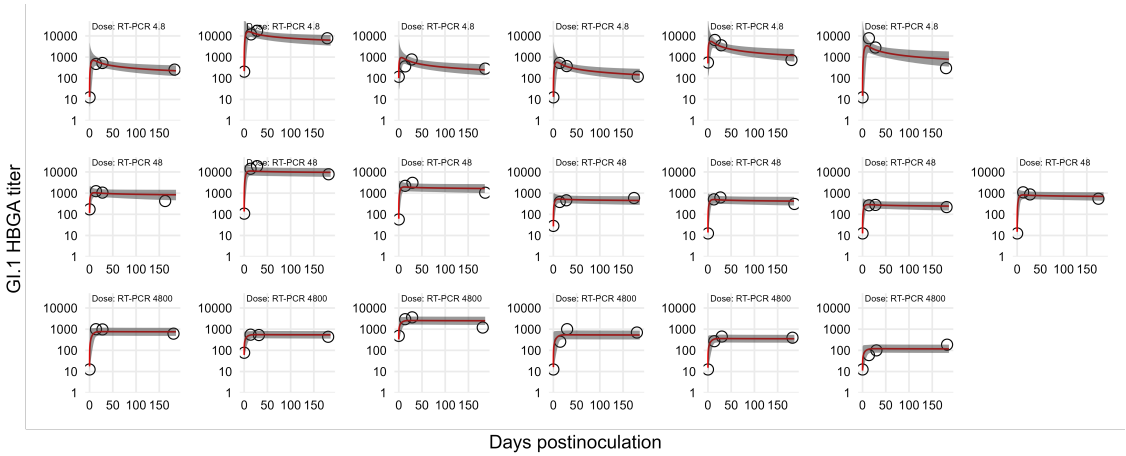

Figure B.4: Fitted individual kinetics of GI.1 HBGA antibody in the HC study (Power-law decay). The lines show means of estimations. The colored areas show 89% equal-tailed credible intervals (CI).

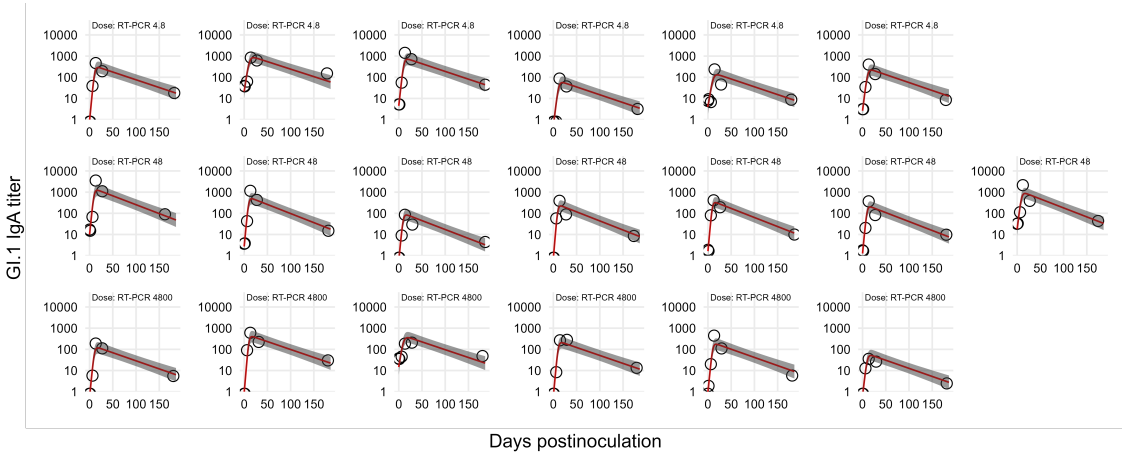

Figure B.5: Fitted individual kinetics of GI.1 HBGA antibody in the HC study (Power-law decay). The lines show means of estimations. The colored areas show 89% equal-tailed credible intervals (CI).

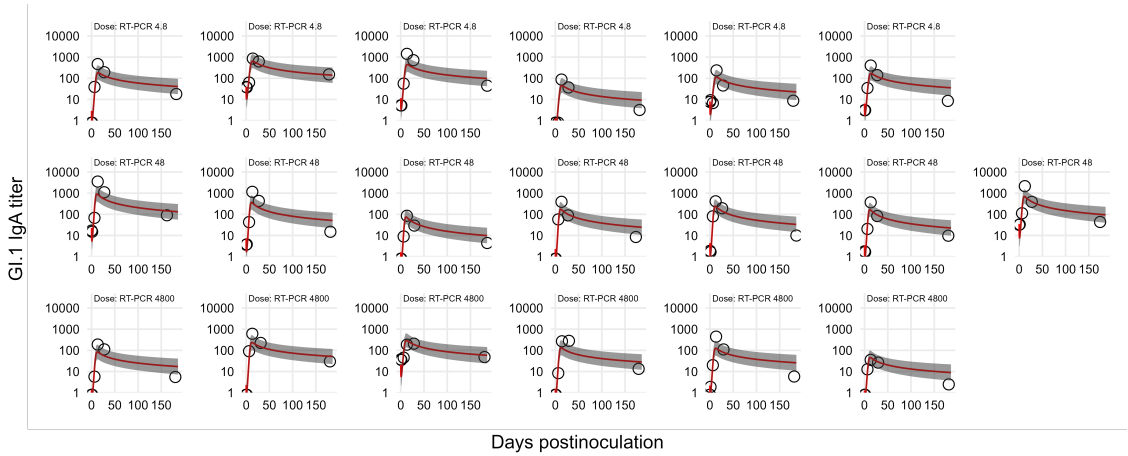

Figure B.6: Fitted individual kinetics of GI.1 IgA antibody in the HC study (Power-law decay). The lines show means of estimations. The colored areas show 89% equal-tailed credible intervals (CI).

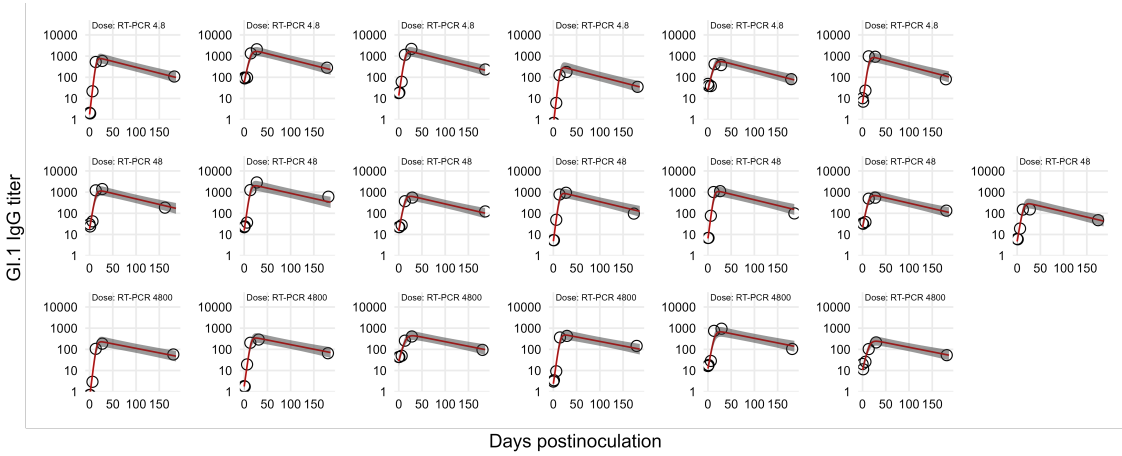

Figure B.7: Fitted individual kinetics of GI.1 IgG antibody in the HC study (Exponential decay). The lines show means of estimations. The colored areas show 89% equal-tailed credible intervals (CI).

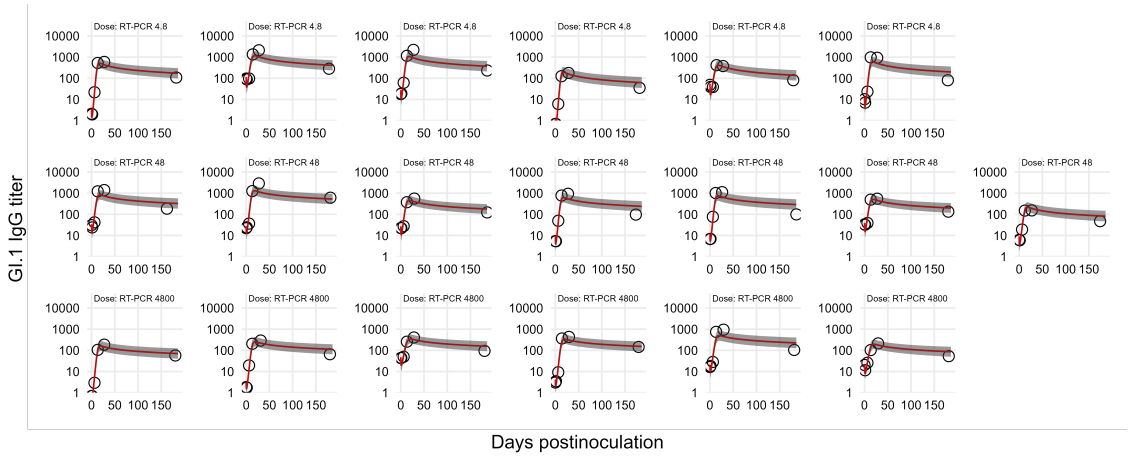

Figure B.8: Fitted individual kinetics of GI.1 IgG antibody in the HC study (Power-law decay). The lines show means of estimations. The colored areas show 89% equal-tailed credible intervals (CI).

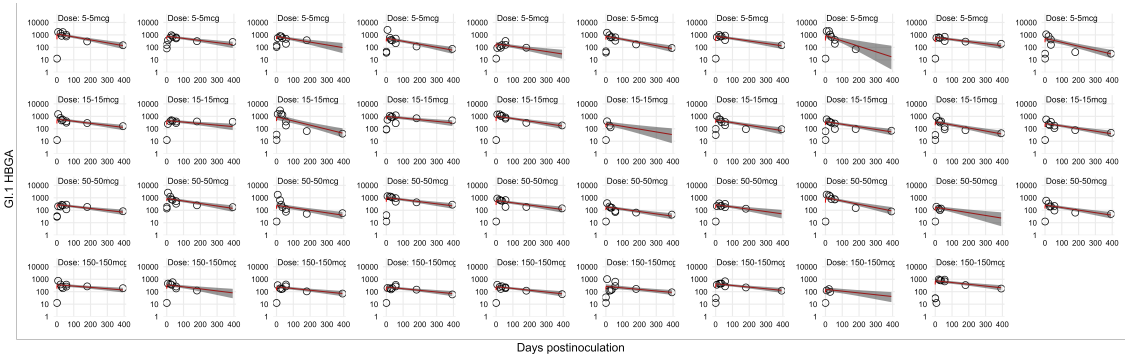

Figure B.9: Fitted individual kinetics of GI.1 HBGA antibody in the HV study (Exponential decay). The lines show means of estimations. The colored areas show 89% equal-tailed credible intervals (CI).

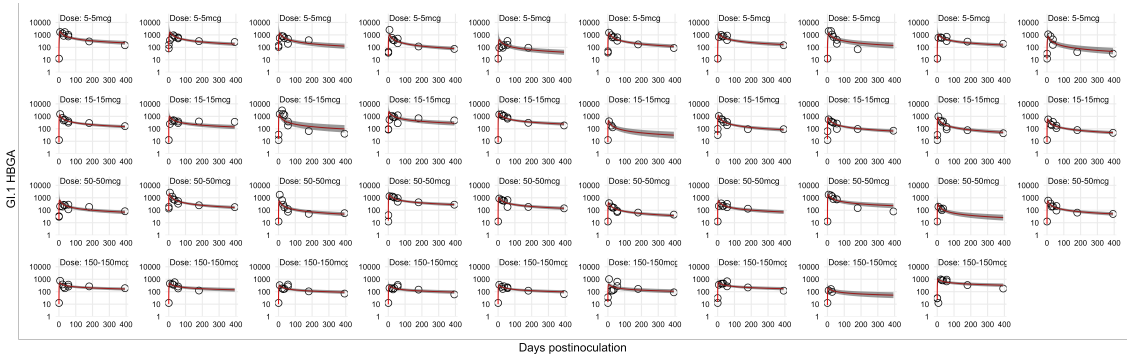

Figure B.10: Fitted individual kinetics of GI.1 HBGA antibody in the HV study (Exponential decay). The lines show means of estimations. The colored areas show 89% equal-tailed credible intervals (CI).

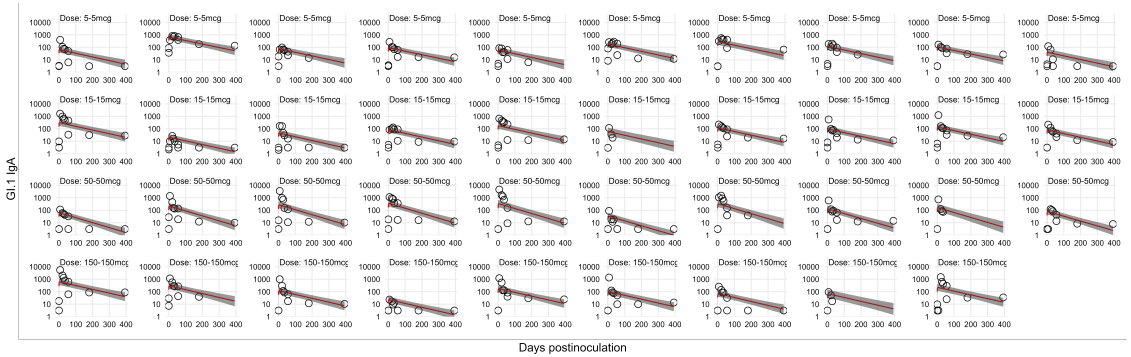

Figure B.11: Fitted individual kinetics of GI.1 IgA antibody in the HV study (Exponential decay). The lines show means of estimations. The colored areas show 89% equal-tailed credible intervals (CI).

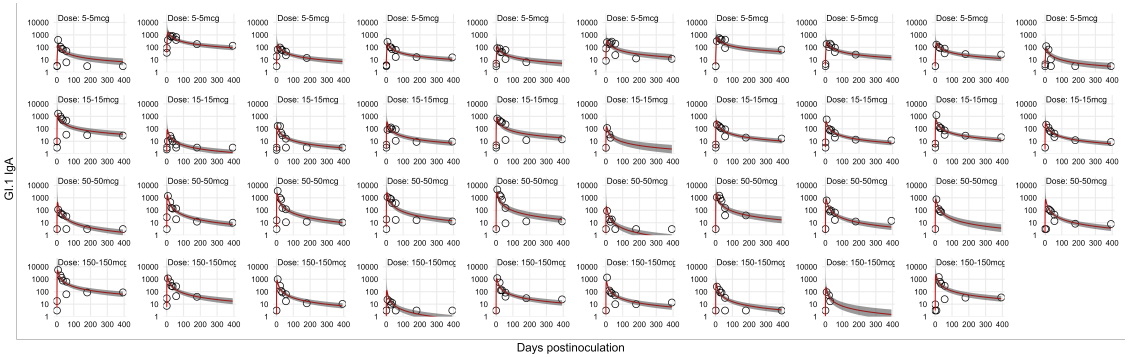

Figure B.12: Fitted individual kinetics of GI.1 IgA antibody in the HV study (Power-law decay). The lines show means of estimations. The colored areas show 89% equal-tailed credible intervals (CI).

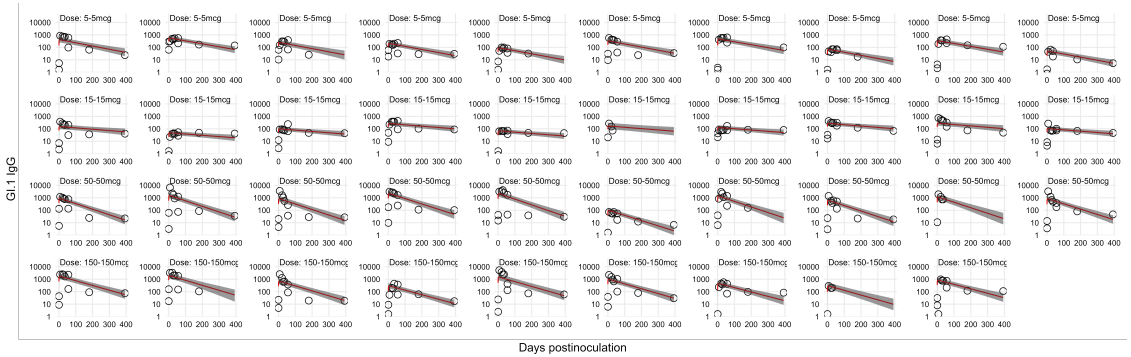

Figure B.13: Fitted individual kinetics of GI.1 IgG antibody in the HV study (Exponential decay). The lines show means of estimations. The colored areas show 89% equal-tailed credible intervals (CI).

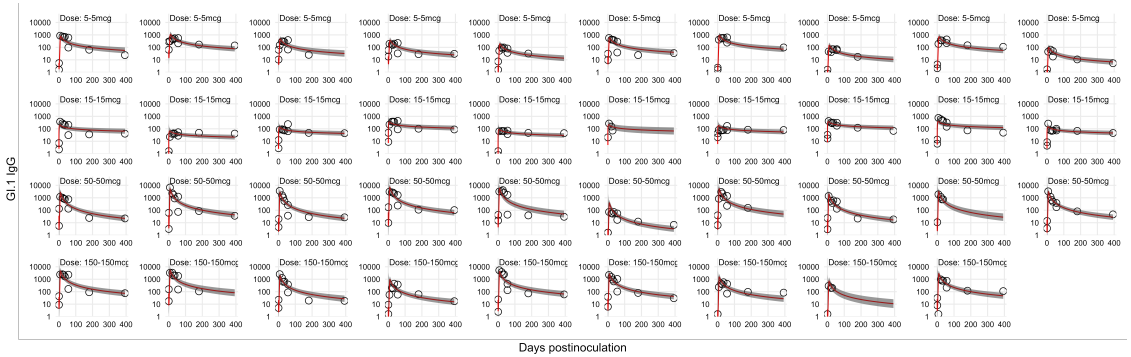

Figure B.14: Fitted individual kinetics of GI.1 IgG antibody in the HV study (Power-law decay). The lines show means of estimations. The colored areas show 89% equal-tailed credible intervals (CI).

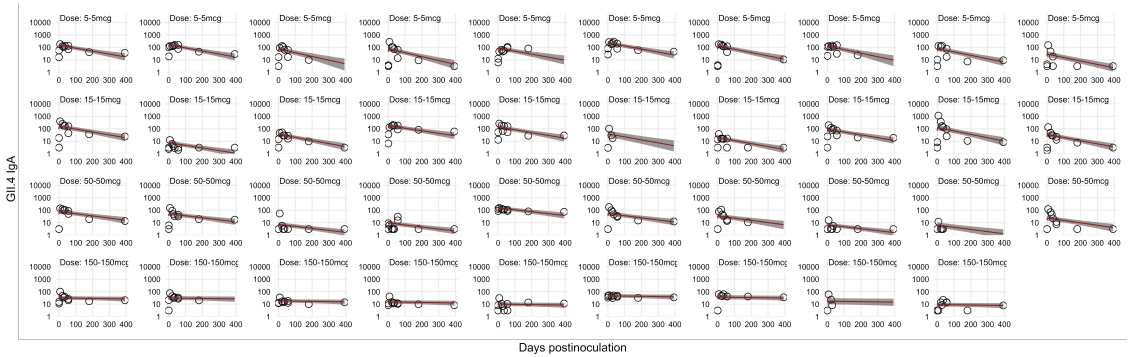

Figure B.15: Fitted individual kinetics of GII.4 IgA antibody in the HV study (Exponential decay). The lines show means of estimations. The colored areas show 89% equal-tailed credible intervals (CI).

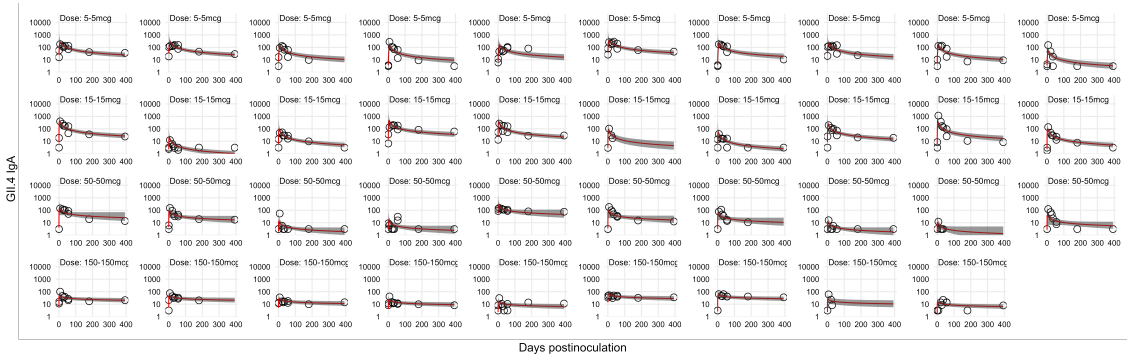

Figure B.16: Fitted individual kinetics of GII.4 IgA antibody in the HV study (Power-law decay). The lines show means of estimations. The colored areas show 89% equal-tailed credible intervals (CI).

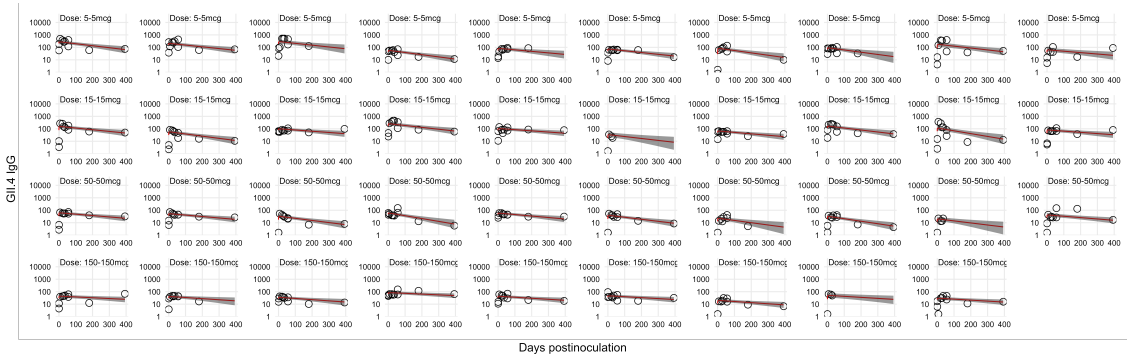

Figure B.17: Fitted individual kinetics of GII.4 IgG antibody in the HV study (Exponential decay). The lines show means of estimations. The colored areas show 89% equal-tailed credible intervals (CI).

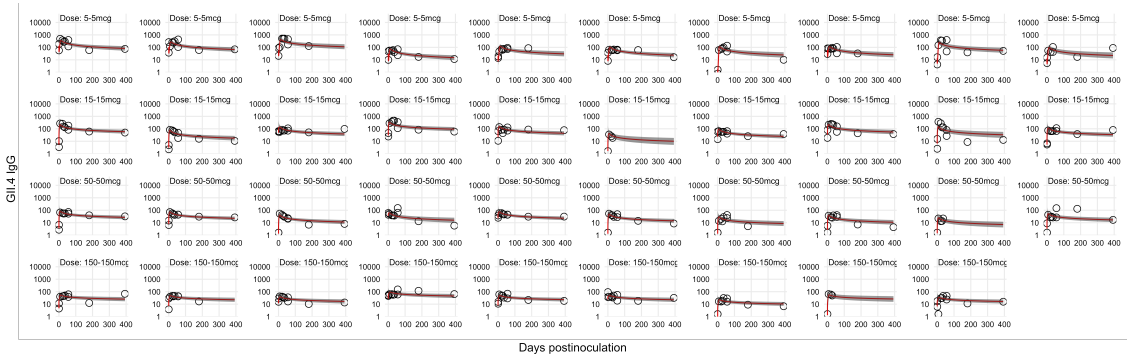

Figure B.18: Fitted individual kinetics of GII.4 IgG antibody in the HV study (Power-law decay). The lines show means of estimations. The colored areas show 89% equal-tailed credible intervals (CI).

APPENDIX C

APPENDIX: IMPACT OF SEASONAL INFLUENZA VACCINE DOSE ON HOMOLOGOUS AND HETEROLOGOUS IMMUNITY

C.1 Description of the multi-center cohort study

Our data came from an ongoing vaccination study. In the study, participants were enrolled before each influenza season. Serum samples were collected and then tested against multiple strains (either contained or not contained in the vaccine) for hemagglutination-inhibition (HAI) antibody titer results at two time points (before and after the vaccination). Therefore, the sample size of HAI titers was much more than the sample size of participants (Figure C.1).

We summarized two special features in the study design (Figure C.2). First, the influenza vaccine used during this study contained either three or four strains. Second, before and after the vaccination, each individual's serum sample was tested with multiple strains for HAI titer results. So, for homologous analysis, several vaccine strains' HAI results may have correlations because they were taken from the same participant. For heterogeneous analysis, multiple HAI titer results came from one participant such that these results also correlated. As a result, we used multilevel models. Lastly, some participants were enrolled more than once across the study seasons, we added another hierarchical setting of random intercept based on participants ID.

Study Flow

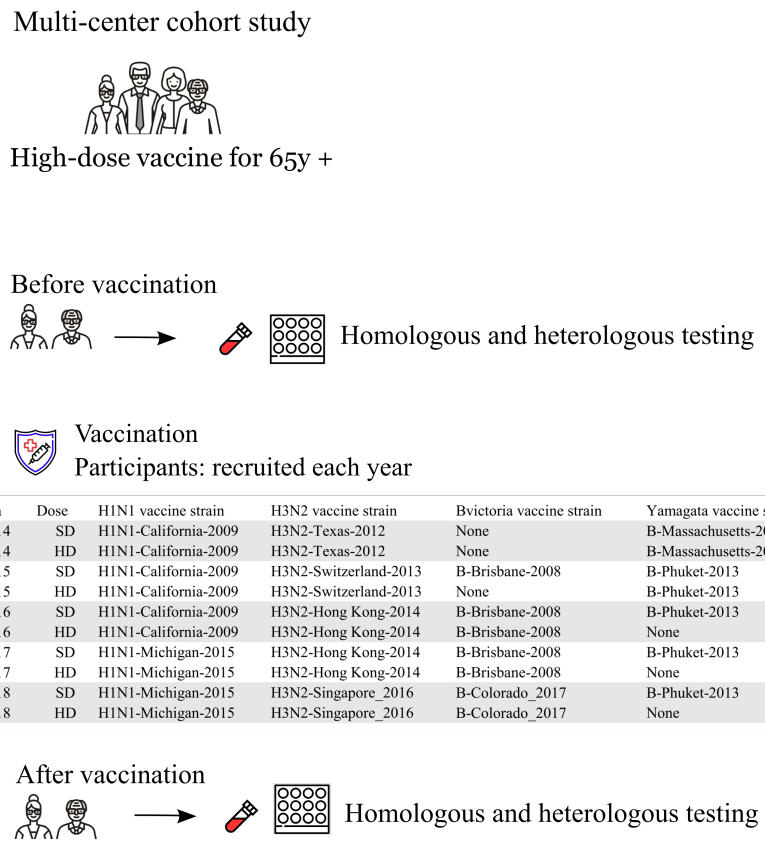

Season	Dose	H1N1 vaccine strain	H3N2 vaccine strain	Bvictoria vaccine strain	Yamagata vaccine strain
2014	SD	H1N1-California-2009	H3N2-Texas-2012	None	B-Massachusetts-2012
2014	HD	H1N1-California-2009	H3N2-Texas-2012	None	B-Massachusetts-2012
2015	SD	H1N1-California-2009	H3N2-Switzerland-2013	B-Brisbane-2008	B-Phuket-2013
2015	HD	H1N1-California-2009	H3N2-Switzerland-2013	None	B-Phuket-2013
2016	SD	H1N1-California-2009	H3N2-Hong Kong-2014	B-Brisbane-2008	B-Phuket-2013
2016	HD	H1N1-California-2009	H3N2-Hong Kong-2014	B-Brisbane-2008	None
2017	SD	H1N1-Michigan-2015	H3N2-Hong Kong-2014	B-Brisbane-2008	B-Phuket-2013
2017	HD	H1N1-Michigan-2015	H3N2-Hong Kong-2014	B-Brisbane-2008	None
2018	SD	H1N1-Michigan-2015	H3N2-Singapore_2016	B-Colorado_2017	B-Phuket-2013
2018	HD	H1N1-Michigan-2015	H3N2-Singapore_2016	B-Colorado_2017	None

Figure C.1: Flow diagram of the multi-center cohort study.

Hierarchical Features

Examples:
ID-1027 in 2014 season
ID-1236 in 2016 season
ID-209 in 2018 season

ID-1027 received vaccine:	ID-1236 received vaccine:	ID-209 received vaccine:
H1N1-California-2009	H1N1-California-2009	H1N1-Michigan-2015
H3N2-Texas-2012	H3N2-Hong Kong-2014	H3N2-Singapore-2016
B-Massachusetts-2012	B-Phuket-2013	B-Colorado-2017
	B-Brisbane-2008	

HAI assay tested strains:

B-Brisbane-2008	B-Colorado-2017	B-Florida-2006	B-Harbin-1994	B-Hong-Kong-2001
B-Malaysia-2004	B-Massachusetts-2012	B-Phuket-2013	B-Sichuan-1999	B-Texas-2011
B-Victoria-1987	B-Victoria-2006	B-Wisconsin-2010	B-Yamagata-1988	H1N1-Beijing-1995
H1N1-Brazil-1978	H1N1-Brisbane-2007	H1N1-California-1978	H1N1-California-2009	H1N1-Chile-1983
H1N1-Denver-1957	H1N1-Fort Monmouth-1947	H1N1-Michigan-2015	H1N1-New Caledonia-1999	H1N1-New Jersey-1976
H1N1-Singapore-1986	H1N1-Solomon Islands-2006	H1N1-South Carolina-1918	H1N1-Texas-1991	H1N1-Ussr-1977
H1N1-Weiss-1943	H3N2-Fujian-2002	H3N2-Hong Kong-1968	H3N2-Hong Kong-2014	H3N2-Mississippi-1985
H3N2-Nanchang-1995	H3N2-New York-2004	H3N2-Panama-1999	H3N2-Perth-2009	H3N2-Port Chalmers-1973
H3N2-Shangdong-1993	H3N2-Sichuan-1987	H3N2-Singapore-2016	H3N2-Switzerland-2013	H3N2-Sydney-1997
H3N2-Texas-1977	H3N2-Texas-2012	H3N2-Uruguay-2007	H3N2-Victoria-2011	H3N2-Wisconsin-2005

Tested strains same to vaccine strains → Homologous model having 10 strains

Tested strains not same to the vaccine strain of
a. H1N1-California-2009 → Heterologous model a
H1N1-South Carolina-1918
H1N1-Weiss-1943
.....
H1N1-Michigan-2015 → Heterologous model b
b. H3N2-Texas-2012
H3N2-Hong Kong-1968
H3N2-Texas-1977
..... → Other 8 heterologous mdoels
H3N2-Hong Kong-2014
....

Figure C.2: The hierarchical features of the study.

C.2 Main multilevel model

C.2.1 Introduction

There were four outcomes based on transformed titer unite, $\log 2(HAI/5)$, namely increase in titer following vaccination, post-vaccination titer, and the categorical versions of those two outcomes, namely seroconversion and seroprotection.

We assumed there was an overall impact of vaccine dose (sometimes also known as an average effect). Because there were multiple strains and seasons, we further assumed there were variations around the overall impact by strains or seasons. Therefore, we used multilevel models. We named the model which estimated an overall impact of vaccine dose and its variation by strains as the strain-specific model. Similarly, we called the model which estimated an overall impact of vaccine dose and its variation by seasons as the vaccine-specific model. In the models, we included the vaccine dose as the main predictor of interest, with age, sex, race and pre-vaccination antibody titer levels as covariates. Continuous variables such as age and pre-vaccination titer were standardized (z-score transformation) before model fitting.

We used Bayesian approaches to estimate parameters in these multi-level models. For the two continuous outcomes (increase in titer following vaccination, post-vaccination titer), we used a linear model. For the binary outcomes (seroconversion and seroprotection), we used a logistic model. Because our model includes pre-vaccination titer as a variable, the titer increase outcome with log2 transformation (post-vaccination titer minus pre-vaccination titer) and the model of post-vaccination titer outcome (with log2 transformation) become mathematically equivalent and produce the

same coefficient estimations for the variable of vaccine dose. Thus, for our analyses where pre-vaccination titer is part of the model, we only report one continuous outcome, namely titer increase.

In homologous models, we filtered the data to only have HAI titer results of the same strain contained in the vaccine (e.g., each row of the data represented participants who received X vaccine strain and their pre- and post-vaccination HAI titer of strain X). In heterologous models, we filtered the data to only have HAI titer results on strains similar to the vaccine strain but not the same as the vaccine strain. For example, when we aim to analyze the heterologous response of H1N1 vaccine strain X, we only keep HAI pre- and post-vaccination titer results of other H1N1 strains of participants who received the vaccine strain X. For H3N2 vaccine strains X, the HAI titer results came from other H3N2 strains, and for X strain of influenza B, the HAI titer results came from other B strains (no subset on lineages).

Models were implemented using the brms package (Bürkner, 2018) in R (R Core Team, 2020).

C.2.2 Model prior setting

Bayesian models need settings of priors. We set our parameter priors based on our study design. In the study, HAI titers were measured with the standard dilution assay with a limit of detection (LOD) as 1:10 and a maximum as 1:20480. After the transformation ("log" 2(HAI/5)), HAI titers values located within a range from zero (LOD) to 12. Therefore, the outcome of titer increase may only vary between -12 to 12 log2 HAI units. For the outcome of seroconversion and seroprotection, because they are binary outcomes, the target probability only can range from 0 to 1.

We aim to have a relatively flat prior-predictive distribution for our outcomes. For the outcome of titer increase, we used normal distribution with mean 0 and standard deviation of 10 (Normal (0,10)) for variable coefficients in the model to have a relatively flat prior-predictive distribution within the range of -12 to 12. By such set, our priors influence the posterior inference weakly (“Prior Choice Recommendations · Stan-Dev/Stan Wiki”, n.d.). For the outcome of seroconversion and seroprotection, narrower priors for variable coefficients are needed to have a relatively flat prior-predictive distribution of the probability in the range of 0 to 1 (McElreath, 2020). Therefore, we used Normal(0,1) as the prior distribution for variable coefficients.

C.2.3 Models of strain-specific analysis

In strain-specific analyses, we aim to estimate the overall vaccine dose impact and its variations by each strain. We used random intercepts for each participant based on IDs (IDs were same across their vaccination seasons) in both homologous and heterologous models because multiple strain specific HAI titer results from the same person may be correlated. In addition, dose-specific random effects for each vaccine strain were also estimated.

Titer increase homologous model

The code of model setting is: titerincrease 0 + dose + (0 + dose| vaccine strains) + scale(age) + race + sex + scale(pre-vaccination titer) + (1 | participant ID)

With the setting of "dose + (0 + dose| vaccine strains)", we modeled the overall vaccine dose impact and its variations by each strain. With the setting of "(1 | participant ID)", we adjust for the correlation among multiple strain-specific HAI titer results from the same person.

The mathematical forms are presented as below:

[Likelihood]:

$$y_{ij} \sim Normal(\mu_{ij}, \sigma^2),\ i : individual,\ j : strain$$

[Linear model]:

$$\begin{aligned}\mu_{ij} = \alpha_{ID[i]} \\ &+ (Dose_{HD} + Dose_{HD[j]})I(Dose_{[i]} = HD) \\ &+ (Dose_{SD} + Dose_{SD[j]})I(Dose_{[i]} = SD) \\ &+ \beta_{sex}x_{sex[i]} + \beta_{race}x_{race[i]} + \beta_{age}x_{age[i]} + \beta_p x_{Pre-vaccine\ titer[ij]}\end{aligned}$$

[Fixed priors]:

$$\sigma \sim \text{Half-Cauchy}\,(0,1)$$

$$Dose_{HD} \sim \text{Normal}(0,10)$$

$$Dose_{SD} \sim \text{Normal}(0,10)$$

$$\beta_{sex} \sim \text{Normal}(0,10)$$

$$\beta_{race} \sim \text{Normal}(0,10)$$

$$\beta_{age} \sim \text{Normal}(0,10)$$

$$\beta_p \sim \text{Normal}(0,10)$$

[Adaptive prior]:

$$\alpha_{ID} \sim \text{Normal}(0, \sigma_\alpha^2)$$

$$\begin{pmatrix} Dose_{HD[j]} \\ Dose_{SD[j]} \end{pmatrix} \sim \text{MVNormal}\left(\begin{pmatrix} 0 \\ 0 \end{pmatrix}, S_{vaccine}\right)$$

[Hyper priors]

$$\sigma_\alpha \sim \text{Half-Cauchy}\,(0,1)$$

$$S_{vaccine} \sim \text{LkjCholesky}(1),$$

where $\alpha_{ID[i]}$ stands for random intercept by participants ID. $Dose_{HD}$ or $Dose_{SD}$ stands for the overall impact of vaccine dose in HD or SD dose group. $Dose_{HD[j]}$ or $Dose_{SD[j]}$ stands for variations of the overall impact of vaccine dose in HD or SD dose group by each strain j. $x_{sex[i]}$, $x_{race[i]}$, $x_{age[i]}$ stand for variables of sex, race, age of the participant with ID = i. $x_{Pre-vaccine\ titer[ij]}$ stands for the pre-vaccination HAI titer of strain j from the sample which was taken from participant i. The prior multivariate normal distribution (MVNormal) for HD and SD of strain j provided flexibility on the correlation between HD and SD on the strain j.

Titer increase heterologous model

The settings of the model were the same as the homologous model. The only difference was the data. In the heterologous model, only heterologous HAI titers results were used.

The mathematical forms are presented as below:

[Likelihood]:

$$(y_{ij}|Vaccine\ strain = v, v \neq j) \sim \text{Normal}(\mu_{ij}, \sigma^2),\ i : individual,\ j : strain$$

$$\begin{aligned}\mu_{ij} = \alpha_{ID[i]} & \\ & + (Dose_{HD} + Dose_{HD[j]})I(Dose_{[i]} = HD) \\ & + (Dose_{SD} + Dose_{SD[j]})I(Dose_{[i]} = SD) \\ & + \beta_{sex}x_{sex[i]} + \beta_{race}x_{race[i]} + \beta_{age}x_{age[i]} + \beta_p x_{Pre-vaccine\ titer[ij]}\end{aligned}$$

[Fixed priors]:

$$\sigma \sim \text{Half-Cauchy}\,(0, 1)$$

$$Dose_{HD} \sim \text{Normal}(0, 10)$$

$$Dose_{SD} \sim \text{Normal}(0, 10)$$

$$\beta_{sex} \sim \text{Normal}(0, 10)$$

$$\beta_{race} \sim \text{Normal}(0, 10)$$

$$\beta_{age} \sim \text{Normal}(0, 10)$$

$$\beta_p \sim \text{Normal}(0, 10)$$

[Adaptive prior]:

$$\alpha_{ID} \sim \text{Normal}(0, \sigma_\alpha^2)$$

$$\begin{pmatrix} Dose_{HD[j]} \\ Dose_{SD[j]} \end{pmatrix} \sim \text{MVNormal}\left(\begin{pmatrix} 0 \\ 0 \end{pmatrix}, S_{vaccine}\right)$$

[Hyper priors]

$$\sigma_\alpha \sim \text{Half-Cauchy}\,(0, 1)$$

$$S_{vaccine} \sim LkjCholesky(1)$$

Seroconversion and Seroprotection homologous model

Most model settings were similar to the titer increase homologous model, but the model link changed to logit.

The mathematical forms are presented as below:

[Likelihood]:

$$y_{ij} \sim Binomial(n = 1, p = p_{ij}),\ i : individual,\ j : strain$$

$$\begin{aligned} logit(p_{ij}) = \alpha_{ID[i]} & \\ & + (Dose_{HD} + Dose_{HD[j]})I(Dose_{[i]} = HD) \\ & + (Dose_{SD} + Dose_{SD[j]})I(Dose_{[i]} = SD) \\ & + \beta_{sex} x_{sex[i]} + \beta_{race} x_{race[i]} + \beta_{age} x_{age[i]} + \beta_{p} x_{Pre-vaccine\ titer[ij]} \end{aligned}$$

[Fixed priors]:

$$Dose_{HD} \sim \text{Normal}(0, 10)$$

$$Dose_{SD} \sim \text{Normal}(0, 10)$$

$$\beta_{sex} \sim \text{Normal}(0, 1)$$

$$\beta_{race} \sim \text{Normal}(0, 1)$$

$$\beta_{age} \sim \text{Normal}(0, 1)$$

$$\beta_{p} \sim \text{Normal}(0, 1)$$

[Adaptive prior]:

$$\alpha_{ID} \sim \text{Normal}(0, \sigma_{\alpha}^2)$$

$$\begin{pmatrix} Dose_{HD[j]} \\ Dose_{SD[j]} \end{pmatrix} \sim \text{MVNormal}\left(\begin{pmatrix} 0 \\ 0 \end{pmatrix}, S_{vaccine} \right)$$

[Hyper priors]

$$\sigma_{\alpha} \sim \text{Half-Cauchy}\,(0, 1)$$

$$S_{vaccine} \sim \text{LkjCholesky}(1)$$

Seroconversion and Seroprotection heterologous model

Most model settings were similar to the titer increase heterologous model, but the model link changed to logit.

The mathematical forms are presented as below:

[Likelihood]:

$$(y_{ij}|Vaccine\ strain = v, v \neq j) \sim Binomial(n = 1, p = p_{ij})$$

$$i : individual,\ j : strain$$

$$\begin{aligned} logit(p_{ij}) = \alpha_{ID[i]} & \\ & + (Dose_{HD} + Dose_{HD[j]})I(Dose_{[i]} = HD) \\ & + (Dose_{SD} + Dose_{SD[j]})I(Dose_{[i]} = SD) \\ & + \beta_{sex}x_{sex[i]} + \beta_{race}x_{race[i]} + \beta_{age}x_{age[i]} + \beta_{p}x_{Pre-vaccine\ titer[ij]} \end{aligned}$$

[Fixed priors]:

$$Dose_{HD} \sim \text{Normal}(0, 10)$$

$$Dose_{SD} \sim \text{Normal}(0, 10)$$

$$\beta_{sex} \sim \text{Normal}(0, 1)$$

$$\beta_{race} \sim \text{Normal}(0, 1)$$

$$\beta_{age} \sim \text{Normal}(0, 1)$$

$$\beta_{p} \sim \text{Normal}(0, 1)$$

[Adaptive prior]:

$$\alpha_{ID} \sim \text{Normal}(0, \sigma_{\alpha}^2)$$

$$\begin{pmatrix} Dose_{HD[j]} \\ Dose_{SD[j]} \end{pmatrix} \sim \text{MVNormal}\left(\begin{pmatrix} 0 \\ 0 \end{pmatrix}, S_{vaccine} \right)$$

[Hyper priors]

$$\sigma_{\alpha} \sim \text{Half-Cauchy}\,(0, 1)$$

$$S_{vaccine} \sim \text{LkjCholesky}(1)$$

C.2.4 Models of vaccine-specific analysis

In vaccine-specific analyses, we aim to estimate the overall vaccine dose impact and its variations by each season. We used random intercepts for each participant based on IDs (IDs were same across their vaccination seasons) in both homologous and heterologous models because multiple strain-specific HAI titer results could come from the same person.

We estimated the overall vaccine dose impact with parameters $Dose_{HD}$ or $Dose_{SD}$, and its variations for each season with parameters $Dose_{HD[s]}$ or $Dose_{SD[s]}$ (s stands for season).

Titer increase homologous model

The code of model setting is: titerincrease 0 + dose + (0 + dose | season) + scale(age) + race + sex + scale(pre-vaccination titer) + (1 | participant ID)

With the setting of "dose + (0 + dose| season)", we modeled the overall vaccine dose impact and its variations by each season. With the setting of "(1 | participant ID)", we let the model account for that that multiple strain-specific HAI titer results could come from the same person.

HAI tested strains were same to vaccine strains. The mathematical forms are presented as below:

[Likelihood]:

$$y_{is} \sim \text{Normal}(\mu_{is}, \sigma^2)$$

$$i : individual,\ s : season$$

$$\begin{aligned}\mu_{ijs} = \alpha_{ID[i]} &\\ &+ (Dose_{HD} + Dose_{HD[s]})I(Dose_{[i]} = HD)\\ &+ (Dose_{SD} + Dose_{SD[s]})I(Dose_{[i]} = SD)\\ &+ \beta_{sex}x_{sex[i]} + \beta_{race}x_{race[i]} + \beta_{age}x_{age[i]} + \beta_p x_{Pre-vaccine\ titer[ijs]}\end{aligned}$$

[Fixed priors]:

$$\sigma \sim \text{Half-Cauchy}\,(0,1)$$

$$Dose_{HD} \sim \text{Normal}(0,10)$$

$$Dose_{SD} \sim \text{Normal}(0,10)$$

$$\beta_{sex} \sim \text{Normal}(0,10)$$

$$\beta_{race} \sim \text{Normal}(0,10)$$

$$\beta_{age} \sim \text{Normal}(0,10)$$

$$\beta_p \sim \text{Normal}(0,10)$$

[Adaptive prior]:

$$\alpha_{ID} \sim \text{Normal}(0, \sigma_\alpha^2)$$

$$\begin{pmatrix} Dose_{HD[s]} \\ Dose_{SD[s]} \end{pmatrix} \sim \text{MVNormal}\left(\begin{pmatrix} 0 \\ 0 \end{pmatrix}, S_{season}\right)$$

[Hyper priors]

$$\sigma_\alpha \sim \text{Half-Cauchy}\,(0,1)$$

$$S_{vaccine} \sim \text{LkjCholesky}(1),$$

where $\alpha_{ID[i]}$ stands for random intercept by participants ID. $Dose_{HD}$ or $Dose_{SD}$ stands for the overall impact of vaccine dose in HD or SD dose group. $Dose_{HD[s]}$ or $Dose_{SD[s]}$ stands for variations of the overall impact of vaccine dose in HD or SD dose group by each season. $x_{sex[i]}$, $x_{race[i]}$, $x_{age[i]}$ stand for variables of sex, race, age of the participant with ID = i. $x_{Pre-vaccine\ titer[ijs]}$ stands for the pre-vaccination HAI titer of strain j from the sample which was taken from participant i in season s. The prior multivariate normal distribution (MVNormal) for HD and SD in season s provided flexibility on the correlation between HD and SD in the same season.

Titer increase heterologous model

HAI tested strains were different from vaccine strains. The mathematical forms are presented as below:

[Likelihood]:

$$y_{is} \sim \text{Normal}(\mu_{is}, \sigma^2)$$

$$i : individual,\ s : season$$

$$\begin{aligned}\mu_{ijs} = \alpha_{ID[i]} &\\ &+ (Dose_{HD} + Dose_{HD[s]})I(Dose_{[i]} = HD)\\ &+ (Dose_{SD} + Dose_{SD[s]})I(Dose_{[i]} = SD)\\ &+ \beta_{sex}x_{sex[i]} + \beta_{race}x_{race[i]} + \beta_{age}x_{age[i]} + \beta_p x_{Pre-vaccine\ titer[ijs]}\end{aligned}$$

[Fixed priors]:

$$\sigma \sim \text{Half-Cauchy}\,(0,1)$$

$$Dose_{HD} \sim \text{Normal}(0,10)$$

$$Dose_{SD} \sim \text{Normal}(0,10)$$

$$\beta_{sex} \sim \text{Normal}(0,10)$$

$$\beta_{race} \sim \text{Normal}(0,10)$$

$$\beta_{age} \sim \text{Normal}(0,10)$$

$$\beta_p \sim \text{Normal}(0,10)$$

[Adaptive prior]:

$$\alpha_{ID} \sim \text{Normal}(0, \sigma_\alpha^2)$$

$$\begin{pmatrix} Dose_{HD[s]} \\ Dose_{SD[s]} \end{pmatrix} \sim \text{MVNormal}\left(\begin{pmatrix} 0 \\ 0 \end{pmatrix}, S_{season}\right)$$

(Hyper-priors)

$$\sigma_\alpha \sim \text{Half-Cauchy}\,(0,1)$$

$$S_{vaccine} \sim \text{LkjCholesky}(1)$$

Seroconversion and Seroprotection homologous model

HAI tested strains were same to vaccine strains. The mathematical forms are presented as below:

[Likelihood]:

$$y_{is} \sim Binomial(n = 1, p = p_{is})$$

$$i : individual,\ s : season$$

$$\begin{aligned} p_{is} = \alpha_{ID[i]} & \\ & + (Dose_{HD} + Dose_{HD[s]})I(Dose_{[i]} = HD) \\ & + (Dose_{SD} + Dose_{SD[s]})I(Dose_{[i]} = SD) \\ & + \beta_{sex}x_{sex[i]} + \beta_{race}x_{race[i]} + \beta_{age}x_{age[i]} + \beta_{p}x_{Pre-vaccine\ titer[ijs]} \end{aligned}$$

[Fixed priors]:

$$Dose_{HD} \sim \text{Normal}(0, 10)$$

$$Dose_{SD} \sim \text{Normal}(0, 10)$$

$$\beta_{sex} \sim \text{Normal}(0, 1)$$

$$\beta_{race} \sim \text{Normal}(0, 1)$$

$$\beta_{age} \sim \text{Normal}(0, 1)$$

$$\beta_{p} \sim \text{Normal}(0, 1)$$

[Adaptive prior]:

$$\alpha_{ID} \sim \text{Normal}(0, \sigma_{\alpha}^2)$$

$$\begin{pmatrix} Dose_{HD[s]} \\ Dose_{SD[s]} \end{pmatrix} \sim \text{MVNormal}\left(\begin{pmatrix} 0 \\ 0 \end{pmatrix}, S_{season} \right)$$

(Hyper-priors)

$$\sigma_{\alpha} \sim \text{Half-Cauchy}\,(0, 1)$$

$$S_{vaccine} \sim \text{LkjCholesky}(1)$$

Seroconversion and Seroprotection heterologous model

HAI tested strains were different from vaccine strains. The mathematical forms are presented as below:

[Likelihood]:

$$y_{is} \sim Binomial(n = 1, p = p_{is})$$

$$i : individual,\ s : season$$

$$\begin{aligned} p_{is} = \alpha_{ID[i]} & \\ & + (Dose_{HD} + Dose_{HD[s]})I(Dose_{[i]} = HD) \\ & + (Dose_{SD} + Dose_{SD[s]})I(Dose_{[i]} = SD) \\ & + \beta_{sex}x_{sex[i]} + \beta_{race}x_{race[i]} + \beta_{age}x_{age[i]} + \beta_{p}x_{Pre-vaccine\ titer[ijs]} \end{aligned}$$

[Fixed priors]:

$$Dose_{HD} \sim \text{Normal}(0, 10)$$

$$Dose_{SD} \sim \text{Normal}(0, 10)$$

$$\beta_{sex} \sim \text{Normal}(0, 1)$$

$$\beta_{race} \sim \text{Normal}(0, 1)$$

$$\beta_{age} \sim \text{Normal}(0, 1)$$

$$\beta_{p} \sim \text{Normal}(0, 1)$$

[Adaptive prior]:

$$\alpha_{ID} \sim \text{Normal}(0, \sigma_{\alpha}^2)$$

$$\begin{pmatrix} Dose_{HD[s]} \\ Dose_{SD[s]} \end{pmatrix} \sim \text{MVNormal}\left(\begin{pmatrix} 0 \\ 0 \end{pmatrix}, S_{season} \right)$$

(Hyper-priors)

$$\sigma_{\alpha} \sim \text{Half-Cauchy}\,(0, 1)$$

$$S_{vaccine} \sim \text{LkjCholesky}(1)$$

C.3 Further analyses

We performed a number of additional analyses to describe data and explore the sensitivity of our main results. In the sensitivity analysis, we included SD recipients of any age. We also used Bayesian generalized linear models for 65+ years old population. In addition, we used 1:1 dose group propensity score matched data (using the nearest neighbor matching algorithm (Ho et al., 2007/ed) with Bayesian generalized linear models as a sensitivity analysis of both data and modeling approaches. Coefficients were summarized with median and 89% equal-tailed credible interval (CI) (McElreath, 2020).

C.3.1 Description analyses

Strain-specific description

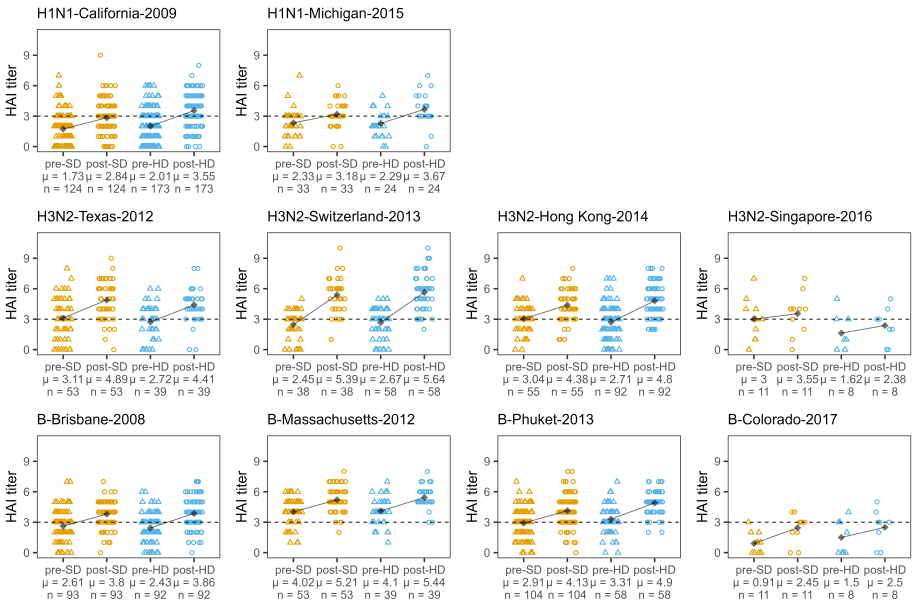

Figure C.3: Homologous pre- and post- vaccination titer. The dashed horizontal line is the seroprotection criterion. criterion.

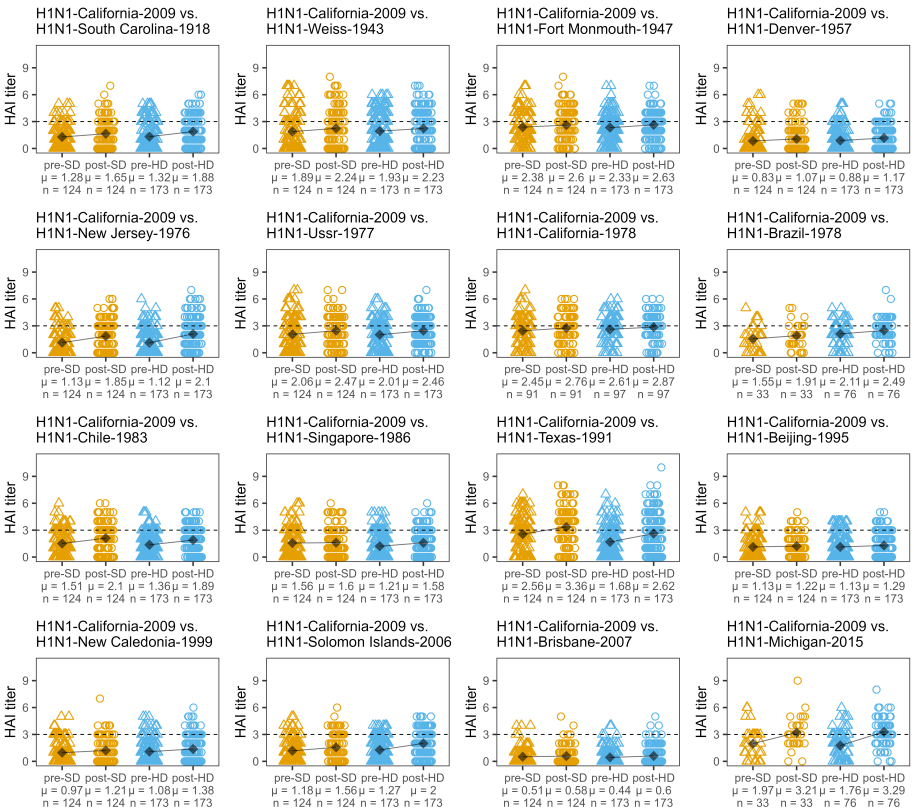

Figure C.4: Heterologous pre- and post- vaccination titer (H1N1-California-2009). The dashed horizontal line is the seroprotection criterion.

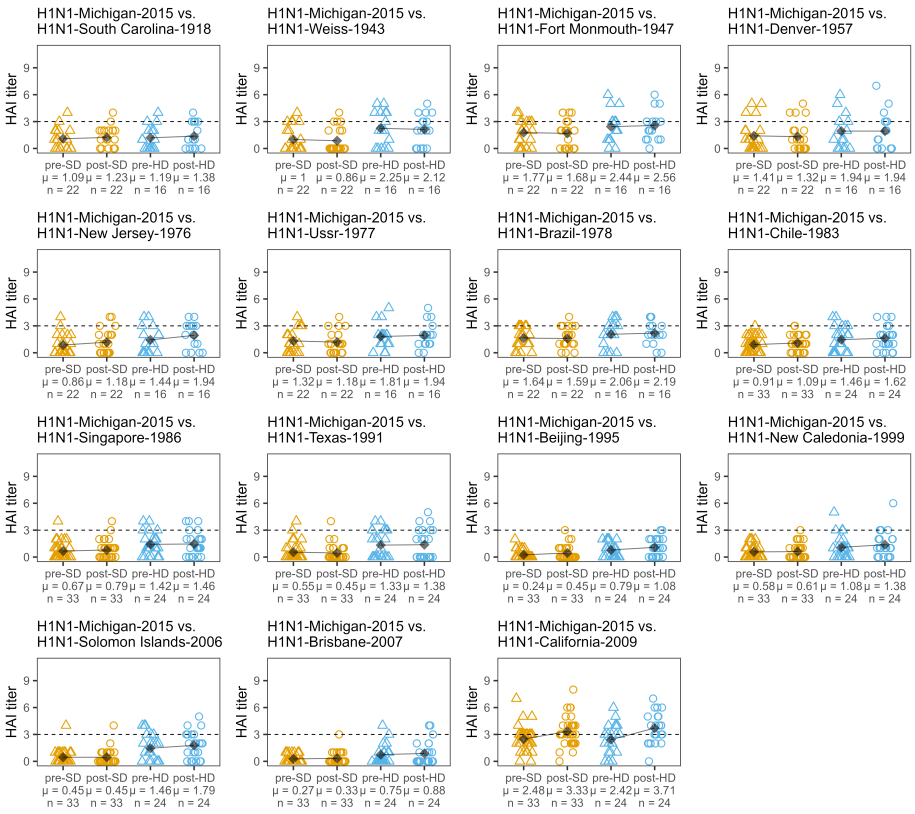

Figure C.5: Heterologous pre- and post- vaccination titer (H1N1-Michigan-2015). The dashed horizontal line is the seroprotection criterion.

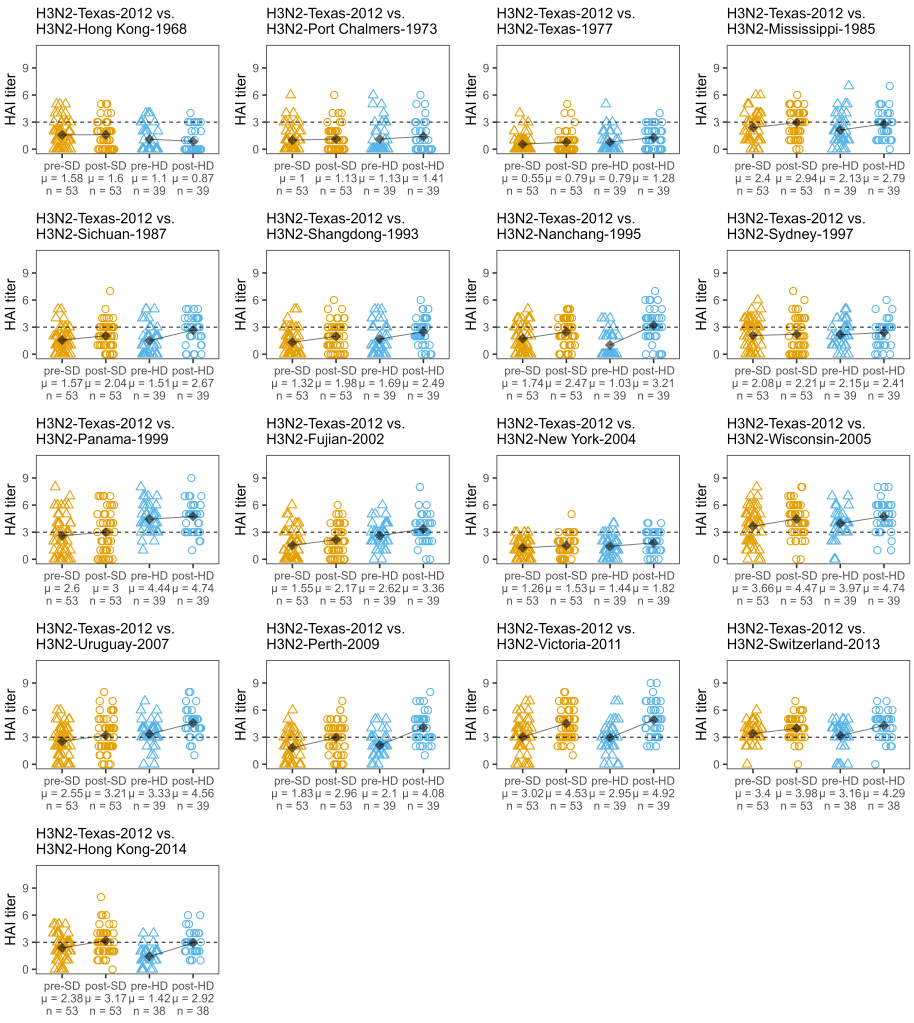

Figure C.6: Heterologous pre- and post- vaccination titer (H3N2-Texas-2012). The dashed horizontal line is the seroprotection criterion.

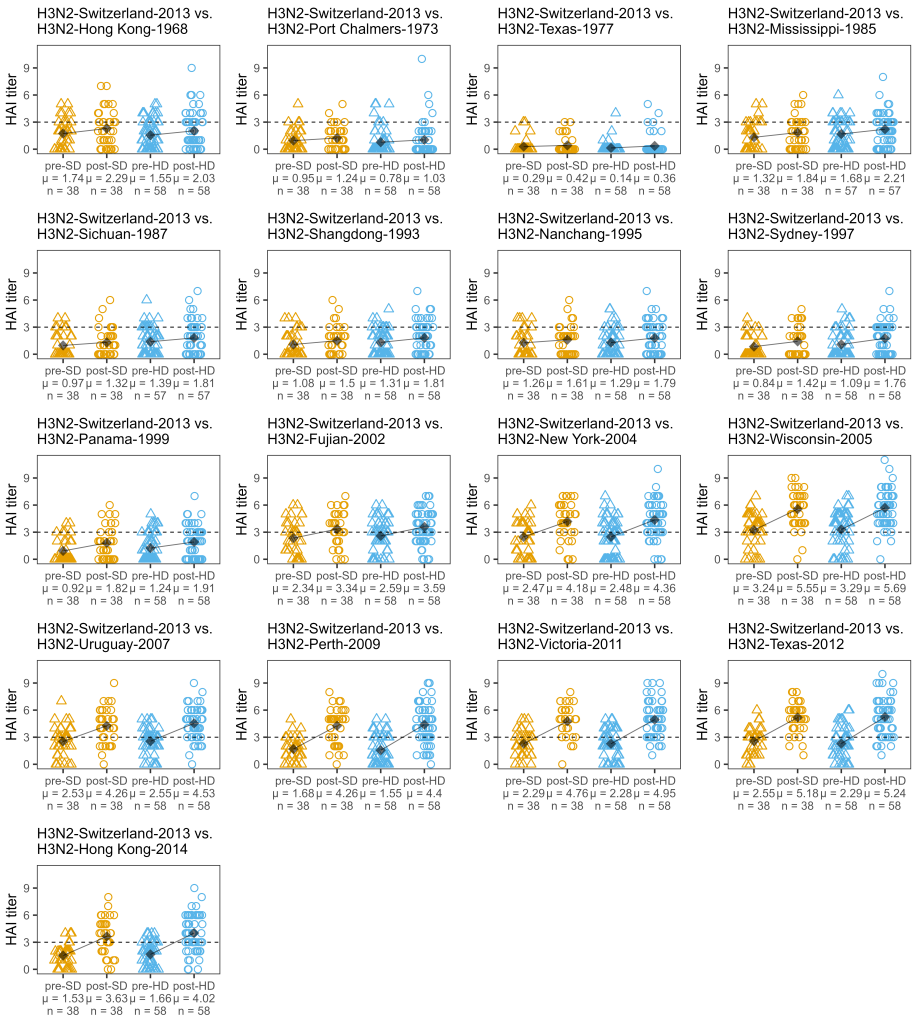

Figure C.7: Heterologous pre- and post- vaccination titer (H3N2-Switzerland-2013). The dashed horizontal line is the seroprotection criterion.

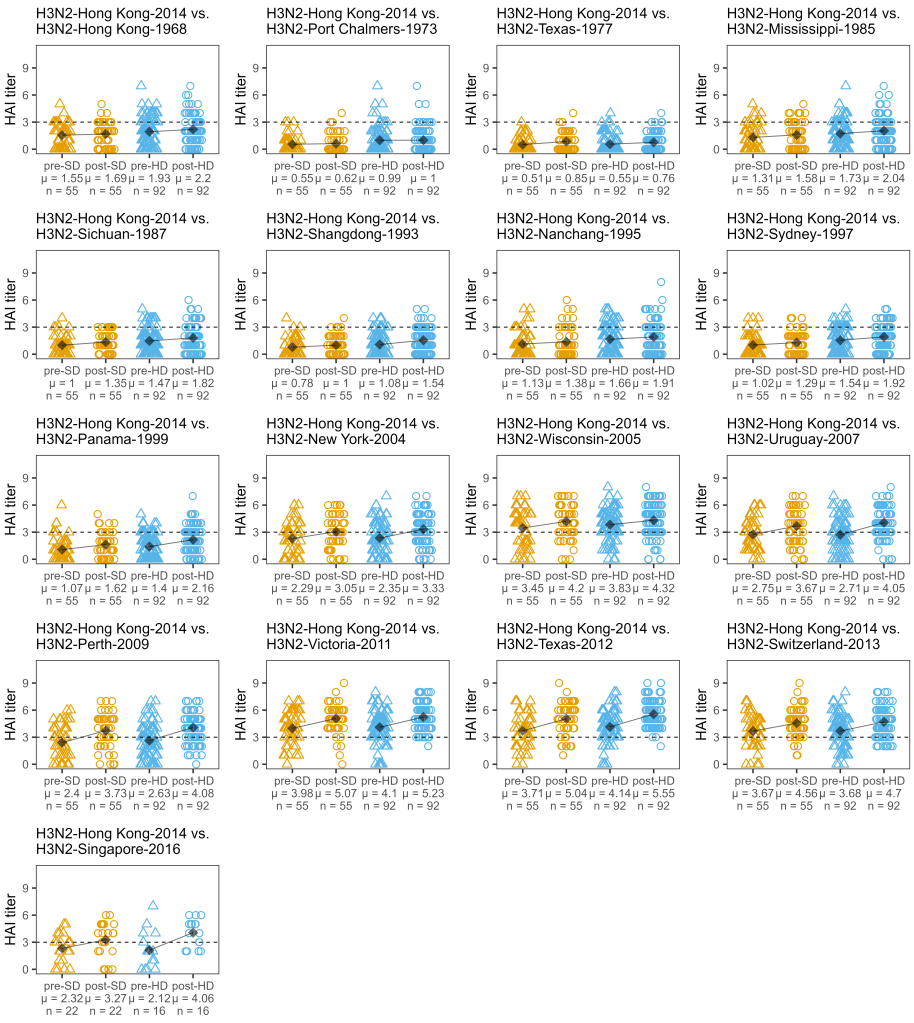

Figure C.8: Heterologous pre- and post- vaccination titer (H3N2-Hong Kong-2014). The dashed horizontal line is the seroprotection criterion.

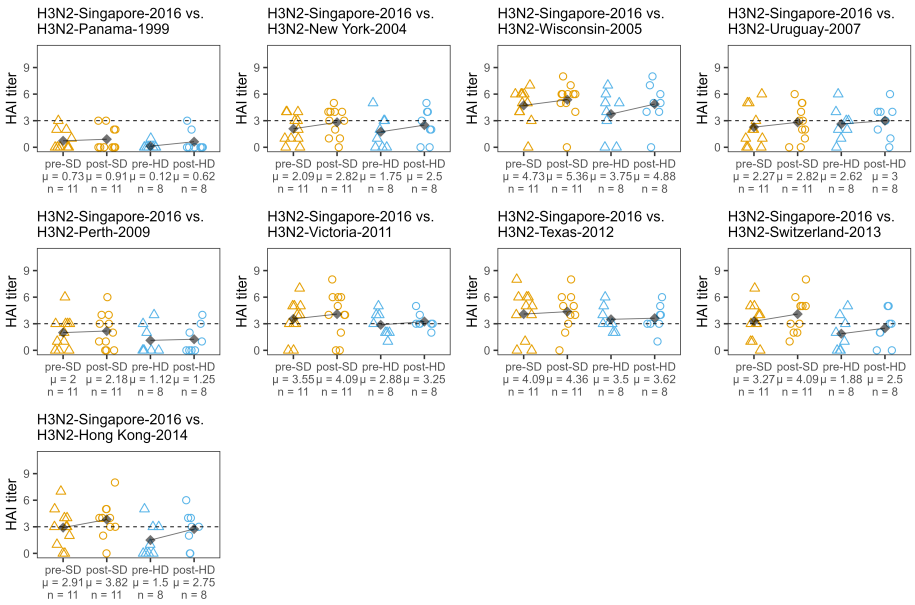

Figure C.9: Heterologous pre- and post- vaccination titer (H3N2-Singapore-2016). The dashed horizontal line is the seroprotection criterion.

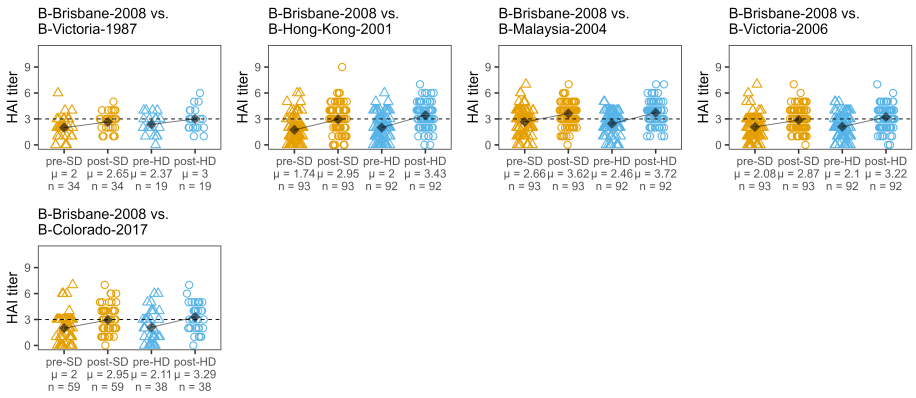

Figure C.10: Heterologous pre- and post- vaccination titer (B-Brisbane-2008). The dashed horizontal line is the seroprotection criterion.

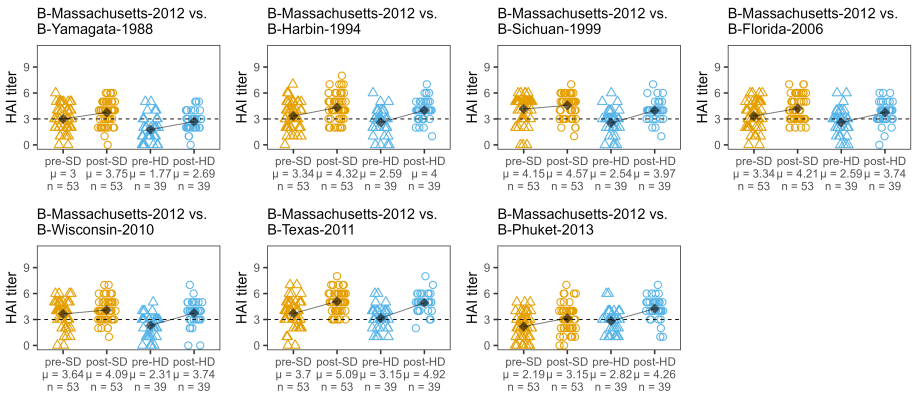

Figure C.11: Heterologous pre- and post- vaccination titer (B-Massachusetts-2012). The dashed horizontal line is the seroprotection criterion.

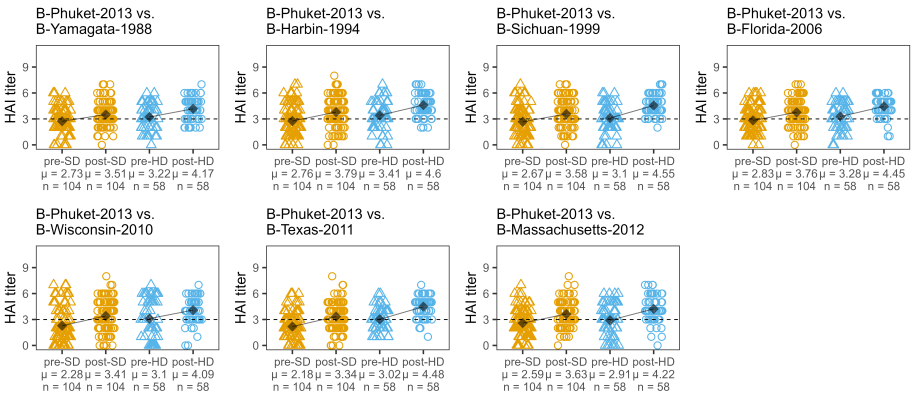

Figure C.12: Heterologous pre- and post- vaccination titer (B-Phuket-2013). The dashed horizontal line is the seroprotection criterion.

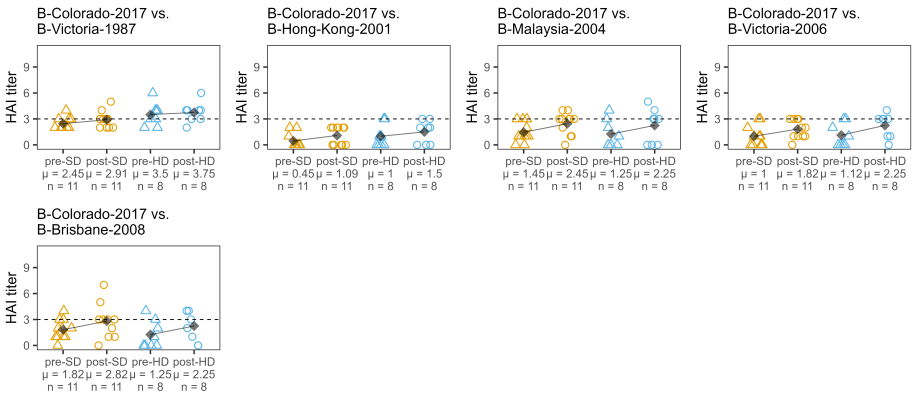

Figure C.13: Heterologous pre- and post- vaccination titer (B-Colorado-2017). The dashed horizontal line is the seroprotection criterion.

Vaccine-specific description

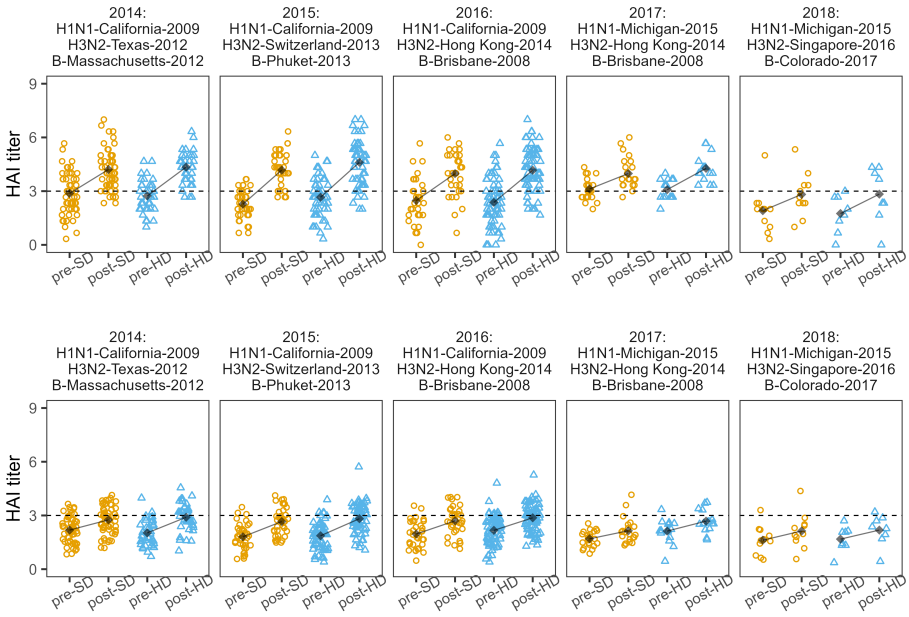

Figure C.14: Pre- and post- vaccination titer by each vaccine. The top row is homologous response, the bottom row is the heterologous response

Repeated vaccinations

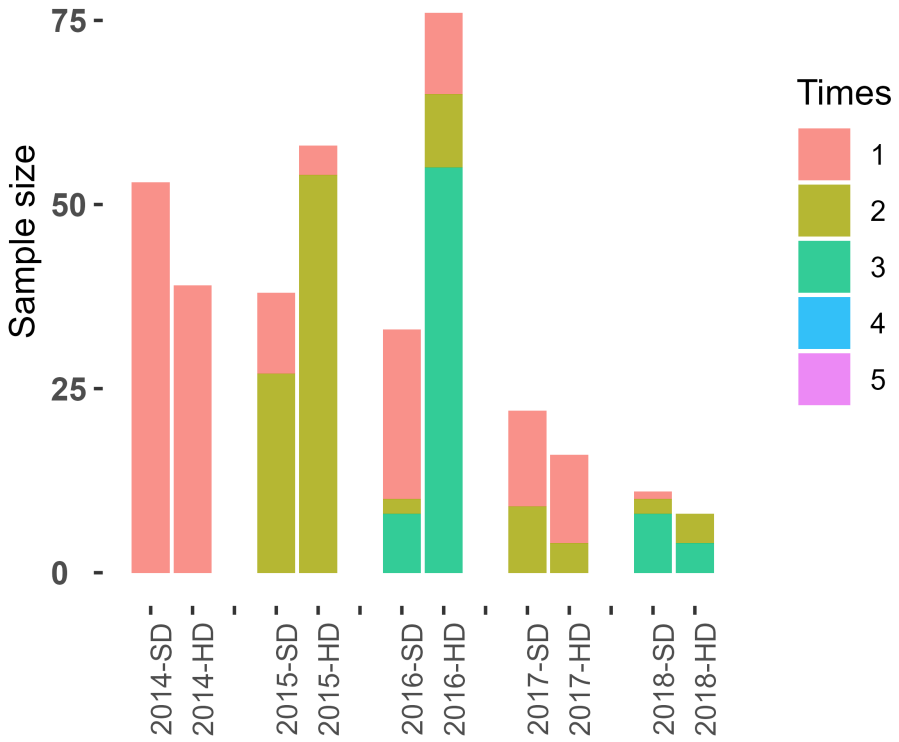

Figure C.15: Repeated vaccination description

C.3.2 Additional results of the main model

This section contains seroconversion and seroprotection heterologous results, as well as the coefficients of sex in either strain-specific and vaccine-specific analyses.

Seroconversion and seroprotection heterologous results

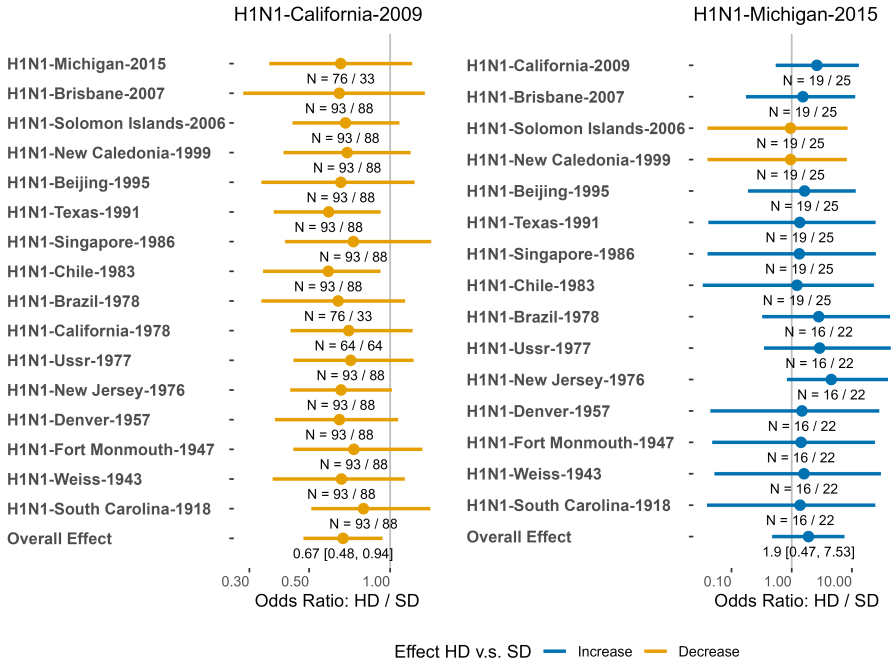

Figure C.16: The impact of HD vaccine compared to SD on strain-specific heterologous seroconversion (H1N1 strains). The median and 89% equal-tailed credible interval (CI) of the overall effect (HD vs SD) are shown. The numbers under each line show the sample size (HD/SD) for that specific strain or the overall effect size.

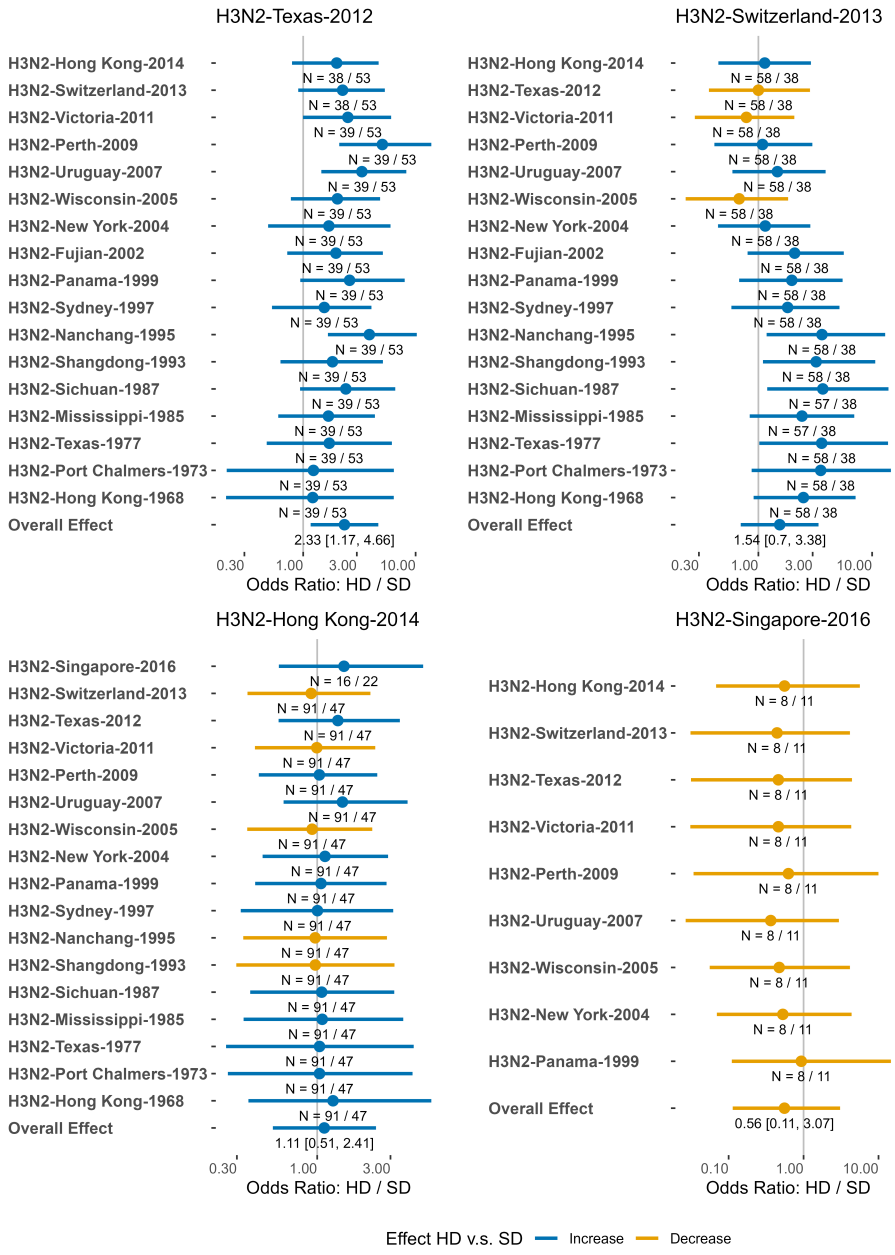

Figure C.17: The impact of HD vaccine compared to SD on strain-specific heterologous seroconversion (H3N2 strains). The median and 89% equal-tailed credible interval (CI) of the overall effect (HD vs. SD) are shown. The numbers under each line show the sample size (HD/SD) for that specific strain or the overall effect size.

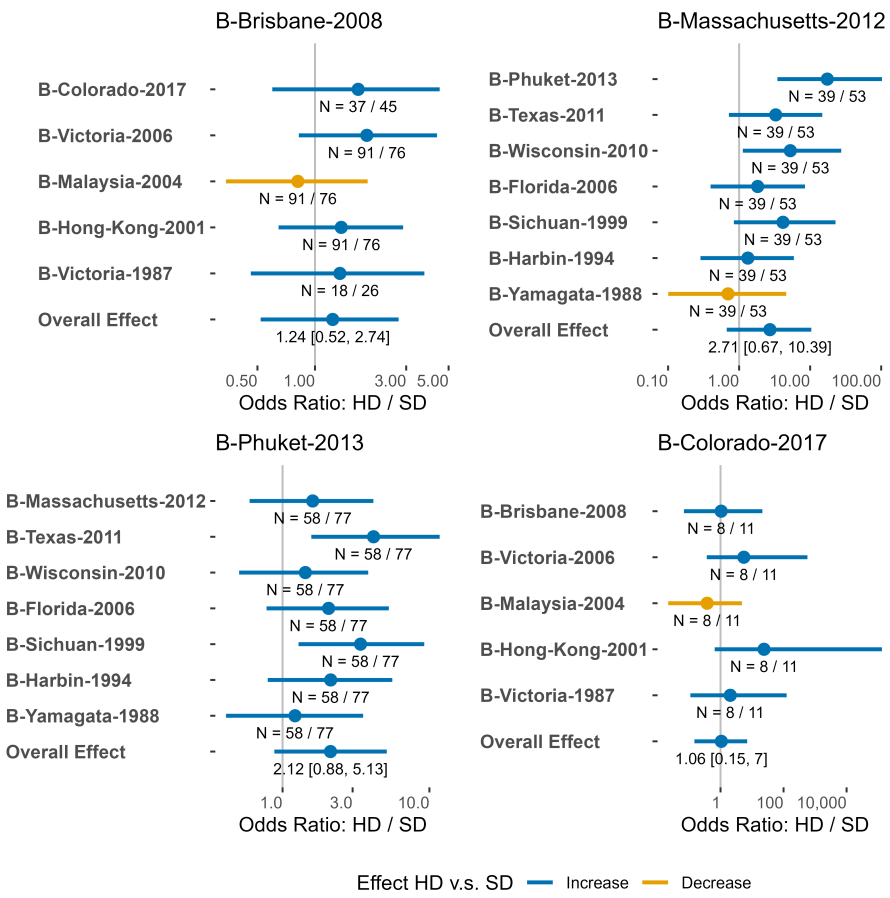

Figure C.18: The impact of HD vaccine compared to SD on strain-specific heterologous seroconversion (B strains). The median and 89% equal-tailed credible interval (CI) of the overall effect (HD vs. SD) are shown. The numbers under each line show the sample size (HD/SD) for that specific strain or the overall effect size.

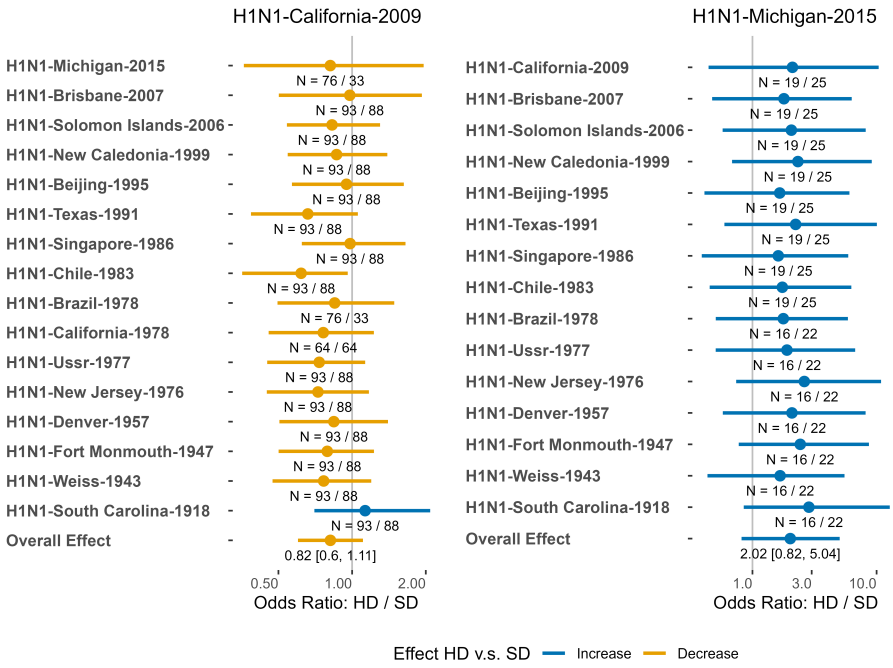

Figure C.19: The impact of HD vaccine compared to SD on vaccine-specific heterologous seroprotection (H1N1 strains). The median and 89% equal-tailed credible interval (CI) of the overall effect (HD vs. SD) are shown. The numbers under each line show the sample size (HD/SD) for that specific strain or the overall effect size.

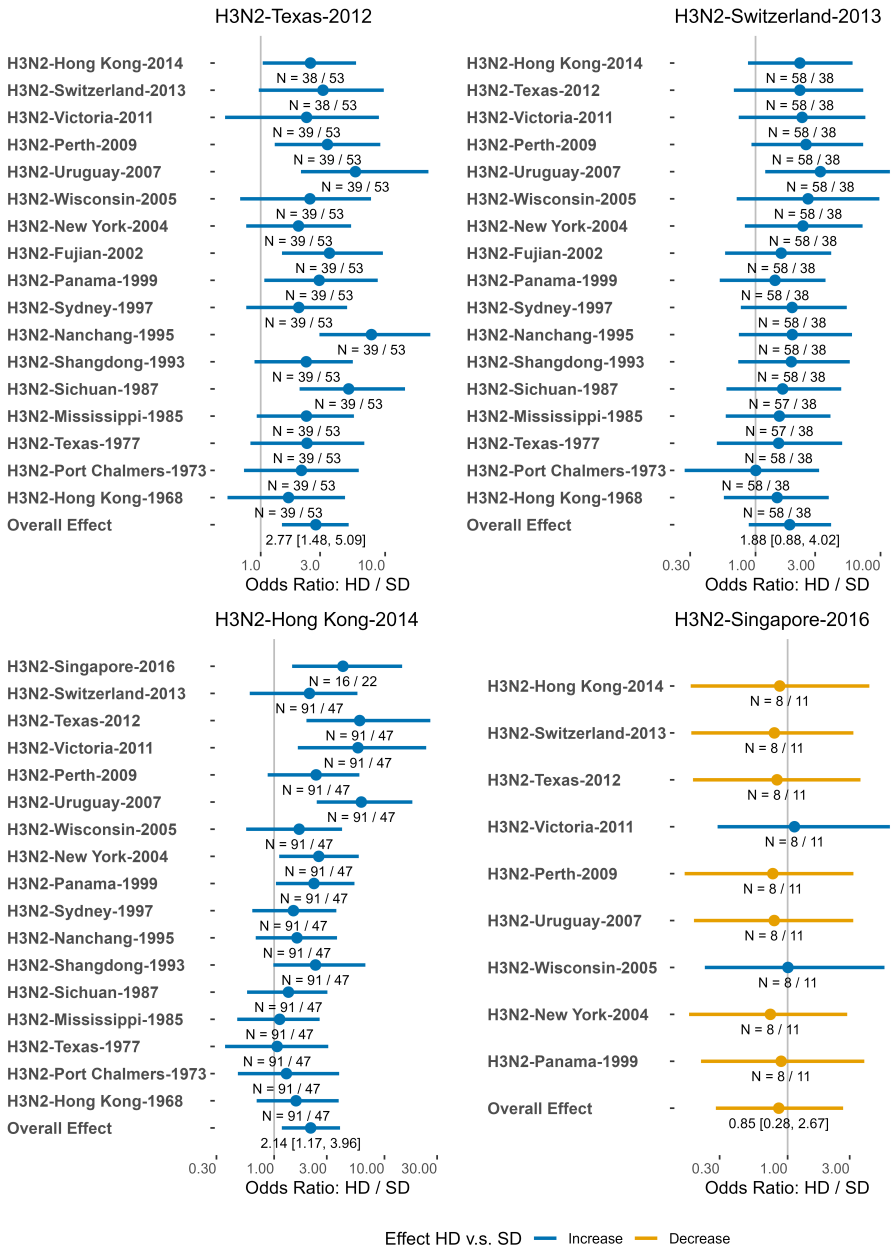

Figure C.20: The impact of HD vaccine compared to SD on vaccine-specific heterologous seroprotection (H3N2 strains). The median and 89% equal-tailed credible interval (CI) of the overall effect (HD vs. SD) are shown. The numbers under each line show the sample size (HD/SD) for that specific strain or the overall effect size.

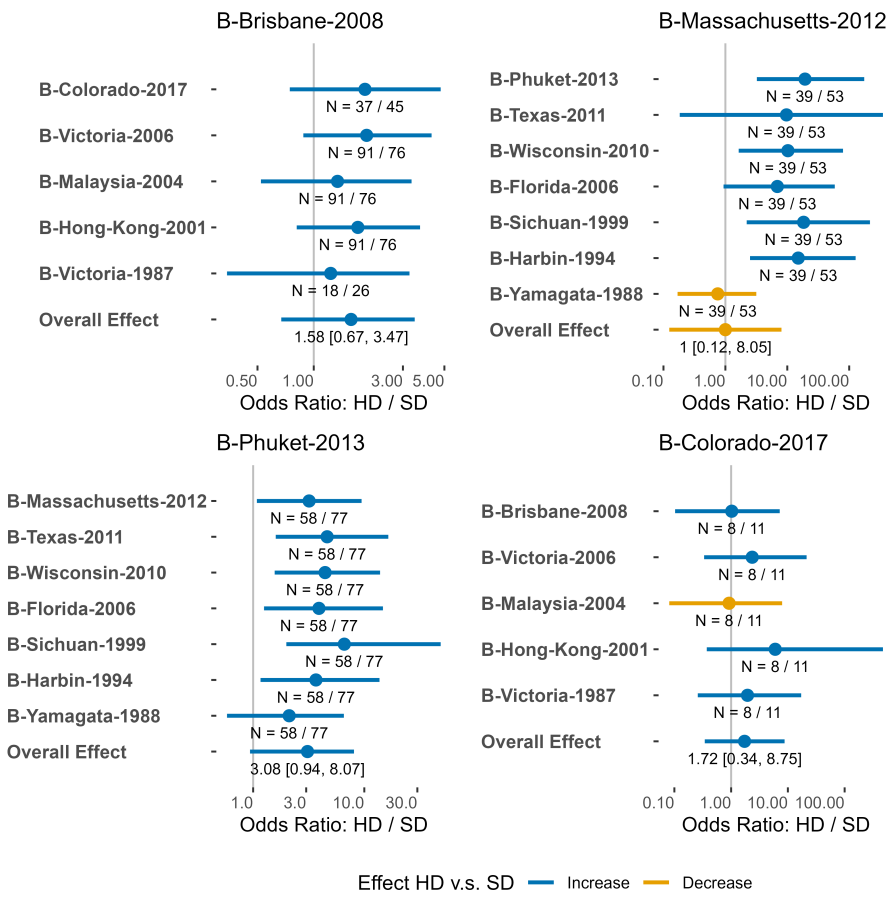

Figure C.21: The impact of HD vaccine compared to SD on vaccine-specific heterologous seroprotection (B strains). The median and 89% equal-tailed credible interval (CI) of the overall effect (HD vs. SD) are shown. The numbers under each line show the sample size (HD/SD) for that specific strain or the overall effect size

Impact of sex

We extracted coefficients of the covariate sex in the main model to show its impact.

Table C.1: The impact of gender in vaccine-specific analyses

Type of outcome	Outcome	Estimation (Male v.s. Female)
Homologous	Titer increase	-0.35, 89%CI: -0.53 to -0.16
Heterologous	Titer increase	-0.19, 89%CI: -0.31 to -0.07
Homologous	Seroconversion	0.71, 89%CI: 0.52 to 0.97
Heterologous	Seroconversion	0.64, 89%CI: 0.49 to 0.84
Homologous	Seroprotection	0.91, 89%CI: 0.59 to 1.43
Heterologous	Seroprotection	0.84, 89%CI: 0.64 to 1.1

C.3.3 Sensitivity analysis

To explore the robustness of the main results, we compared results by using different data and model approaches.

Multilevel model (including young SD participants)

We first included participants younger than 65 years old into SD group.

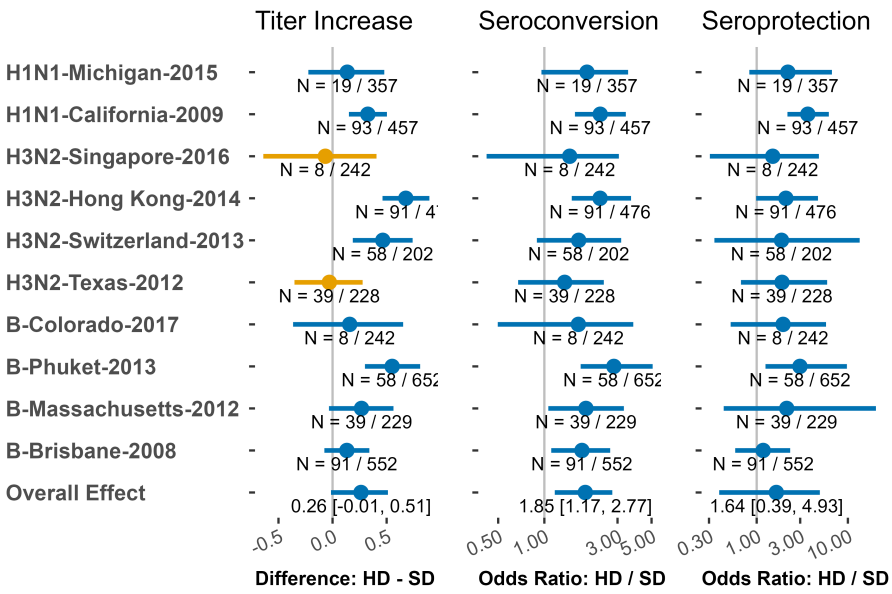

Figure C.22: The impact of HD vaccine compared to SD on strain-specific homologous responses. The median and 89% equal-tailed credible interval (CI) of the overall effect (HD vs. SD) are shown. The numbers under each line show the sample size (HD/SD) for that specific strain or the overall effect size.

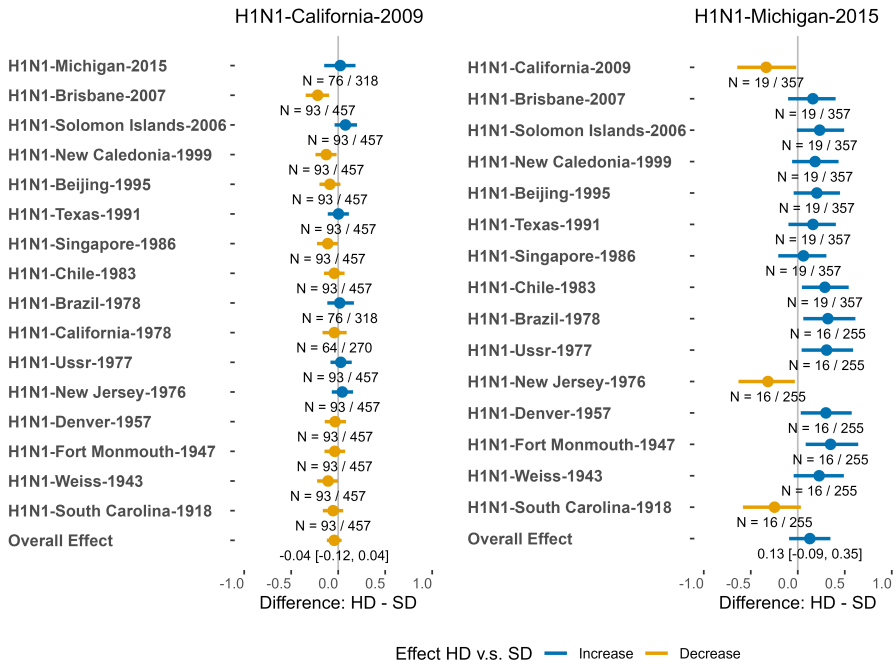

Figure C.23: The impact of HD vaccine compared to SD on strain-specific heterologous titer increase (H1N1 strains). The median and 89% equal-tailed credible interval (CI) of the overall effect (HD vs. SD) are shown. The numbers under each line show the sample size (HD/SD) for that specific strain or the overall effect size.

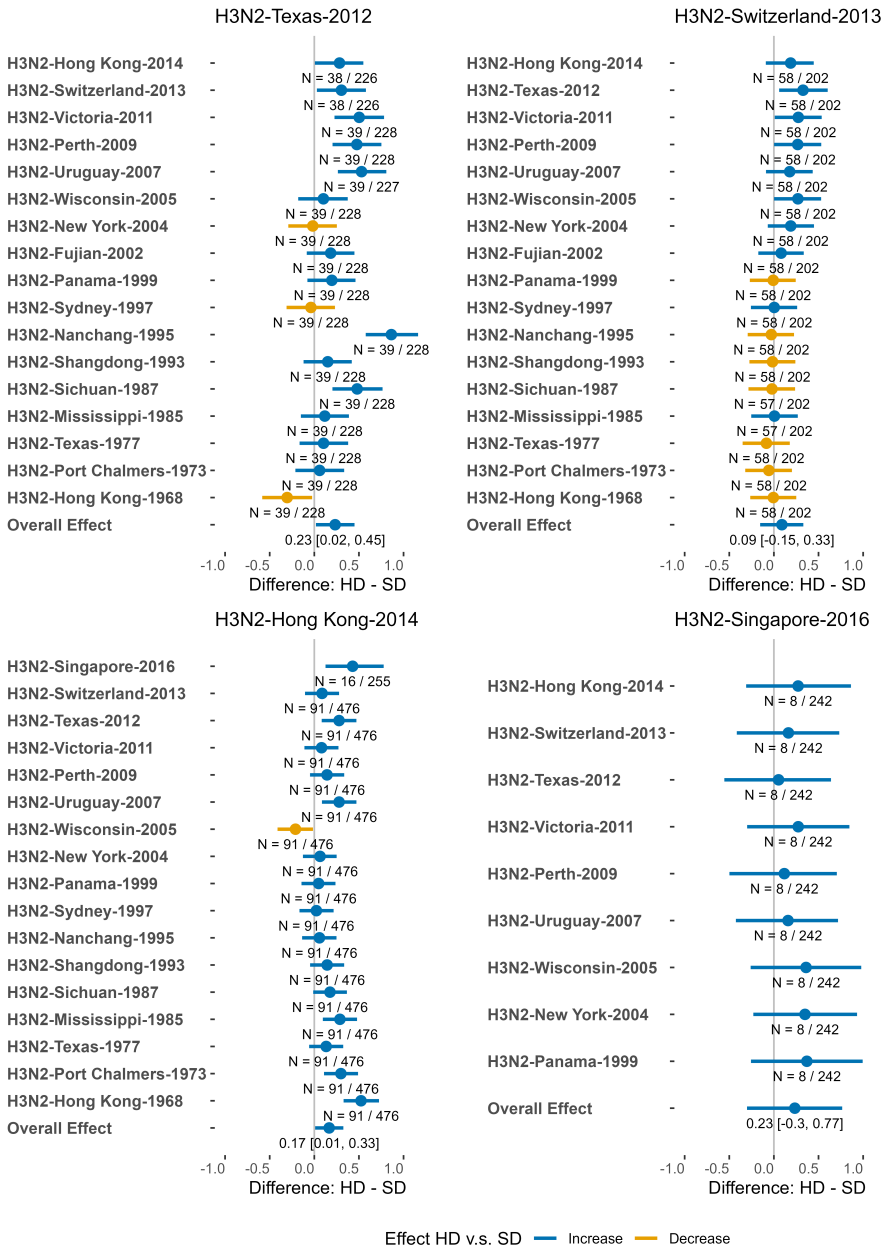

Figure C.24: The impact of HD vaccine compared to SD on strain-specific heterologous titer increase (H3N2 strains). The median and 89% equal-tailed credible interval (CI) of the overall effect (HD vs. SD) are shown. The numbers under each line show the sample size (HD/SD) for that specific strain or the overall effect size.

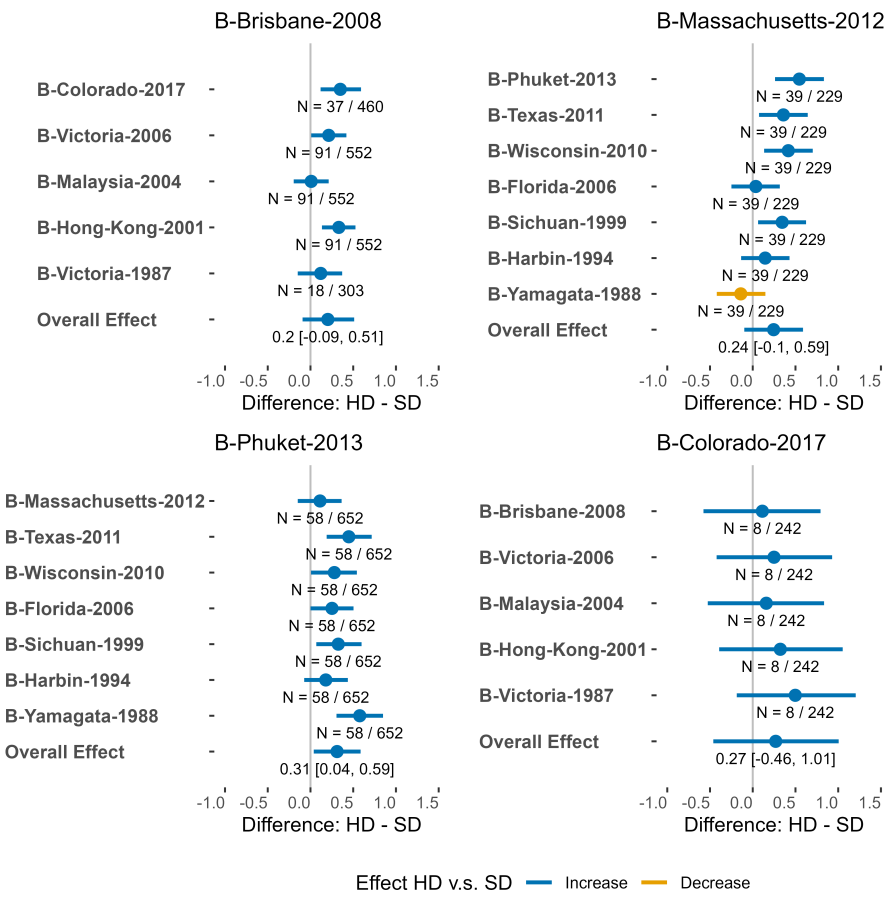

Figure C.25: The impact of HD vaccine compared to SD on strain-specific heterologous titer increase (B strains). The median and 89% equal-tailed credible interval (CI) of the overall effect (HD vs. SD) are shown. The numbers under each line show the sample size (HD/SD) for that specific strain or the overall effect size.

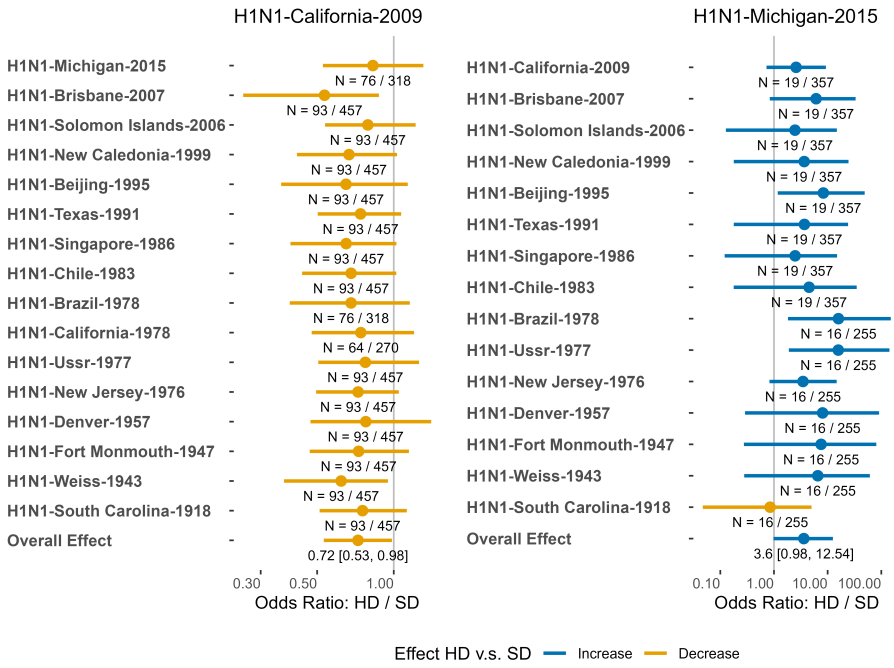

Figure C.26: The impact of HD vaccine compared to SD on strain-specific heterologous seroconversion (H1N1 strains). The median and 89% equal-tailed credible interval (CI) of the overall effect (HD vs. SD) are shown. The numbers under each line show the sample size (HD/SD) for that specific strain or the overall effect size.

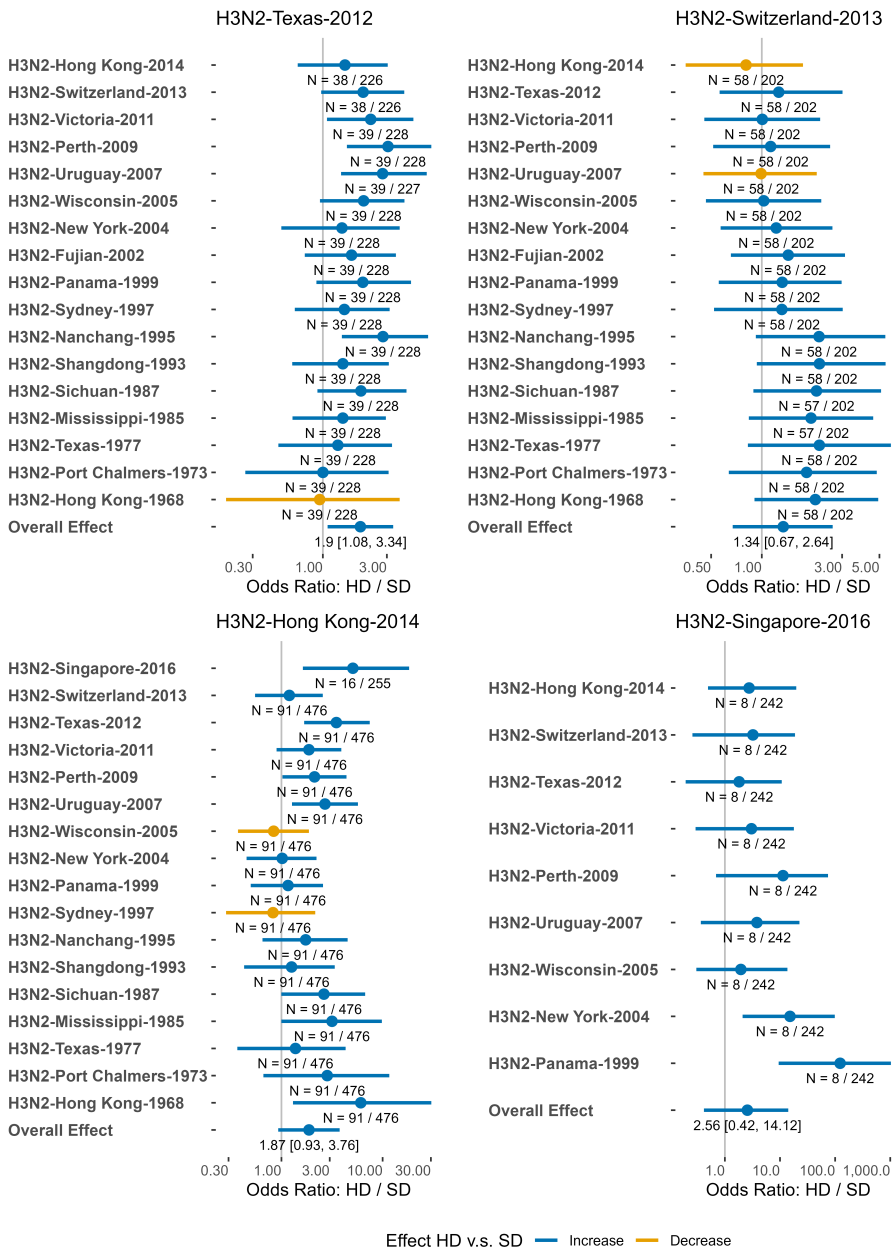

Figure C.27: The impact of HD vaccine compared to SD on strain-specific heterologous seroconversion (H3N2 strains). The median and 89% equal-tailed credible interval (CI) of the overall effect (HD vs. SD) are shown. The numbers under each line show the sample size (HD/SD) for that specific strain or the overall effect size.

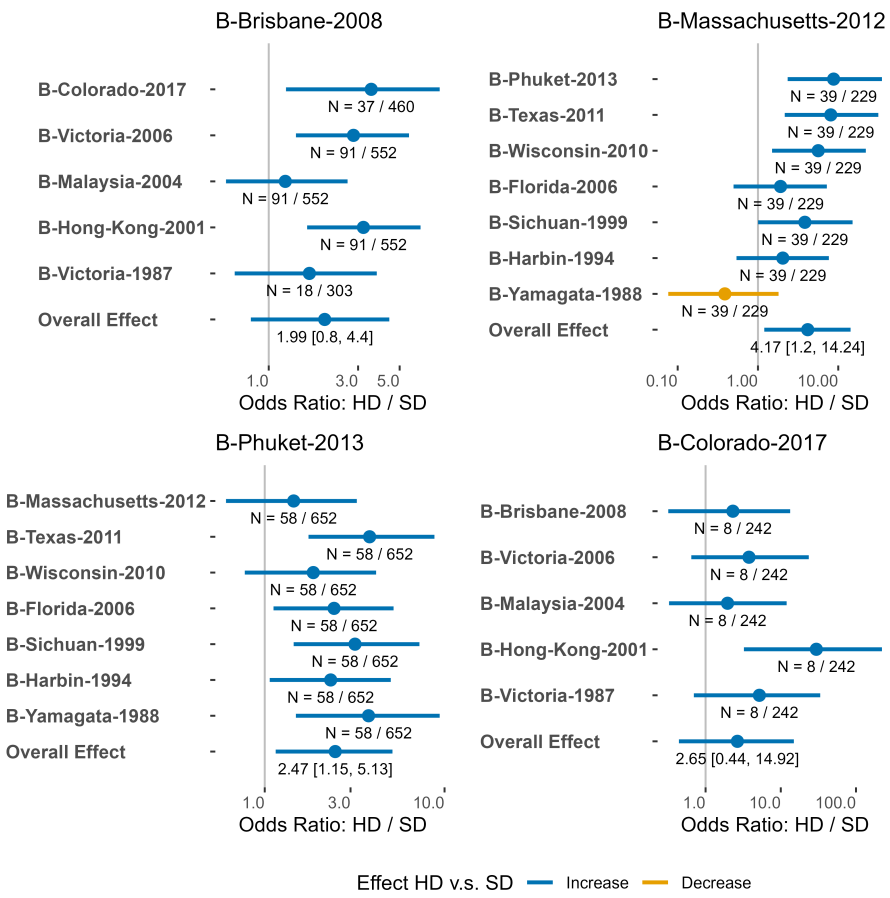

Figure C.28: The impact of HD vaccine compared to SD on strain-specific heterologous seroconversion (B strains). The median and 89% equal-tailed credible interval (CI) of the overall effect (HD vs. SD) are shown. The numbers under each line show the sample size (HD/SD) for that specific strain or the overall effect size.

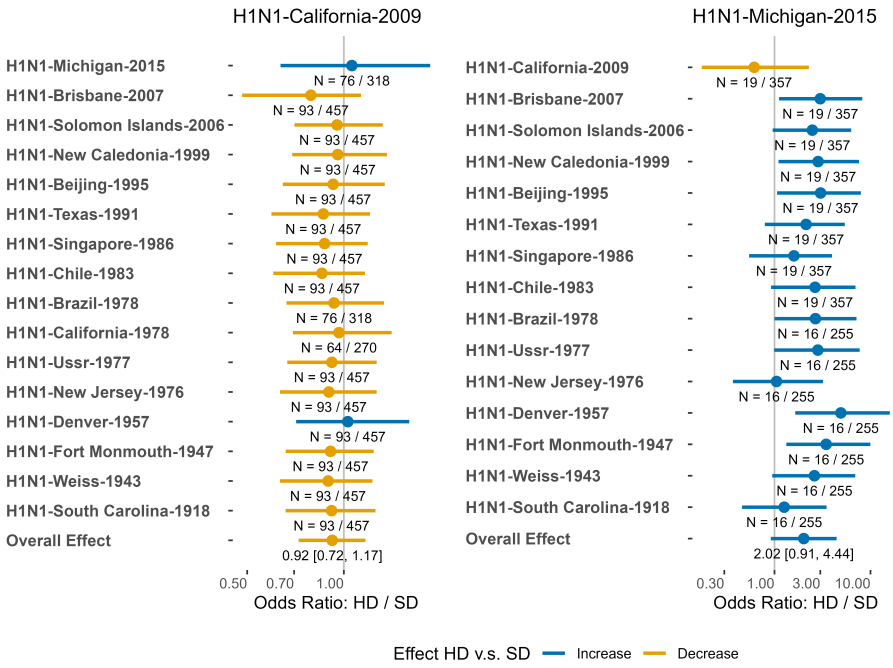

Figure C.29: The impact of HD vaccine compared to SD on strain-specific heterologous seroprotection (H1N1 strains). The median and 89% equal-tailed credible interval (CI) of the overall effect (HD vs. SD) are shown. The numbers under each line show the sample size (HD/SD) for that specific strain or the overall effect size.

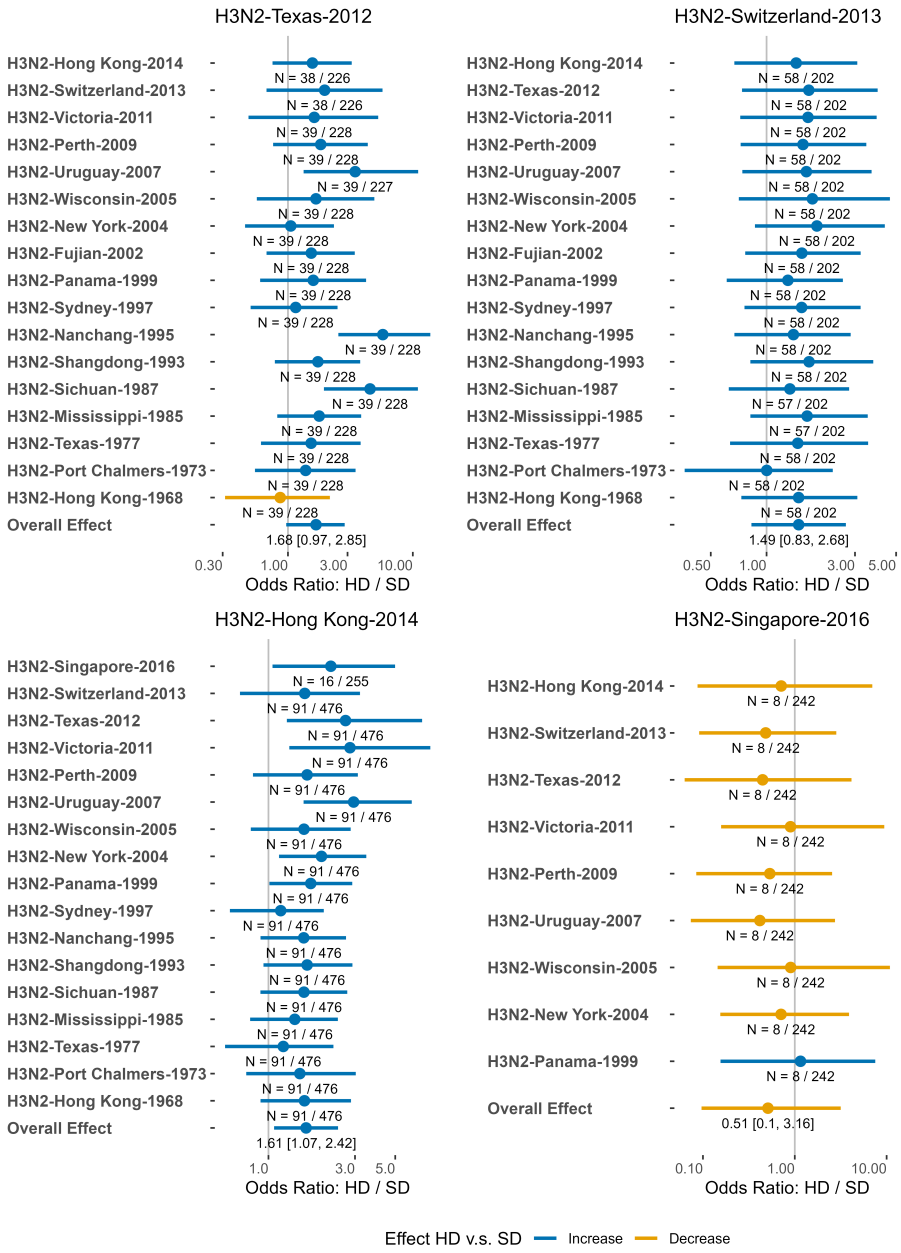

Figure C.30: The impact of HD vaccine compared to SD on strain-specific heterologous seroprotection (H3N2 strains). The median and 89% equal-tailed credible interval (CI) of the overall effect (HD vs. SD) are shown. The numbers under each line show the sample size (HD/SD) for that specific strain or the overall effect size.

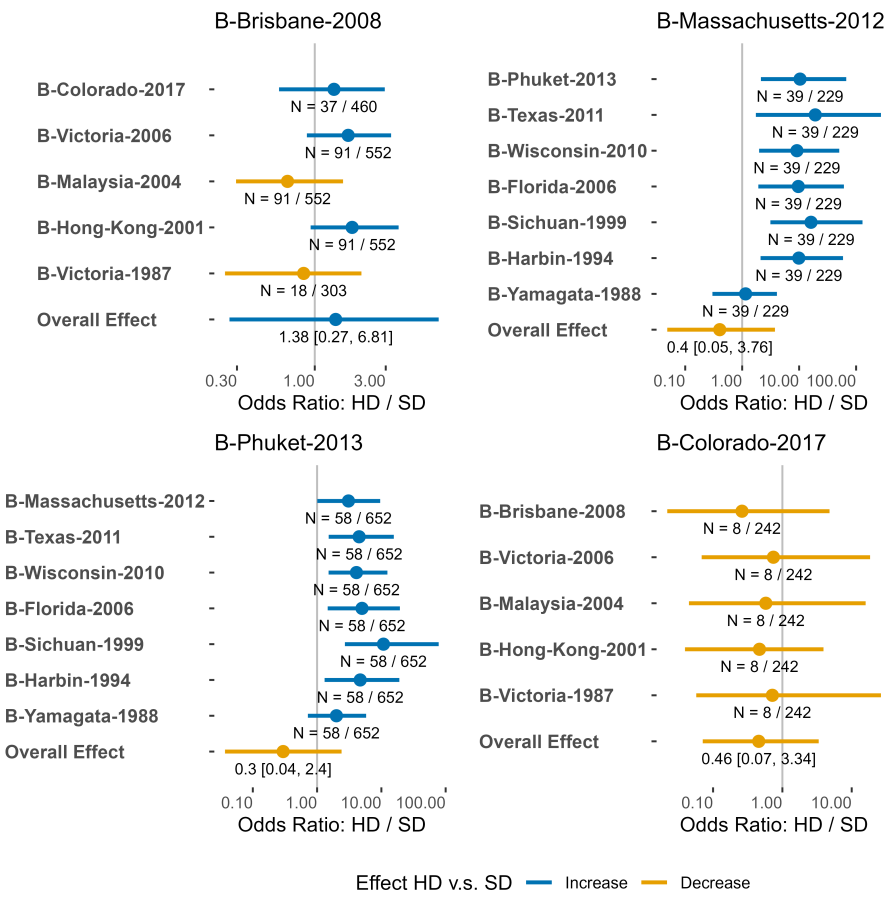

Figure C.31: The impact of HD vaccine compared to SD on strain-specific heterologous seroprotection (B strains). The median and 89% equal-tailed credible interval (CI) of the overall effect (HD vs. SD) are shown. The numbers under each line show the sample size (HD/SD) for that specific strain or the overall effect size.

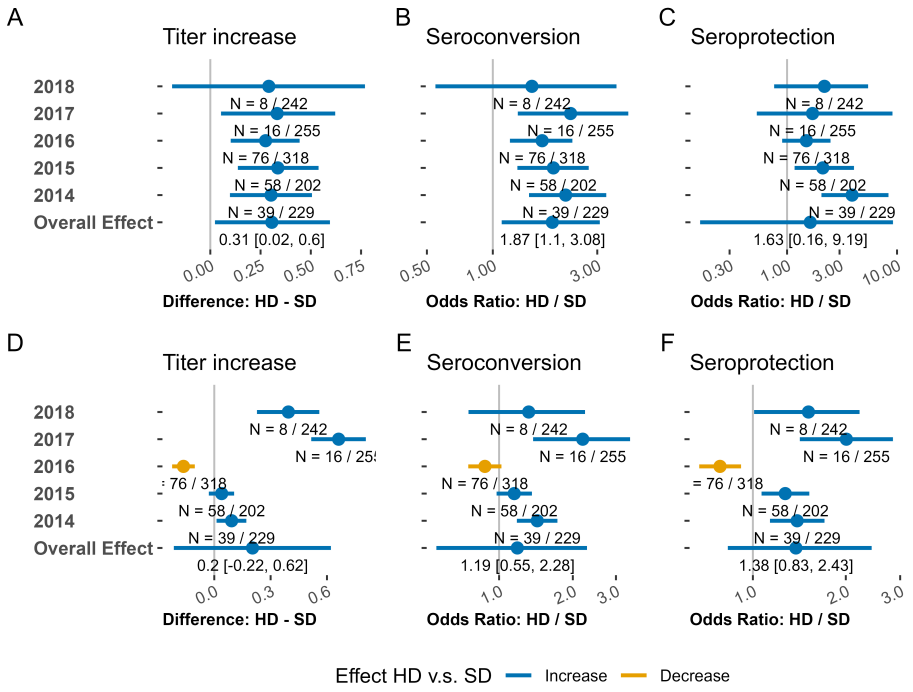

Figure C.32: The impact of HD vaccine compared to SD on vaccine-specific analyses. The median and 89% equal-tailed credible interval (CI) of the overall effect (HD vs. SD) are shown. The numbers under each line show the sample size (HD/SD) for that specific strain or the overall effect size. The top row shows homologous responses (A to C), the bottom row is heterologous (D to F).

Generalized linear models

We used generalized linear model to estimate the impact of vaccine dose by pairs of each vaccine strain and HAI tested strain. Therefore, in coefficient plots, coefficients came from different models.

The impact of HD vaccine compared to SD on strain-specific homologous response

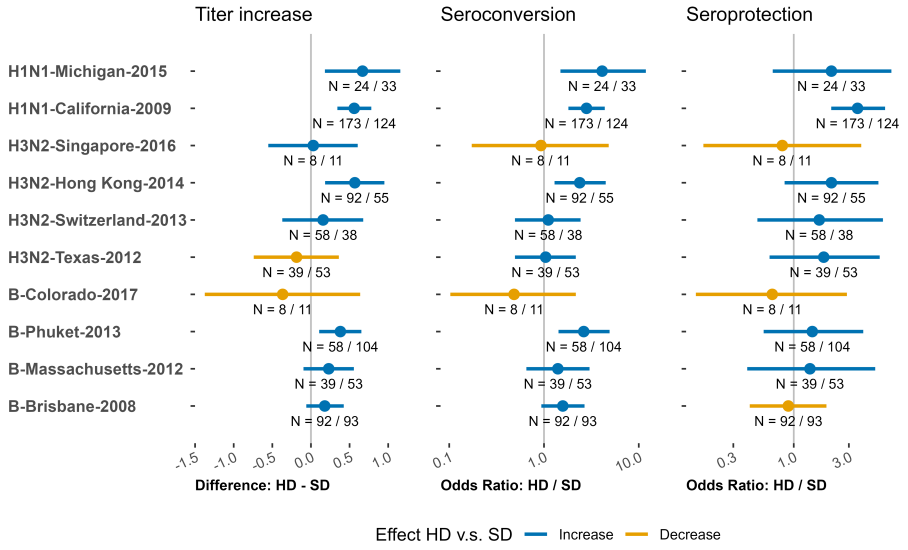

Figure C.33: The impact of HD vaccine compared to SD on strain-specific, homologous HAI titer increase. The median and 89% equal-tailed credible interval (CI) of the overall effect (HD vs. SD) are shown. The numbers under each line show the sample size (HD/SD) for that specific strain or the overall effect size.

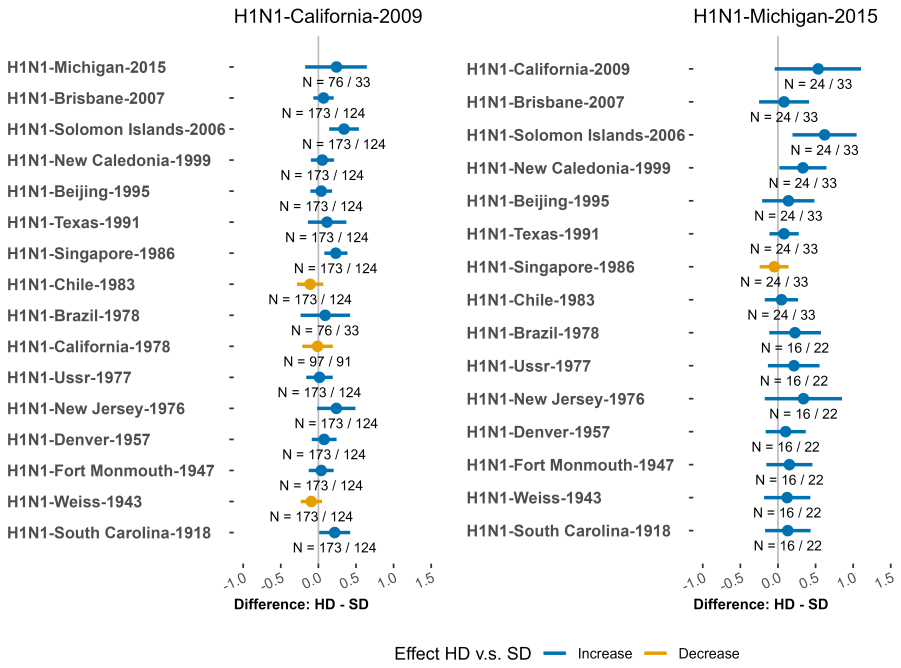

Figure C.34: The impact of HD vaccine compared to SD on strain-specific, heterologous HAI titer increase (H1N1 strains). The median and 89% equal-tailed credible interval (CI) of the overall effect (HD vs. SD) are shown. The numbers under each line show the sample size (HD/SD) for that specific strain or the overall effect size.

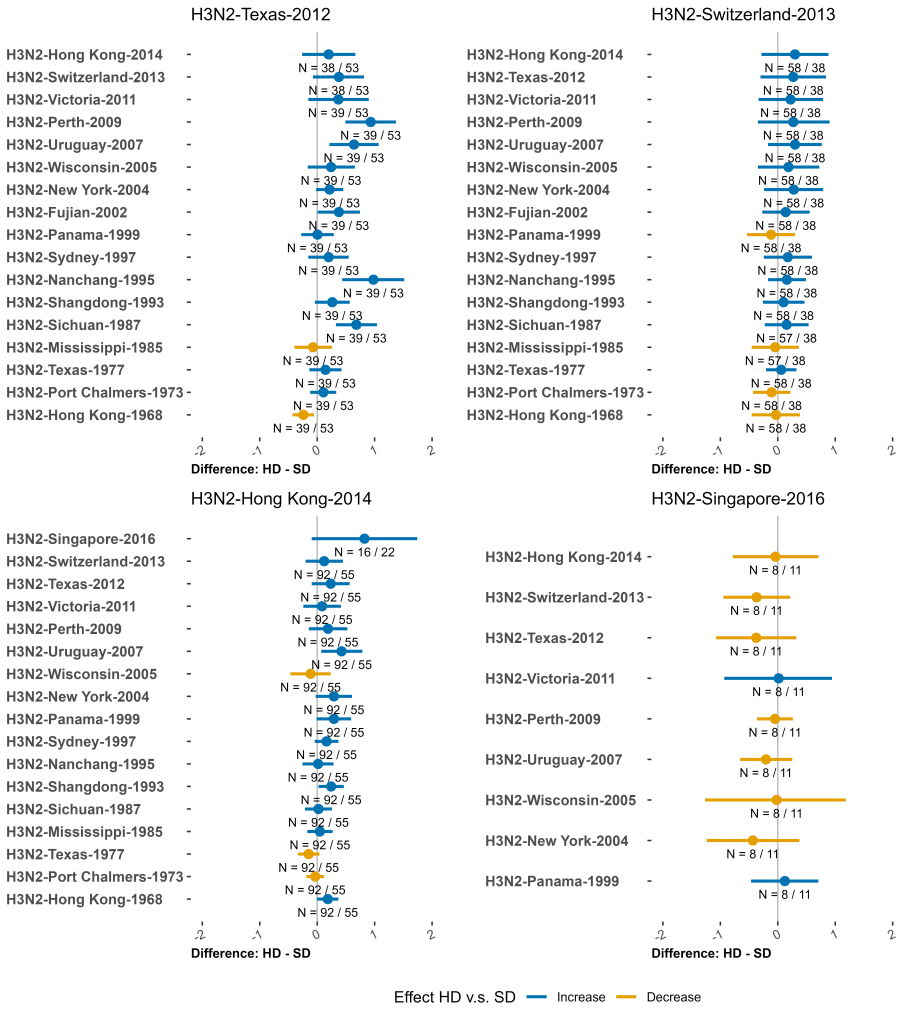

Figure C.35: The impact of HD vaccine compared to SD on strain-specific, heterologous HAI titer increase (H3N2 strains). The median and 89% equal-tailed credible interval (CI) of the overall effect (HD vs. SD) are shown. The numbers under each line show the sample size (HD/SD) for that specific strain or the overall effect size.

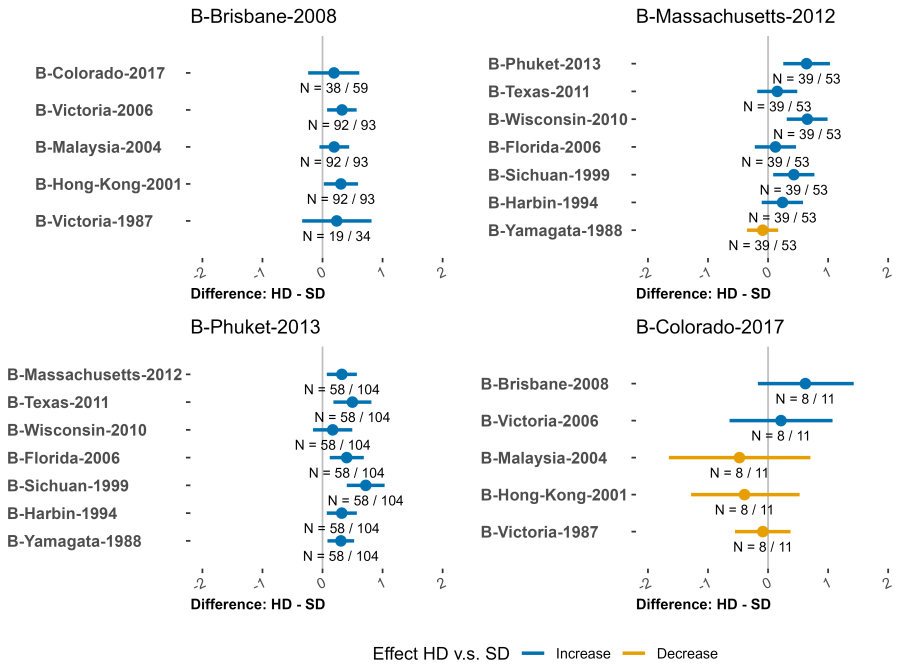

Figure C.36: The impact of HD vaccine compared to SD on strain-specific, heterologous HAI titer increase (B strains). The median and 89% equal-tailed credible interval (CI) of the overall effect (HD vs. SD) are shown. The numbers under each line show the sample size (HD/SD) for that specific strain or the overall effect size.

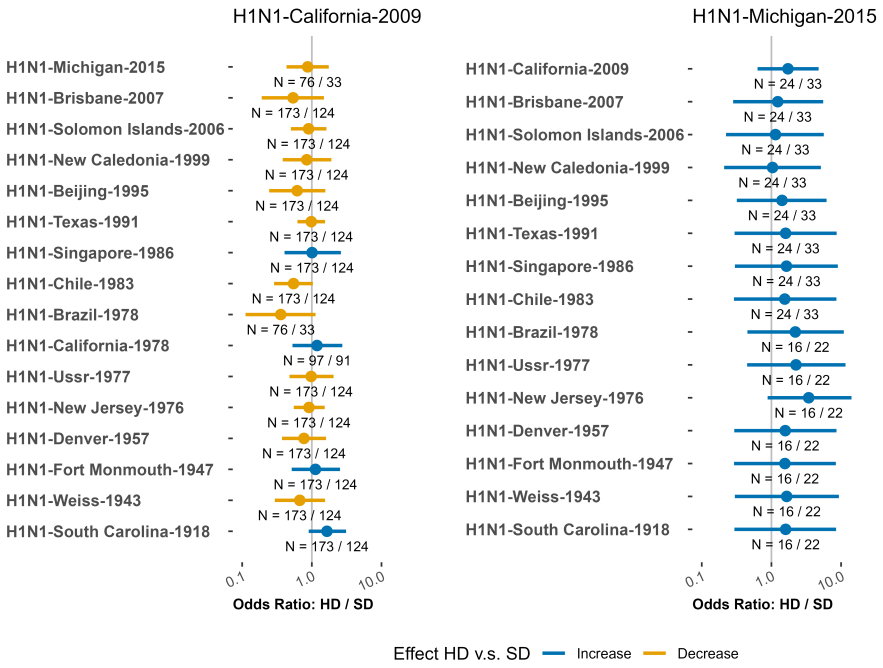

Figure C.37: The impact of HD vaccine compared to SD on strain-specific heterologous seroconversion (H1N1 strains). The median and 89% equal-tailed credible interval (CI) of the overall effect (HD vs. SD) are shown. The numbers under each line show the sample size (HD/SD) for that specific strain or the overall effect size

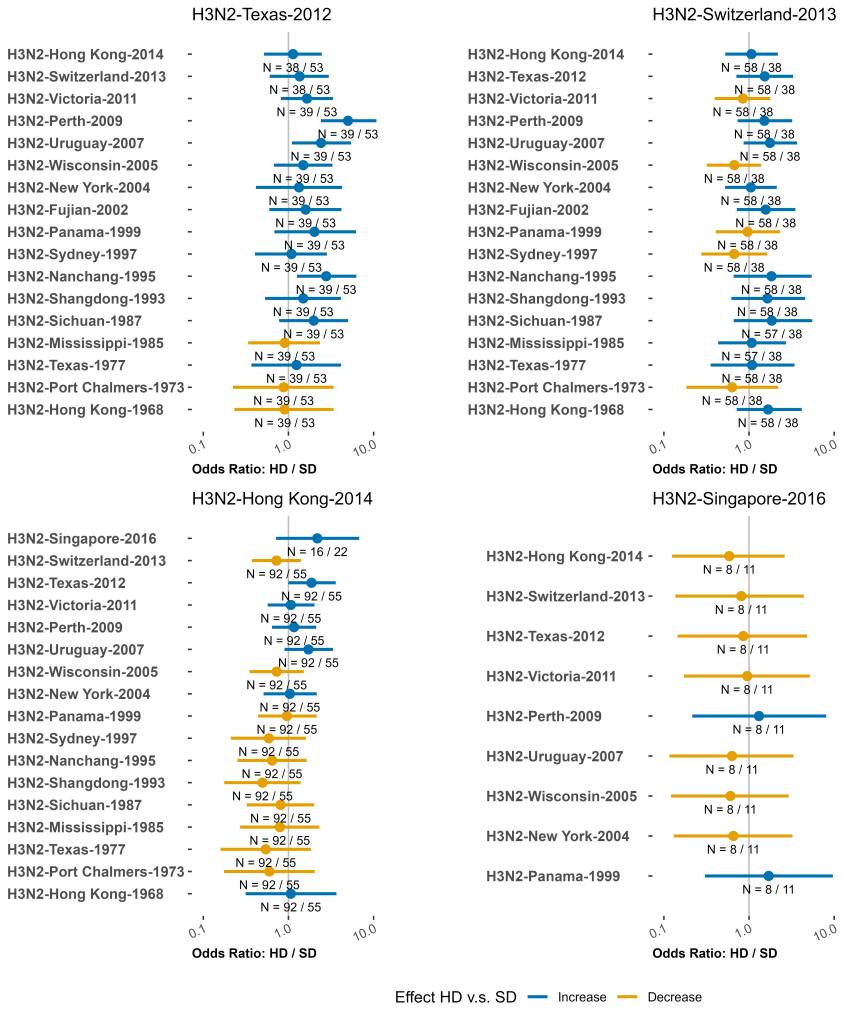

Figure C.38: The impact of HD vaccine compared to SD on strain-specific heterologous seroconversion (H3N2 strains). The median and 89% equal-tailed credible interval (CI) of the overall effect (HD vs. SD) are shown. The numbers under each line show the sample size (HD/SD) for that specific strain or the overall effect size.

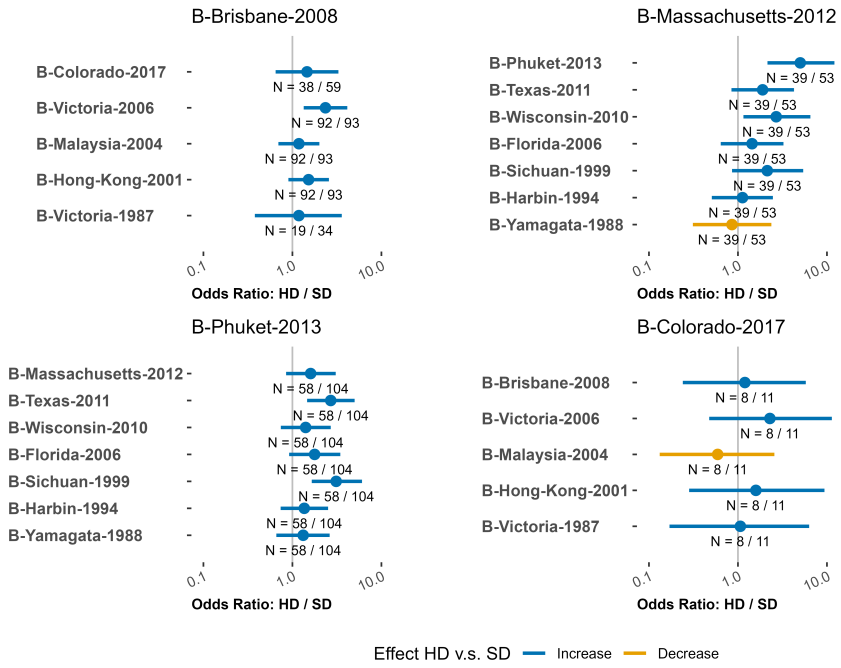

Figure C.39: The impact of HD vaccine compared to SD on strain-specific heterologous seroconversion (B strains). The median and 89% equal-tailed credible interval (CI) of the overall effect (HD vs. SD) are shown. The numbers under each line show the sample size (HD/SD) for that specific strain or the overall effect size.

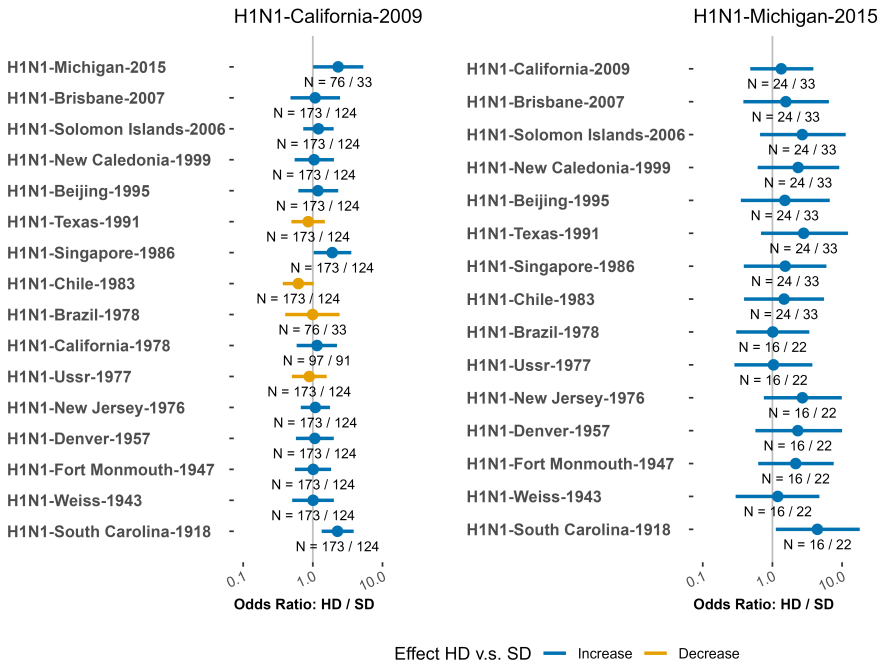

Figure C.40: The impact of HD vaccine compared to SD on strain-specific heterologous seroprotection (H1N1 strains). The median and 89% equal-tailed credible interval (CI) of the overall effect (HD vs. SD) are shown. The numbers under each line show the sample size (HD/SD) for that specific strain or the overall effect size.

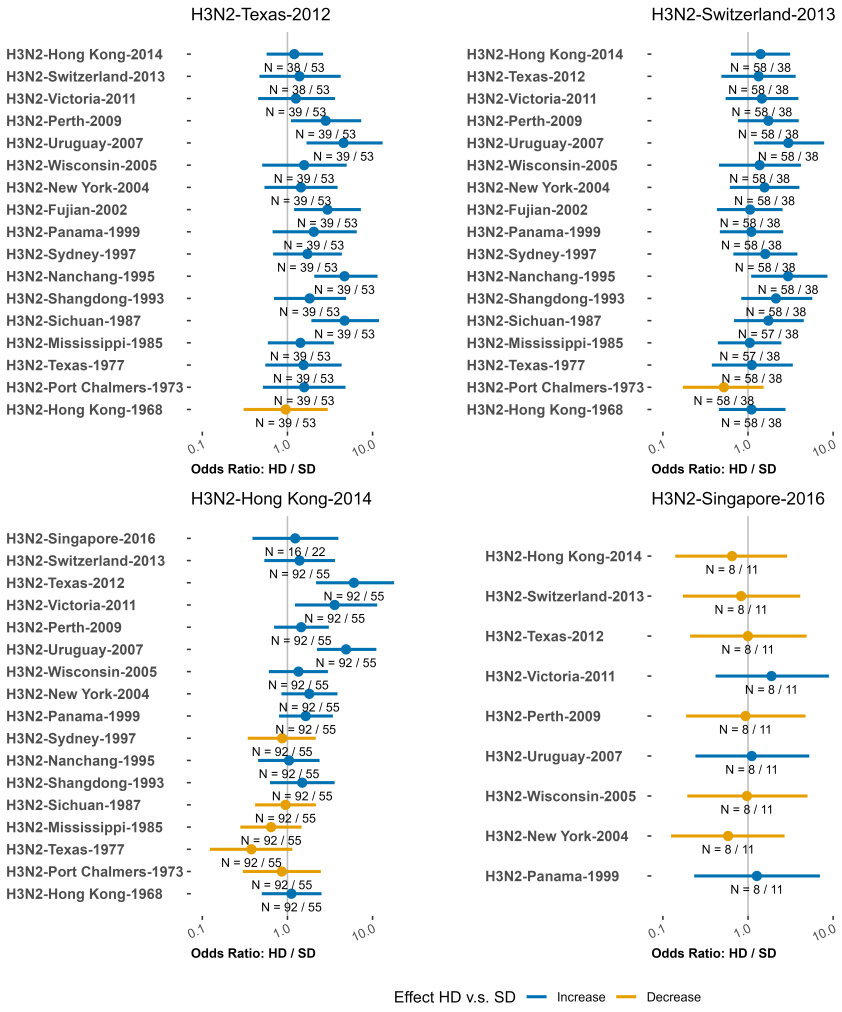

Figure C.41: The impact of HD vaccine compared to SD on strain-specific heterologous seroprotection (H3N2 strains). The median and 89% equal-tailed credible interval (CI) of the overall effect (HD vs. SD) are shown. The numbers under each line show the sample size (HD/SD) for that specific strain or the overall effect size.

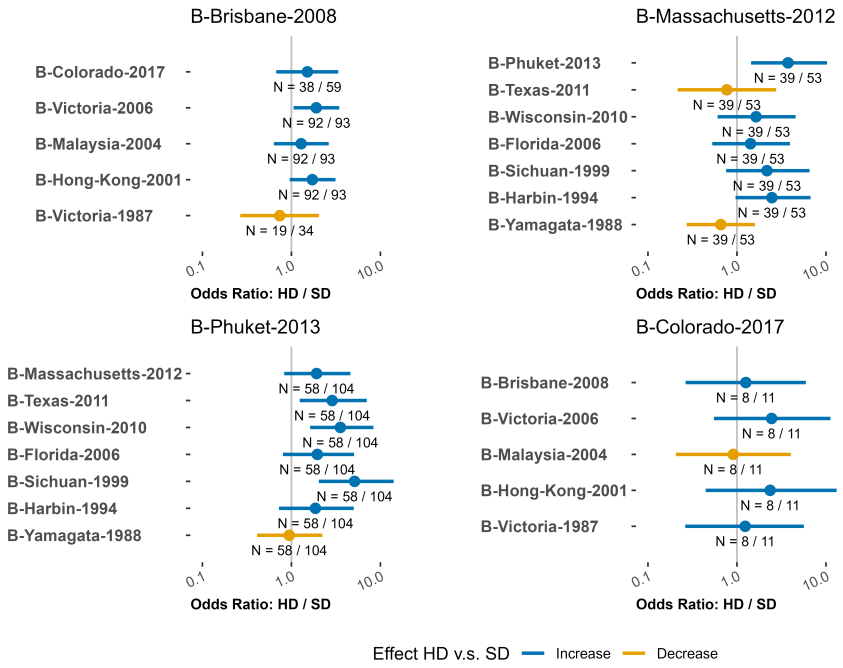

Figure C.42: The impact of HD vaccine compared to SD on strain-specific heterologous seroprotection (B strains). The median and 89% equal-tailed credible interval (CI) of the overall effect (HD vs. SD) are shown. The numbers under each line show the sample size (HD/SD) for that specific strain or the overall effect size.

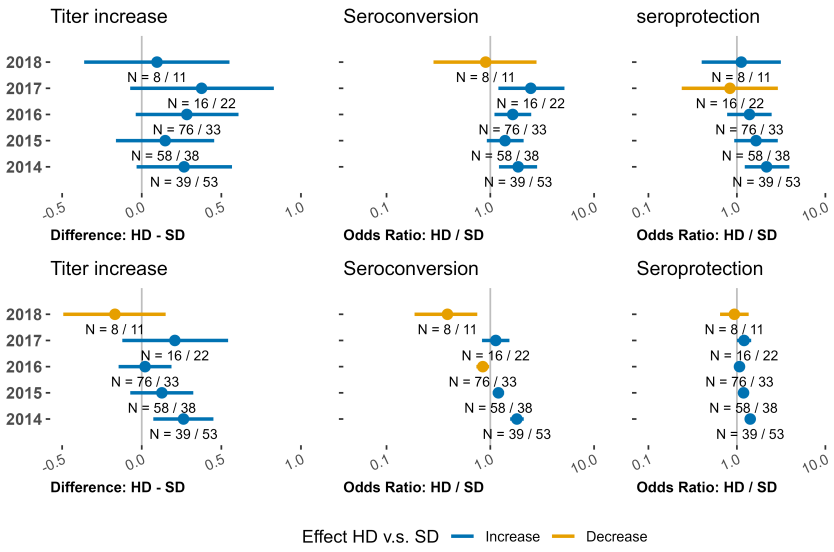

Figure C.43: The impact of HD vaccine compared to SD on vaccine-specific HAI responses. The median and 89% equal-tailed credible interval (CI) of the overall effect (HD vs. SD) are shown. The numbers under each line show the sample size (HD/SD) for that specific strain or the overall effect size. The top row shows homologous responses, the bottom row is heterologous.

Propensity score matching model

We use the same model setting as the generalized linear model with data based on propensity score matching. We used 1:1 matching on variables of age, sex, pre-vaccine titer and race (using the nearest neighbor matching algorithm (Ho et al., 2007/ed).

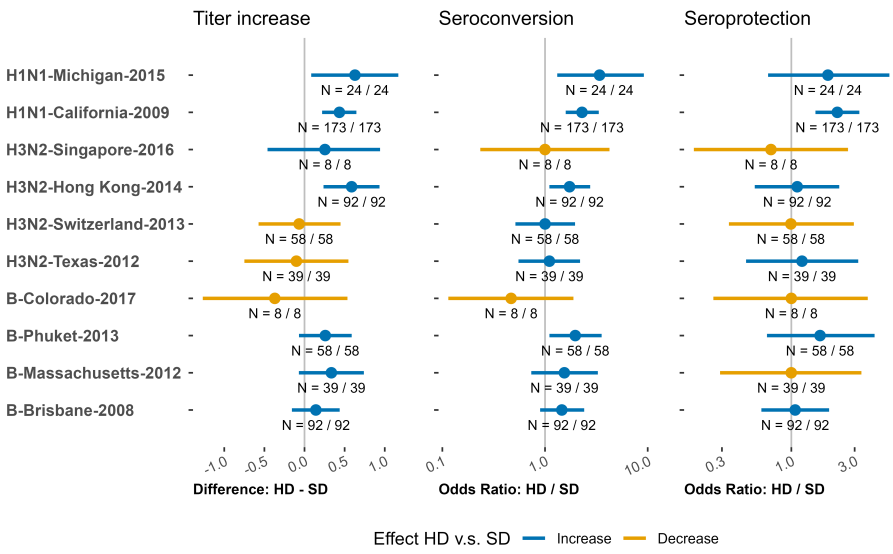

Figure C.44: The impact of HD vaccine compared to SD on strain-specific, homologous HAI titer increase. The median and 89% equal-tailed credible interval (CI) of the overall effect (HD vs. SD) are shown. The numbers under each line show the sample size (HD/SD) for that specific strain or the overall effect size.

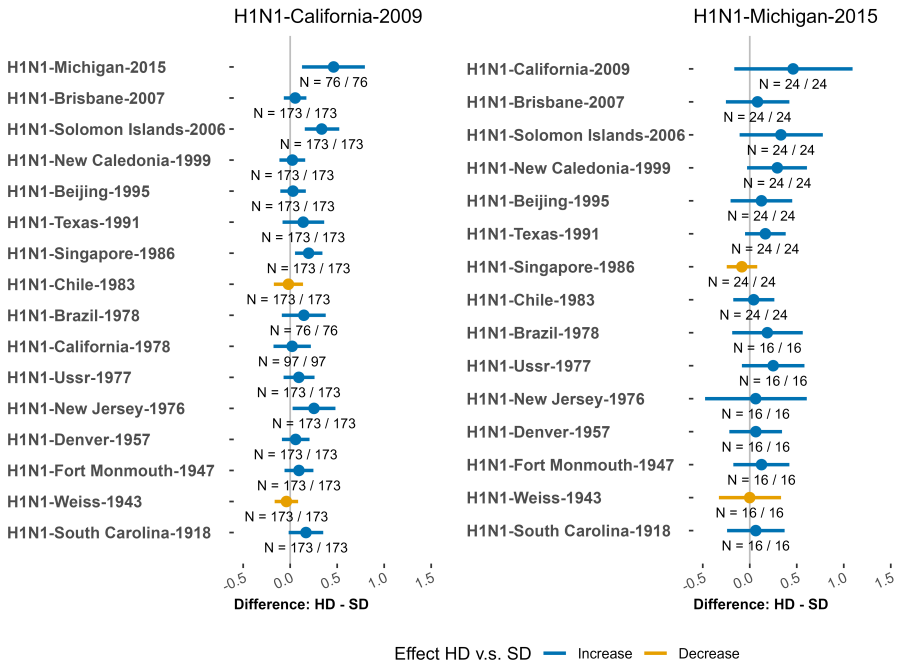

Figure C.45: The impact of HD vaccine compared to SD on strain-specific, heterologous HAI titer increase (H1N1 strains). The median and 89% equal-tailed credible interval (CI) of the overall effect (HD vs. SD) are shown. The numbers under each line show the sample size (HD/SD) for that specific strain or the overall effect size.

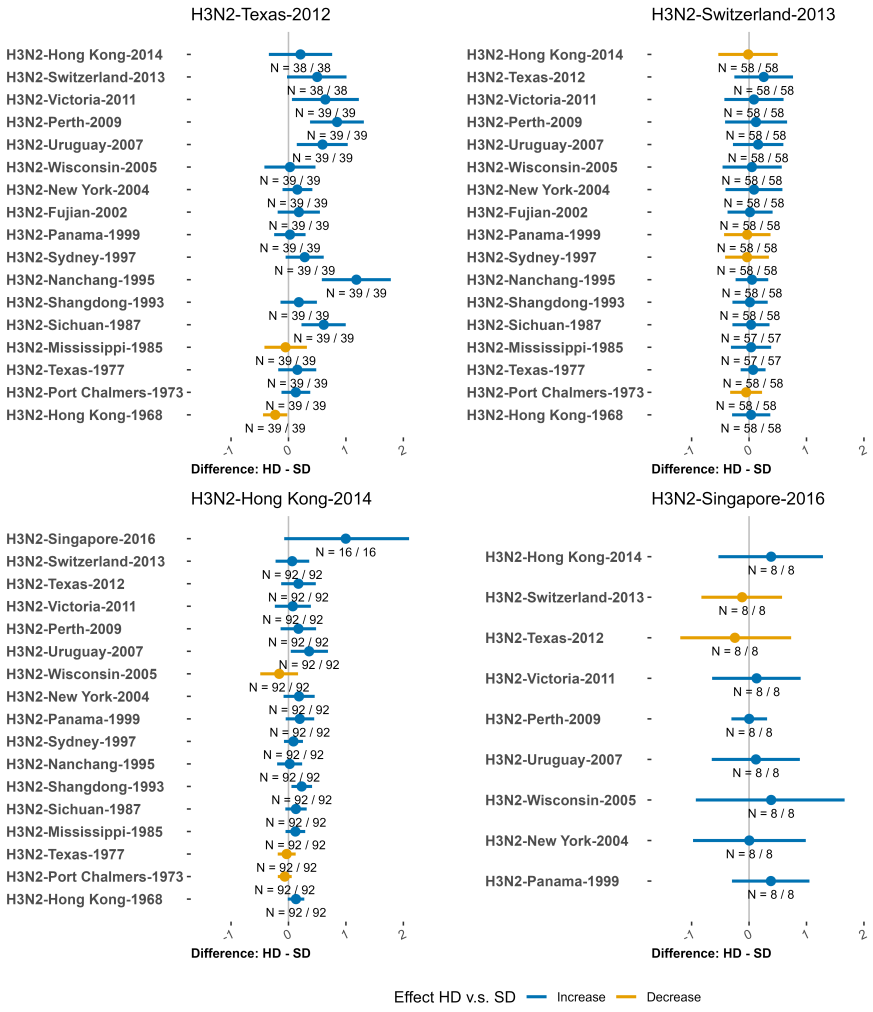

Figure C.46: The impact of HD vaccine compared to SD on strain-specific, heterologous HAI titer increase (H3N2 strains). The median and 89% equal-tailed credible interval (CI) of the overall effect (HD vs. SD) are shown. The numbers under each line show the sample size (HD/SD) for that specific strain or the overall effect size.

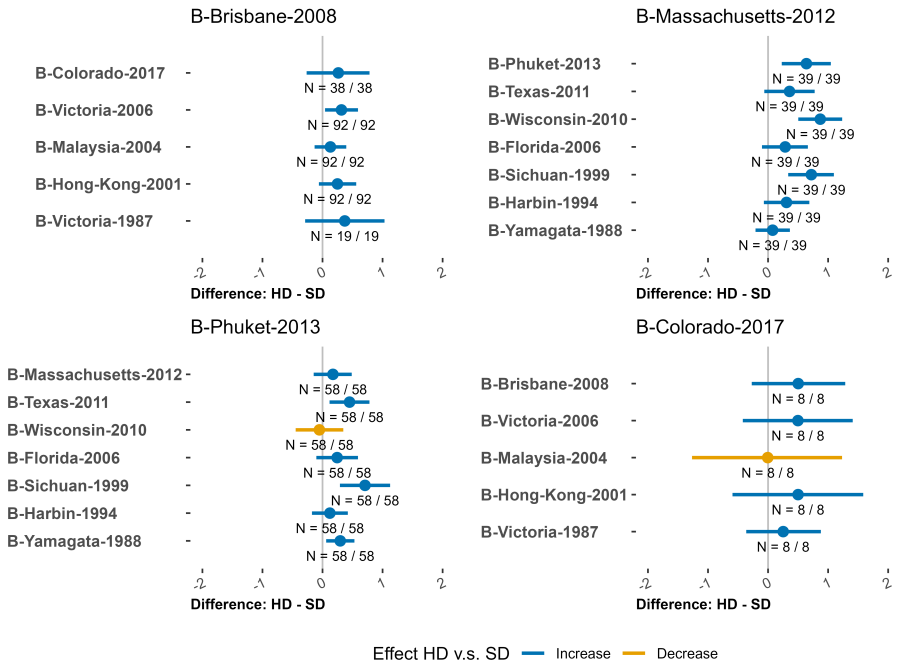

Figure C.47: The impact of HD vaccine compared to SD on strain-specific, heterologous HAI titer increase (B strains). The median and 89% equal-tailed credible interval (CI) of the overall effect (HD vs. SD) are shown. The numbers under each line show the sample size (HD/SD) for that specific strain or the overall effect size.

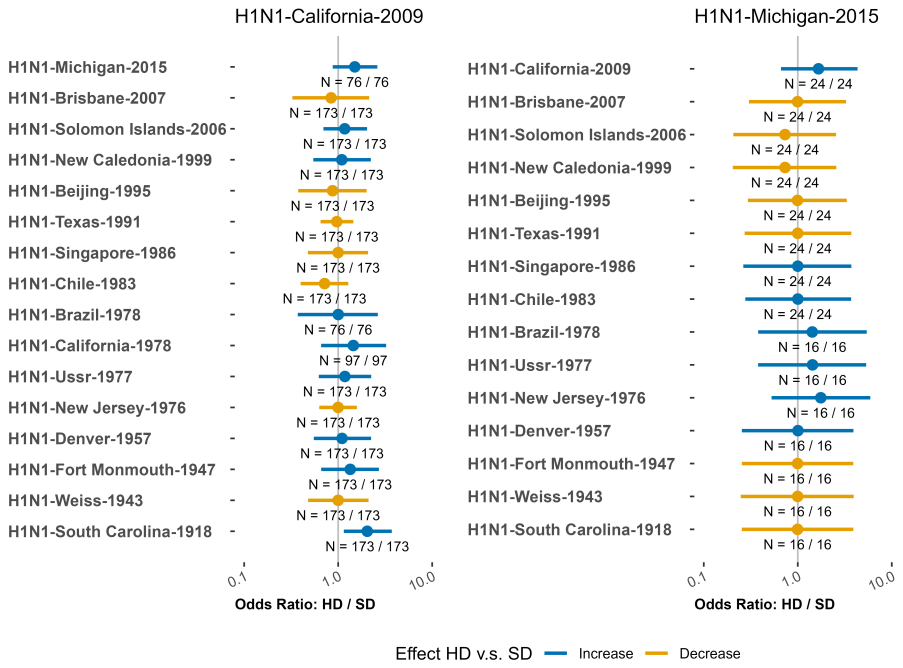

Figure C.48: The impact of HD vaccine compared to SD on strain-specific heterologous seroconversion (H1N1 strains). The median and 89% equal-tailed credible interval (CI) of the overall effect (HD vs. SD) are shown. The numbers under each line show the sample size (HD/SD) for that specific strain or the overall effect size

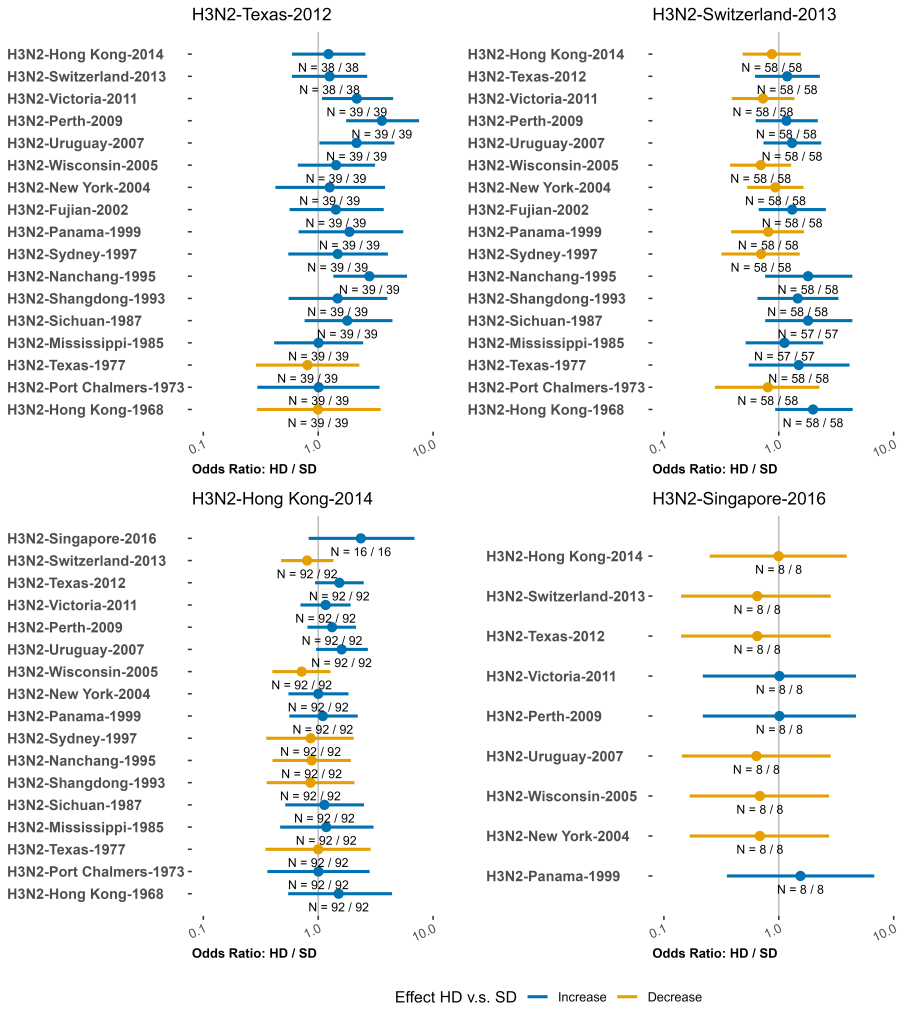

Figure C.49: The impact of HD vaccine compared to SD on strain-specific heterologous seroconversion (H3N2 strains). The median and 89% equal-tailed credible interval (CI) of the overall effect (HD vs. SD) are shown. The numbers under each line show the sample size (HD/SD) for that specific strain or the overall effect size.

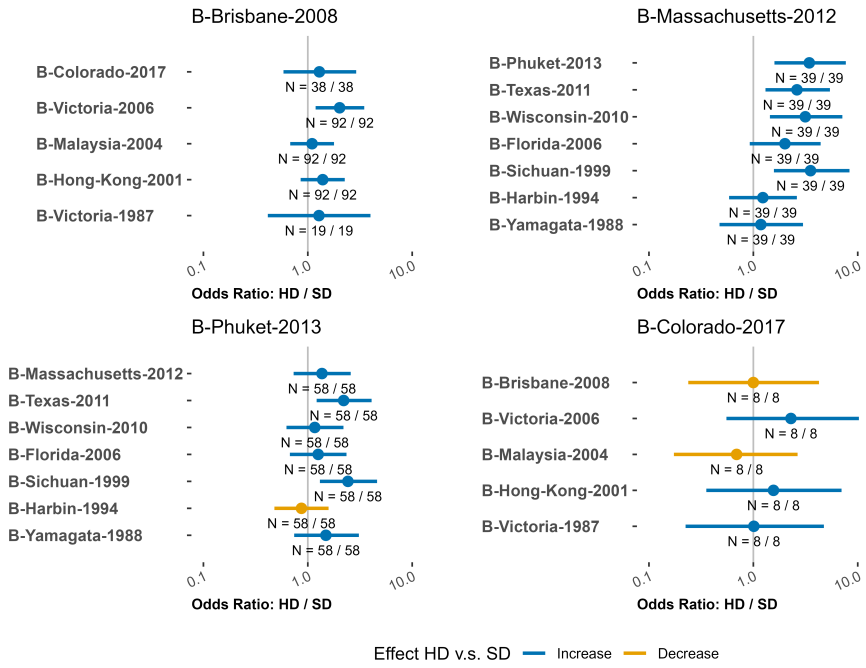

Figure C.50: The impact of HD vaccine compared to SD on strain-specific heterologous seroconversion (B strains). The median and 89% equal-tailed credible interval (CI) of the overall effect (HD vs. SD) are shown. The numbers under each line show the sample size (HD/SD) for that specific strain or the overall effect size.

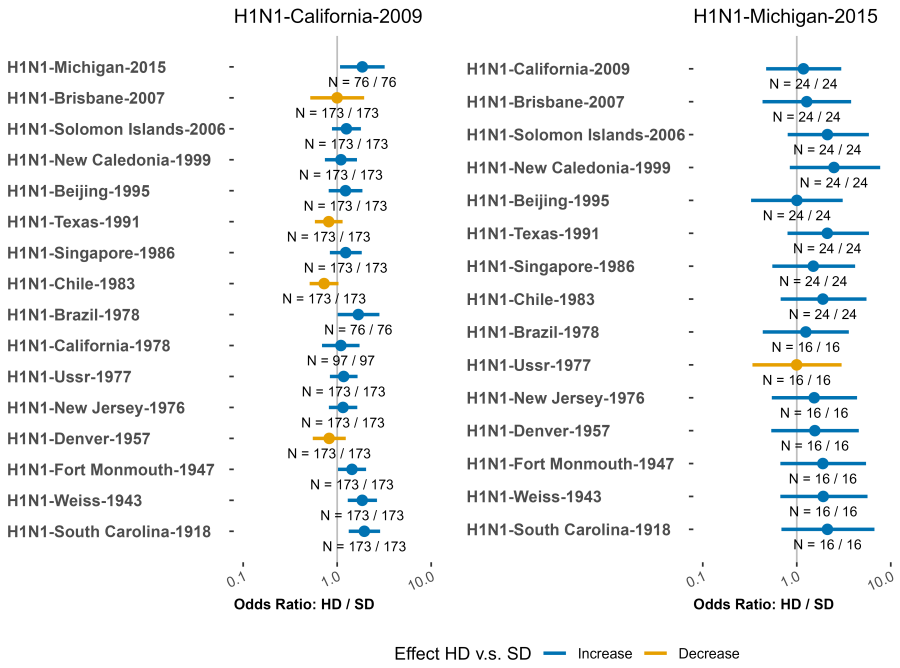

Figure C.51: The impact of HD vaccine compared to SD on strain-specific heterologous seroprotection (H1N1 strains). The median and 89% equal-tailed credible interval (CI) of the overall effect (HD vs. SD) are shown. The numbers under each line show the sample size (HD/SD) for that specific strain or the overall effect size.

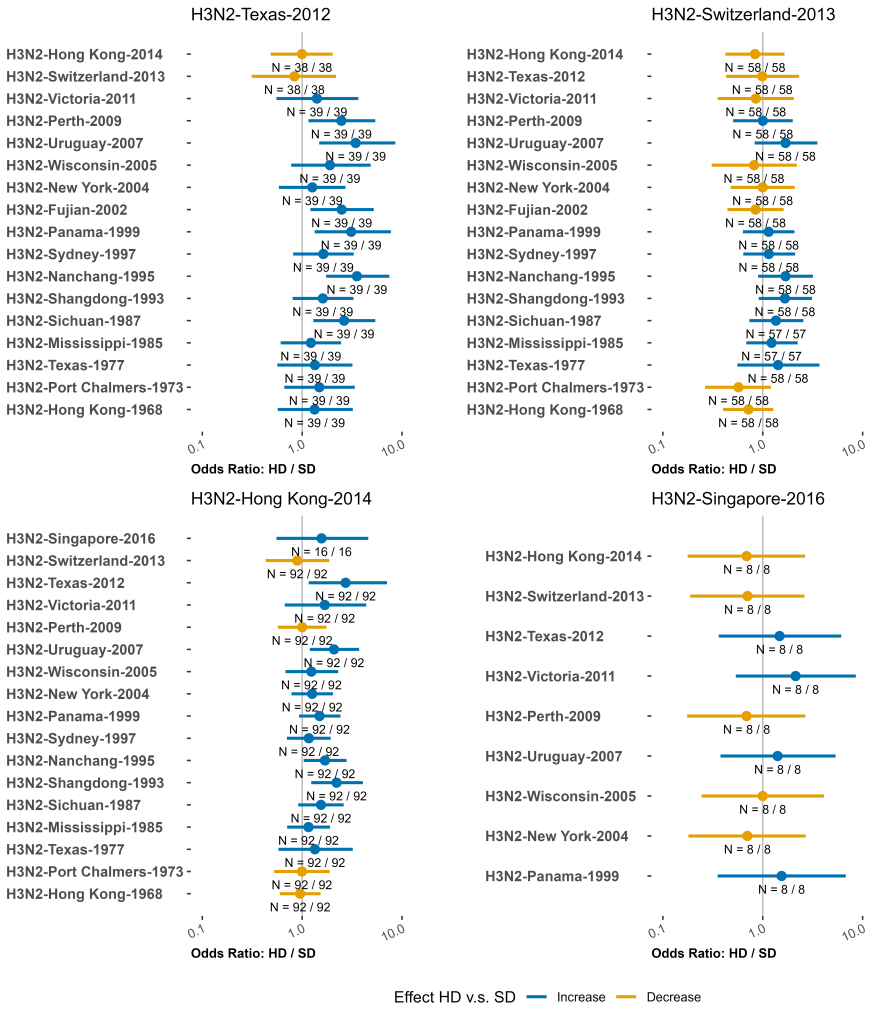

Figure C.52: The impact of HD vaccine compared to SD on strain-specific heterologous seroprotection (H3N2 strains). The median and 89% equal-tailed credible interval (CI) of the overall effect (HD vs. SD) are shown. The numbers under each line show the sample size (HD/SD) for that specific strain or the overall effect size.

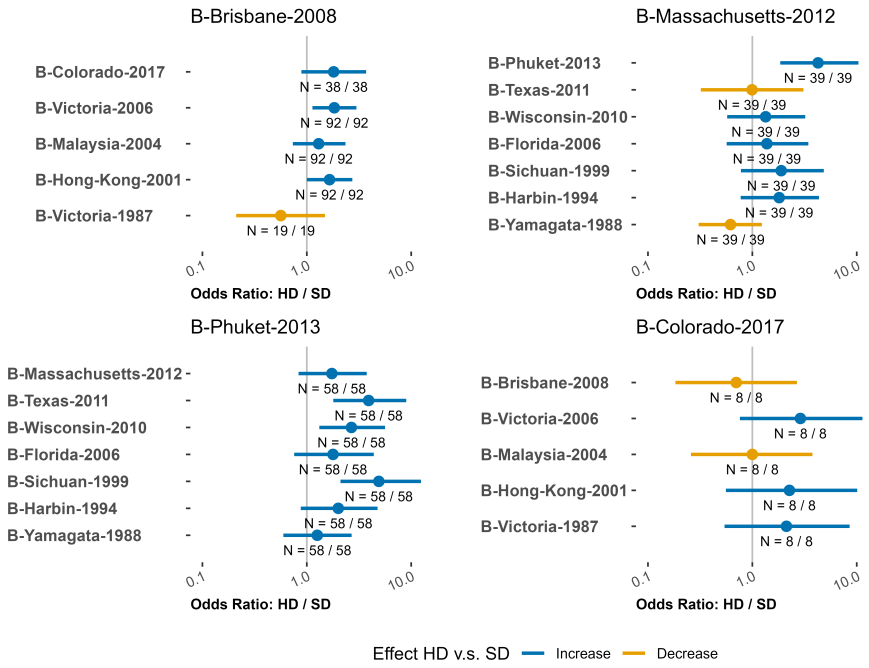

Figure C.53: The impact of HD vaccine compared to SD on strain-specific heterologous seroprotection (B strains). The median and 89% equal-tailed credible interval (CI) of the overall effect (HD vs. SD) are shown. The numbers under each line show the sample size (HD/SD) for that specific strain or the overall effect size.

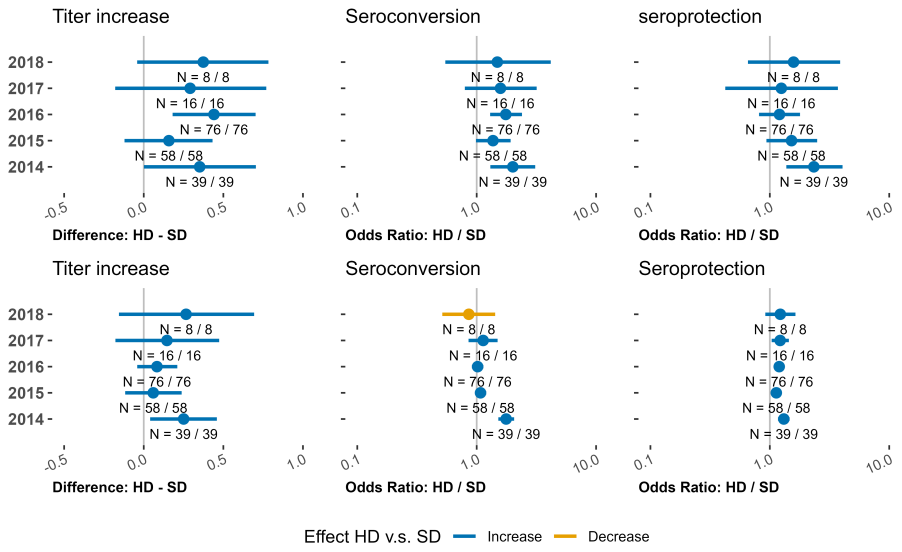

Figure C.54: The impact of HD vaccine compared to SD on vaccine-specific HAI responses. The median and 89% equal-tailed credible interval (CI) of the overall effect (HD vs. SD) are shown. The numbers under each line show the sample size (HD/SD) for that specific strain or the overall effect size. The top row shows homologous responses, the bottom row is heterologous.